Mathematical and Computational Modelling of Stochastic Partial Differential Equations Applied to Advanced Materials

by

Inayatullah Soomro

A thesis submitted in partial fulfilment for the requirements for the degree of Doctor of Philosophy at the University of Central Lancashire

September 2016

STUDENT DECLARATION FORM

I declare that while registered as a candidate for the research degree, I have not been a registered candidate or enrolled student for another award of the University or other academic or professional institution.

I declare that no material contained in the thesis has been used in any other submission for an academic award and is solely my own work.

Signature of Candidate 

Date: 20 September 2016

Type of award: **Doctor of Philosophy**

School: **Physical Sciences and computing**

Abstract

Soft materials have received increasing attention in the research community as promising candidates due to their potential applications in the field of nanotechnology. These applications include separation of membranes with nano-pores, templates for nano-electronics, novel catalysts and drug delivery nano-particles. Block copolymers have a fascinating property of self-assembly and are an important class of soft materials. Confinement of the block copolymers is a very important tool for obtaining new morphologies compared to bulk systems. In a confined system, interfacial interactions, symmetry breaking, structural frustration, curvature and confinement-induced entropy loss play vital roles in the formation of different morphologies compared to the bulk systems. In this study classical lamella, cylinder and sphere forming morphologies were investigated under geometric confinements. The Cell Dynamics Simulation (CDS) method was used to study block copolymers under geometric confinements by physically motivated discretizations. The CDS simulation method was implemented in curvilinear coordinates systems to study accurately nanostructure formations of block copolymer materials on curved surfaces. The CDS method provides a balance between computational speed and physical accuracy. The novel nanostructures were obtained with various film thicknesses, pore radii and with symmetric boundary conditions on the film interfaces.

The formations of the lamella confined in the circular annular pore systems include: concentric lamella, curved lamella, T-junctions, U-shaped, V-shaped, W-shaped, Y-shaped and star shaped. Cylindrical and sphere forming systems confined in circular annular pores showed novel packing arrangements along the spiral lines and in the concentric circular rings. Meanwhile, a new set of CDS parameters with a high temperature taken into consideration allowed study of the sphere forming system. The confined lamellae in the cylindrical pores show novel nanostructures like helical

lamella, concentric lamella and perpendicular to the pore surface lamella. This study reveals novel formation of tilted standing up cylinders packed into the concentric circular rings confined in the cylindrical pores. The cylindrical forming system confined in the cylindrical pores and spherical pores showed parallel and perpendicular cylinders; curved cylinders, straight short cylinders, cylinders packed in concentric layers and perforated holes. Sphere forming systems displayed various packing arrangements in the cylindrical pores and the spherical pores geometries like hexagonal, pentagonal, square, rhombus, concentric rings and along the vertices of the concentric quadrilateral. The obtained novel nanostructures confined in the spherical pores are onion-like nanostructures, stacked lamellar, perforated holes, standing lamella and coexistence of lamella, cylinder and sphere morphologies.

Contents

List of Figures V
List of Tables XIV
Acknowledgements XV
Nomenclature XVI
Greek Letters XVII
CHAPTER ONE 1
1. Introduction and aim of the investigation 1
1.1. Introduction and motivation of the study 1
1.2. Outline of thesis 2
1.3. Aims and objectives 4
CHAPTER TWO 5
2. Block copolymers under geometric confinements: A literature review 5
2.1. Overview 5
2.2. Block copolymers in planar thin films 12
2.3. Block copolymers confined in cylindrical pores 14
2.4. Block copolymers confined in spherical pores 18
CHAPTER THREE 21
3. Implementation of CDS method in polar, cylindrical and spherical coordinate systems 21
3.1. Overview 21
3.2. CDS and its implementation in polar, cylindrical and spherical coordinate systems 24
3.3. Discretisation of Laplacian in the polar coordinate system 28
3.4. Discretisation of Laplacian in the cylindrical coordinate system 30
3.5. Discretisation of Laplacian in the spherical coordinate system 33
3.6. Simulations of binary fluid 36
CHAPTER FOUR 38
4. Block copolymer system confined in circular annular pores 38
4.1. Introduction 38
4.2. Results and discussions 39
4.2.1. Asymmetric lamellae forming system confined in circular annular pores 39
4.2.2. Symmetric lamella forming system confined in circular annular pores ... 55
4.2.3. Cylindrical forming system confined in circular annulus pores 57

4.2.4. Spherical forming system confined in circular annular pores 62
4.3. Summary 69
CHAPTER FIVE 72
5. Block copolymers confined in cylindrical pores 72
5.1. Introduction 72
5.2. Results and discussions 73
5.2.1. Lamella forming system confined in cylindrical pores 73
5.2.2. Cylindrical forming system confined in cylindrical pores 81
5.2.3. Spherical forming system confined in cylindrical pores 92
5.3. Summary 104
CHAPTER SIX 106
6. Diblock copolymer system confined in spherical pores 106
6.1. Introduction 106
6.2. Results and discussion 107
6.2.1. Lamella forming system confined in spherical pores 107
6.2.2. Cylindrical forming system confined in spherical pores 116
6.2.3. Sphere forming system confined in spherical pores 124
6.3. Summary 132
CHAPTER SEVEN 134
7. Conclusions and Future work 134
7.1. Block copolymers confined in the circular annular pores 134
7.2. Block copolymers confined in cylindrical pores 135
7.3. Block copolymers confined in spherical pores 138
7.4. Future work 139
References 140

List of Figures

Figure 2.1: The bulk phase diagram of diblock copolymer system [25]. The horizontal axis shows volume fraction of A segment of polymer system, vertical axis on the left illustrates Flory-huggins interaction parameter and vertical axis on the right presents the decreasing temperature parameter. In the diagram (LAM) indicates lamella phase, (HEX) indicates hexagonal packed cylindrical phase, (BCC) is for body-centred-cubic spheres phase and (GYR) refers to the bi-continues complex gyroid phase in the bulk system. 8

Figure 2.2: AB diBlock copolymers nanostructures in the bulk systems [22]. 10

Figure 2.3: Schematic diagrams of different architectures of block copolymers. The green represents the block A, red one represents the block B and the blue one represents block C. (a) A-B diblock copolymer, (b) A-B-A triblock copolymer, (c) Grafted or branched A-B diblock copolymer, (d) Star A-B-C triblock copolymer, (e) Linear A-B-C triblock copolymer. 11

Figure 3.1: Polar mesh diagram. 28

Figure 3.2: Cylindrical mesh diagram [82]. 30

Figure 3.3: Sphere grid system diagram [83] 33

Figure 3.4: Phase separation for binary fluid were obtained on 1 million time steps, in a pore system with the interior radius of the pore system was fixed at r_a = 3.0 and the grid sizes are (a) 30x360 (b) 60x360 37

Figure 4.1: Evolutions of asymmetric lamellae system on 1 million time steps confined in various circular annular pore sizes with the interior radius of the pore was fixed at $r_a = 3.0$ and the exterior radius of pore was expanded to obtain various pore sizes: (a) evolution of asymmetric lamella in the pore system size *d = 1,* pore system induces alternating lamella strips (b) evolution of asymmetric lamella in the pore system size *d = 2,* system patterned into Y-shaped, U-shaped and perforated holes morphologies (c)

evolution of asymmetric lamella in the pore system size $d = 3$, pore shows Y-shaped or tilted Y-shaped star shaped and W-shaped patterns (d) evolution of asymmetric lamella in the pore system size $d = 4$, system induces Y-shaped, W-shaped U-shaped and a few perforated holes (e) evolution of asymmetric lamella in the pore system size $d = 5$, patterns are two arm stars and single arm star with a perforated hole at the centre of the star (f) evolution of asymmetric lamella in the pore system size $d = 6$, induced nanostructures include perforated holes morphology (g) evolution of asymmetric lamella in the pore system size $d = 8$, mixed morphologies (h) evolution of asymmetric lamella in the pore system size $d = 10$, alternating lamella strips normal to the exterior circular boundary. 41

Figure 4.2: Evolution of asymmetric lamellae system on 1 million time steps in the pore system with the interior radius of pore system was fixed at $r_a = 5.0$ and the exterior radius r_b of the pore system was expanded to obtain various pore sizes, pore size of the systems: (a) evolution of nanodomains in the pore size $d = 2$, system show alternating lamella strips normal to the circular boundaries, perforated holes and Y-shaped defects (b) evolution of lamella patterns in the pore system size $d = 3$ system induces lamella strips and Y-shaped defects (c) evolution of the asymmetric lamella system in the pore size $d = 4$ induced morphologies are Y-shape, U-shape, W-shape and star shape lamellae with a perforated hole at the centre of the star (d) nanostructure evolution in the pore size $d = 5$ induces diverse lamella patterns.....45

Figure 4.3: The asymmetric lamellae system in the expanded pore size with the interior radius of pore system was fixed at $r_a = 7$: (a) the system size $d = 2$, system induces alternating parallel lamella strips normal to the circular boundaries, Y-shaped, W-shaped and star shaped patterns (b) the system size $d = 3$, induced patterns including a few alternating lamella strips normal to the circular boundaries, Y-shaped, W-shaped and star shaped defects.....46

Figure 4.4: Asymmetric lamellae system under one dimensional confinement obtained on 1 million time steps, the interior radius of the pore system was fixed at r_a=3.0 and the pore sizes of systems are (a) *d = 1,* pore system induces three alternating concentric lamella rings (b) *d = 2.5,* pore system induces seven alternating concentric lamella rings (c) *d = 3,* system induced concentric lamella and strip lamella (d) *d = 4,* system induced concentric lamella and dislocations (e) *d = 6,* system patterned with mixed lamella morphologies. 48

Figure 4.5: Evolution of asymmetric lamellae system on 1 million time steps under geometric confinement, interacting circular walls has affinity with the B segment of polymer system, interaction strength was applied $\alpha = 0.2$, the interior radius of the pore system was fixed at r_a = *3,* whereas system was expanded by the exterior radius of the pore system and pore system size are (a) *d = 1,* system patterned into concentric lamella (b) *d = 2.5,* system induces concentric lamella with very few dislocations (c) *d = 3,* concentric lamella, perforated holes and dislocations (d) *d = 4,* mixed patterns..... 49

Figure 4.6: Asymmetric lamellae system under one dimensional confinement into expanded pore system with the interior radius was fixed at r_a = *5* and the pore size of the systems are (a) *d = 2.5* (b) *d = 3* (c) *d = 4.* 51

Figure 4.7: Asymmetric lamellae system under geometric confinement, circular walls have affinity to the B segment of the polymer system, the interior radius of the pore systems was fixed at r_a = *5,* and the pore sizes are (a) *d = 2* (b) *d = 2.5* (c) *d = 3* (d) *d = 4.* 52

Figure 4.8: Asymmetric lamellae system under geometric confinement, the interaction strength was applied $\alpha = 0.2$, the expanded pore system with the interior radius of the pores were fixed at r_a = *7* and pore sizes of the systems are (a) *d = 2.5* (b) *d = 3.5*..... 53

Figure 4.9: Lamellae system under geometric confinement, circular walls have affinity to the B segment of the polymer system, the interior radius of the pore system was fixed

at r_a = *7*, the pore size expanded by the exterior radius of the pore system, pore sizes are (a) *d = 2.5* (b) *d = 3.5.* 54

Figure 4.10: Symmetric lamellae forming system confined in circular annular pores with the interior radius of the pore system was fixed at r_a = 3.0 and the pore sizes are (a) 2 (b) 4 (c) 6. 56

Figure 4.11: Symmetric lamellae system under geometric confinement with the interior radius of the pore system was fixed at r_a = 3.0 and pore sizes of the system are (a) *d = 3* (b) *d = 6.* 57

Figure 4.12: Cylindrical system in the pore geometry with pore sizes (a) *d = 1* (b) *d = 2* (c) *d = 3* (e) *d = 4* (f) *d = 6*..... 58

Figure 4.13: Cylindrical systems confined under interfacial circular walls having affinity to A block and the pore size of systems are (a) *d = 2* (b) *d = 3* (c) *d = 4* (d) *d = 6.*..... 60

Figure 4.14: Cylindrical systems with interfacial affinity to B block and the pore size of the systems are (a) *d = 2* (b) *d = 3* (c) *d = 4* (d) *d = 6.0.* 61

Figure 4.15: Sphere system in the circular annular pore geometry and the pore sizes are (a) *d = 2* (b) *d = 3* (c) *d = 4* (d) *d = 6.*..... 63

Figure 4.16: Sphere forming system with modified CDS parameter system and pore system sizes are (a) *d = 2* (b) *d = 3* (c) *d = 4* (d) *d = 6.*..... 64

Figure 4.17: sphere forming system with system subject to the affinity of interacting walls to A block and system size (a) *d = 2* (b) *d = 3* (c) *d = 4* (d) *d = 6.* 65

Figure 4.18: Sphere system with preferential attractive wall for monomer B and the pore system size are (a) *d = 2* (b) *d = 3.*..... 66

Figure 4.19: Sphere forming system with modified CDS parameter system subject to the affinity of interacting walls to A block and system sizes are (a) *d = 2* (b) *d = 3* (c) *d = 4* (d) *d = 6.* 67

Figure 4.20: Sphere forming system with modified CDS parameter system subject to the affinity of interacting walls to A block and system size (a) *d = 2* (b) *d = 3* (c) *d = 4* (d) *d = 6.* 68

Figure 5.1: Lamella system confined in neutral cylindrical pores, with pore system where interior radius was fixed at r_a *= 3* and the pore size (a) *d = 0.5* (b) *d = 1.5* (c) *d = 2.* 74

Figure 5.2: Lamellae system confined in the neutral cylindrical pores, interior radius of pore system fixed at r_a *= 5* and pore size (a) *d = 0.5* (b) pore size *d = 1* (c) *d = 1.5* (d) *d = 2* (e) *d = 2.5* (f) *d = 3.* 75

Figure 5.3: Lamella system with interfacial surfaces, the pore system with interior radius fixed at r_a *= 3* and the pore sizes are (a) *d = 1.0* (b) *d = 1.5.* 76

Figure 5.4: Lamella system with interfacial surfaces, interior radius of the pore surface was fixed at $r_a = 5$ and the pore sizes are (a) *d = 1.0* (b) *d = 1.5*(c) *d = 2.5* (d) *d = 3.0.* 77

Figure 5.5: Cylindrical system confined by interfacial surfaces perpendicular to the pore system and the pore size and pore lengths are (a) *d = 1.6* and *h = 1.6* (b) *d = 2.5* and *h = 1.0* (c) *d = 2.5* and *h = 2.5.* 79

Figure 5.6: Two dimensional confinement of cylindrical system with the pore sizes and the pore lengths are (a) *d = 1.0* and *h = 1* (b) *d = 1.0* and *h = 1.6.* 81

Figure 5.7: Cylindrical forming system confined in neutral surfaces, in a pore system with the interior radius fixed at r_a *= 3*, the pore sizes of the system are (a) *d = 1* (b) *d = 1.5* (c) *d = 3.* 82

Figure 5.8: Cylindrical morphology in the neutral cylindrical pores with a pore system whose the interior radius was fixed at $r_a = 5$ and the pore size of systems are (a) *d = 0.5* (b) *d = 1.0* (c) *d = 1.5.* 84

Figure 5.9: Cylinder system under interfacial surfaces in a pore system with the interior radius fixed at $r_a = 3$ and the pore sizes of system are (a) *d = 1* (b) *d = 1.5* (c) *d = 2* (d) *d = 2.5* (e) *d = 3.* 85

Figure 5.10: Cylindrical forming system under surface interacting parameter $\alpha = 2$, the interior radius of pore system is fixed at $r_a = 5$, the length of pore was fixed at *h = 6,* $0 \le \theta \le 2\pi$ and the pore sizes are (a) *d = 0.9* (b) *d= 1.0* (c) *d = 1.5* with the interior layer (d) *d = 2* (e) *d = 2.5* (f) *d = 3.* 86

Figure 5.11: Cylindrical forming system with fixed pore size *d =5,* whereas, the height was varied for different values of lattice. 89

Figure 5.12: cylindrical system obtained with interaction parameter $\alpha = 0.4$, the pore size and the pore lengths respectively are (a) d = 1.6 and *h* = 1.6 (b) d = 1.5 and *h* = 4 (c) d = 2 and *h*=4. 91

Figure 5.13: Sphere forming system in neutral cylindrical pore systems with low temperature CDS parameter system, the interior radius of pore system was fixed at r_a = *3* and the pore sizes are (a) *d =2.5* (b) *d = 3.0.* 93

Figure 5.14: Sphere system obtained by low temperature CDS parameter system, the pore system has the interior radius fixed at r_a *=5* and pore sizes in the images are (a) *d = 0.5* (b) *d = 1* (c) *d = 1.5.* 93

Figure 5.15: Sphere system obtained by modified CDS parameters system with high temperature in a pore system with the interior radius fixed at r_a *= 3* and the pore sizes are (a) *d = 1* (b) *d = 2* (c) *d = 2.5.* 95

Figure 5.16: Sphere system obtained with modified CDS parameter system in a pore system whose interior radius were fixed at r_a *= 0.5*and the pore sizes of the systems are (a) *d = 0.5* (b) *d = 1* (c) *d = 1.5* (d) *d = 2* (e) *d = 2.5* (f) *d = 3.* 96

Figure 5.17: Sphere system with interacting parallel circular walls having preferential affinity with majority segment of the polymer system, in a pore system with interior

radius of the pore were fixed at $r_a = 3$ and the pore sizes of the system are (a) *d = 1.5* (b) *d = 2* (c) *d = 2.5.* 98

Figure 5.18: Sphere system under interfacial cylindrical surfaces and size of pore systems are (a) *d = 1.5* (b) *d = 2* (c) *d = 2.5* (d) *d = 0.3.* 99

Figure 5.19: Sphere system under geometric confinement applied through cross sections of cylindrical pore system with the pore size and the pore length are respectively (a) *d = 1.5, h = 1.2* (b) *d = 2.5, h = 2.5* (c) *d = 3.0, h = 3.0.* 101

Figure 5.20: Sphere system under two dimensional confinements with system size and length are respectively (a) *d = h = 1.5* (b) *d = h = 2.5* (c) *d = h = 3.0.* 103

Figure 6.1: Asymmetric lamellae system in spherical pores with neutral surfaces, the interior radius of the pores were fixed at $r_a = 3$ and the pore sizes of the systems are (a) *d = 0.5* (b) *d = 1* (c) *d = 1.5* (d) *d = 3.* 108

Figure 6.2: Asymmetric lamella system in the pore surface with the interior radius fixed at $r_a = 5$ and shell sizes are (a) *d = 0.5* (b) *d = 1* (c) *d = 1.5* (d) *d = 3.* 110

Figure 6.3: Asymmetric lamella system in spherical pore with the interior radius of the pore system fixed at $r_a = 7$ and the spherical pore sizes are (a) *d = 0.5* (b) *d = 1* (c) *d = 1.5* (d) *d = 3.* 111

Figure 6.4: Lamella systems with interfacial surfaces, the pore surface having the interior radius fixed at $r_a = 3$ and the pore sizes are (a) *d = 1* (b) *d = 1.5.*.....112

Figure 6.5: Lamella systems confined by interfacial interfaces, with pore surface having the interior radius fixed at $r_a = 5$ and the pore sizes are (a) *d = 1* (b) *d = 1.5.*.....113

Figure 6.6: lamella systems confined by interacting interfaces, with the pore surface having the interior radius fixed at $r_a = 7$ and the pore sizes are (a) *d = 1* (b) *d = 1.5* (c) *d = 2.0* (d) *d = 2.5* (e) *d = 3.0.*.....114

Figure 6.7: Cylindrical forming system confined in neutral spherical pores with the interior radius of the pore surface fixed at $r_a = 5$ and the pore sizes are (a) *d = 0.5* (b) *d = 1* (c) *d = 2.5* (d) *d = 3.0.* 117

Figure 6.8: Cylindrical forming system confined in neutral spherical pores with the interior radius of the pore surface fixed at $r_a = 7$ and the pore sizes are (a) *d = 0.5* (b) *d = 2.0* (c) *d = 2.5* (d) *d = 3.0.* 119

Figure 6.9: Cylinder system confined by parallel spherical interfaces in a spherical pore with the interior radius fixed at $r_a = 5$ and the pore surface sizes are (a) *d = 1* (b) *d = 1.5* (c) *d = 2.5.* 121

Figure 6.10: Cylinder system confined by parallel spherical interfaces in a spherical pore with the interior radius fixed at $r_a = 7$ and the pore surface sizes are (a) *d = 1* (b) *d = 1.5* (c) *d = 2.0.* 123

Figure 6.11: Modified sphere system in the neutral pore surfaces with the interior radius of the pore surface fixed at $r_a = 3$ and the pore sizes are (a) *d = 0.5* (b) *d = 1.0.* 125

Figure 6.12: Modified sphere system in the neutral pore surfaces with the interior radius of the pore surface fixed at $r_a = 5$ and the pore sizes are (a) *d = 0.5* (b) *d = 1.0* (c) *d = 1.5.* 126

Figure 6.13: Sphere system obtained by modified CDS parameter system in the neutral pore surfaces with the interior radius of the pore surface fixed at $r_a = 7$ and the pore sizes are (a) *d = 0.5* (b) *d = 1.0* (c) *d = 1.5.* 127

Figure 6.14: Sphere system confined by parallel to the pore walls, with the interior radius of the pore surface fixed at $r_a = 5$ and the pore surface sizes are (a) *d = 1.5* (b) *d = 2.0* (c) *d = 2.5.* 129

Figure 6.15: Sphere system confined by parallel to the pore walls, with the interior radius of the pore surface fixed at $r_a = 7$ and the pore surface sizes are (a) *d = 1.5* (b) *d = 2.0* (c) *d = 2.5*.....131

List of Tables

Table 1: Computational parameters used in the simulation results 39

Table 2: CDS Parameters for asymmetric lamella forming system 40

Table 3: CDS parameters for symmetric lamella system 55

Table 4 Modified CDS parameters for sphere forming system 64

Table 5: CDS parameter system for asymmetric lamella forming system 74

Table 6: CDS parameter system with low temperature for sphere forming system 92

Table 7: Modified CDS parameter system for sphere forming system 95

Table 8: CDS parameter system for sphere forming system for low temperature 98

Table 9: CDS parameter system for asymmetric lamella forming system 107

Table 10: CDS parameter system for cylindrical forming system 116

Table 11: Modified CDS parameter system for sphere forming system with high temperature 124

Table 12: CDS parameters for sphere forming system with low temperature 128

Acknowledgements

I am grateful to all the people who provided support, encouragement, advice and friendship during my studies at the University of Central Lancashire. It is a great pleasure to acknowledge all of them here.

I would like to first express my sincere gratitude to my supervisors, Dr Dung Ly and Prof Dr Waqar Ahmed for their vital guidance, patience and encouragements during the study. I am thankful for your confidence in me and your eagerness.

I also would like to thank you Prof Dr Andrei Zvelindovsky and Dr Marco Pinna for their valuable support.

I would like to thank you, my colleagues and friends of University of Central Lancashire and Preston city for their valuable motivations and help.

I wish to acknowledge the Shah Abdul Latif University Khairpur, Sindh, Pakistan and Higher Education Commission (HEC) Pakistan for funding and support during the study.

In the last but not the least, enormous and special thanks to my family members for their support and love. I am especially grateful to my wife; in my absence she provided care and love to my kids. This journey would not have been possible without the support of my wife, my mother and rest of family members. I dedicate this thesis to all my family members.

Nomenclature

A----------Phenomenological constant

B ----------Chain-length dependence to the free energy

A----------Phenomenological constant

B----------Phenomenological constant

D ----------Positive constant for diffusion coefficient

F ----------Free energy functional

f_A ----------Global volume fraction of *A* monomers in the diblock polymer system

$f(\psi)$----------Map function

$F(\psi)$----------Free energy functional

$H(\psi)$----------Free energy function

M ----------Phenomenological mobility constant

N_A ----------Number of *A* monomers

N_B ----------Number of *B* monomers

N_r ----------The length of the radial *r* dimension of the lattice system

N_θ ----------The length of the angular dimension of the lattice system

N_z ----------The length of the *z* dimension of the lattice system

N_ϕ ----------The length of the azimuthal angular dimension of the lattice

t ----------Time evolution of order parameter

u ----------Phenomenological constant

v ----------Phenomenological constant

Greek Letters

ψ ----------Order parameter

$\nabla^2\psi$ ----------The Laplacian operator

$\langle\langle\ \rangle\rangle$ ----------The averaging of the stencil in the lattice

ϕ_A ----------Local volume fraction for A monomer

ϕ_B ----------Local volume fraction for B monomer

α -The interaction strength between pore interfaces and one of the segments of the polymer system

τ ----------Temperature-like parameter

Δt----------Time-step

Δr ----------Radial step in the lattice

$\Delta\theta$ ----------The angular step in the lattice

Δz ----------The length steps in the cylindrical lattice

$\Delta\phi$ ----------The azimuthal angular step in the spherical lattice

ε --------weighting factor of nearest neighbour points for laplacian in polar coordinates

ω ---weighting factor of nearest neighbour points for laplacian in cylindrical coordinates

β -- weighting factor of nearest neighbour points for laplacian in spherical coordinates

CHAPTER ONE

1. Introduction and aim of the investigation

1.1. Introduction and motivation of the study

Block copolymers due to their ability to self-assemble into rich nanostructures and potential scientific applications have attracted tremendous scientific interest. Different numbers of ordered equilibrium phases like lamellae, hexagonally packed cylinders, body centred-cubic spheres, and a bi-continues network structure gyroid phases have been identified in diblock copolymer melts. Nanostructure control is a prime goal for researchers and can be achieved by applying external fields, particularly surface fields which are prominent in the confining geometries. Under geometric confinements, more complex structures, different morphologies and symmetry breaking of an ordered structure can be achieved.

In this contribution we focus on mathematical modelling and computer simulations of diblock copolymers (two blocks per molecule) in various confinements. Due to the very large parameter space experimental study of block copolymers is very time consuming. However, computer simulations can help in finding optimal parameters to create new block copolymer materials. Most of the previous computational studies were carried out for block copolymers under geometric confinements by using the Cartesian coordinate system. While, block copolymers confinements in circular, spherical and cylindrical pores using the Cartesian coordinate system could lead to artefacts in the systems. In order to study accurately block copolymer confined in circular, cylindrical and spherical pores the CDS method was employed in polar, cylindrical and spherical coordinate systems. In order to account for curvature effects at each point on the lattice, isotropic

discrete Laplacian operators were derived in polar, cylindrical and spherical coordinate systems. Therefore, this study provides the physical motivated discretization of curved surfaces. A mathematical model for the order parameter which involves partial differential equations was solved by numerical approximations using finite difference schemes. The CDS equations were solved with the appropriate boundary conditions on the circular thin film, the cylindrical pores and the spherical pore surfaces. The CDS simulation codes were developed in the FORTRAN computer language for the evaluations of the order parameter in polar, cylindrical and spherical coordinate systems.

Further, in this study, confinement-induced nanostructure formations have been carried out in the natural geometric environment by using polar, cylindrical and spherical coordinate systems. The curvilinear coordinate systems provide accurate nanostructure formations in the confined systems as compared to the Cartesian coordinate system. In the case of confinement, the effect of interfacial surfaces can also be accurately studied by using polar, cylindrical and spherical coordinate system. The study reveals various novel nanostructures confined in circular annular pores, cylindrical pores and spherical pores with various pore sizes and pore radii.

1.2. Outline of thesis

In this study investigations were carried out on self-assembly of diblock copolymers confined in annular circular pores, hollow cylindrical pores, and spherical nanopores. To study accurately, block copolymers confined in circular annular pores, cylindrical pores, and spherical pores, the CDS method was employed in polar, cylindrical and spherical coordinate systems.

In **Chapter 2** a literature review of block copolymers confined in the planar thin films, the cylindrical pores and the spherical pore is given.

In **chapter 3** the mathematical model and algorithm are discussed in detail. Evaluation of order parameter by partial differential equations and its allied equations which represent the CDS method are discussed in detail. The discretized isotropic forms of Laplacian operators in polar, cylindrical and spherical coordinate systems were derived and discussed.

In **chapter 4** block copolymers are investigated under geometric confinements of the circular annular pores with various film thicknesses and pore radii. Lamella, cylinder, and sphere forming systems are studied in the circular annular pore system with neutral surfaces and interfacial surfaces. Results predicted novel nanostructure in the circular annular pore geometry. Studies are carried out with interacting circular walls having affinity with the majority block as well as the minority block of the polymer system. A new set of CDS parameters for sphere forming system is proposed.

In **chapter 5** studies are carried out on block copolymers confined in the hollow cylindrical pore with various sizes of the pore surfaces, pore lengths and pore radii. Lamella, cylinder, and spherical forming systems are obtained and discussed in the cylindrical pore geometry. The results are obtained and discussed with the neutral pore surfaces and the interfacial pore surfaces having affinity to the majority segment of the polymer system. Block copolymers confined in the cylindrical pores are obtained and discussed with one-dimensional confinements and two-dimensional confinements.

In **chapter 6** studies and investigations are carried out for block copolymers confined in the spherical shell with various thicknesses of the pore surfaces and pore radii. Lamella, cylinder, and sphere systems are obtained and discussed in the spherical pore geometry.

Results are obtained and discussed with neutral pore surfaces as well as interfacial surfaces having affinity to the majority segment of the polymer system.

In **chapter 7** covers conclusions, discussions, and future works of this study.

1.3. Aims and objectives

Following are the aims and objectives of this study.

I. To study and investigate self-assembled diblock copolymers lamella, cylindrical and spherical forming systems confined in annular circular pores by using the CDS method employed in the polar coordinate system.

II. To investigate self-organizing diblock copolymers lamella, cylindrical and spherical forming nanostructures confined in hollow cylindrical pores by using the CDS method employed in the cylindrical coordinate system.

III. To Study and analyses of self-assembling diblock copolymers lamella, cylindrical and spherical forming systems confined in spherical pores by using the CDS method employed in the spherical coordinate system.

CHAPTER TWO

2. Block copolymers under geometric confinements: A literature review

2.1. Overview

The diblock copolymer system is an important class of soft materials which are characterised by a self-assembling property [1, 2]. The self-assembling property enables diblock copolymers for potential scientific applications. [3]. Geometric confinements of block copolymers provide spatial constraints to the molecules of the polymer system. Nano structural control is a prime goal for researchers. Confinement is a significant tool to break the symmetry of an ordered structure [4]. Under the constraint environment, the block copolymers conforms novel nanostructures which is important for significant biological and chemical applications [5]. Block copolymers are one of the classes of soft materials which consist of different polymer blocks covalently connected to each other and the length scale of the ordered structures at nanometer scale is (10-100 nm) [6-8]. AB diblock copolymers are the simplest linear polymer systems which consist of two blocks interconnected covalently to each other [9, 10]. Due to the fact that the phase separation is driven by chemical incompatibilities between the different blocks, they can spontaneously form various patterns of nanostructures depending on block-block interactions, block composition, architecture of blocks, molecular characteristics and furthermore, external conditions such as the geometry of confinement [3, 9, 10]. A number of ordered microdomain structures have been explored in diblock copolymer melts such as lamellae, hexagonally packed cylinders, body-centred arrays of spheres and complex structures such as bi-continuous network structures [7, 10-14]. More

complex block copolymers and various morphologies can be obtained by placing block copolymers under geometrical confinements [6, 10]. Block copolymers under geometrical confinement, conform many fascinating nanostructures that do not tend to conform in the bulk systems. Spatial confinement provides a powerful tool to break the symmetry of an ordered nanostructure [15] and paves the way for fabricating novel morphologies [8]. Under confinement, interfacial interactions, symmetry breaking, structural frustrations and confinement-induced entropy can play vital roles in the nanostructural control of soft materials [10, 16]. The pore is the most reasonable geometry to be considered and its effects on morphology formation are significant for nanotechnology applications and biology [17]. The curvature and interfacial interactions influence microdomains to change their orientation [7]. To avoid the difficulty associated with irregular boundaries or arbitrarily shaped boundaries, the entire physical problem can be transformed into boundary-fitted curvilinear coordinate systems such as polar, spherical and cylindrical coordinates [18]. Cylindrical geometry provides a high degree of curvature imposed on the surface of nanopores which causes a frustration of chain packing at the interface, leading to the formation of new morphologies [15]. Previous studies were done on one-dimensional (thin film) and two-dimensional cylindrical pores confined systems and under three-dimensional confinements (spherical and elliptical) pores [19]. To the best of our knowledge, no one has studied diblock copolymers under geometric confinement using the CDS method applied in polar and cylindrical coordinates. However, it is our aim and desire to fill this gap by providing a complete understanding of applying the CDS method using polar, cylindrical and spherical coordinate systems in the investigation of the soft materials.

Previous studies of block copolymers were carried out by using a square lattice, but unfortunately, these studies did not provide full isotropic results while studying two-dimensional confinements with polar coordinates may give full isotropic results as

being the nature of geometrical coordinates. These confinements may give generalizations and rules about controlling the morphologies as a geometric function. Using CDS, the morphology of thin block copolymers films around a spherical nanoparticle has been investigated to obtain nanoshells with structural control through the interplay between film thicknesses, characteristics of block copolymers, surface parameters, and curvature [20]. Block copolymers confined in cylindrical nanopores have been studied systematically and have found novel structures such as helices and stacked toroids inside the cylindrical pores. These types of confinement-confinement induced morphologies depend on the pore diameter and the surface-polymer interactions, which shows the importance of structural frustration as well as interfacial interactions [14]. Later the pore diameter and surface-polymer interactions were varied systematically to investigate their influence on the self-assembled morphologies and chain conformations. In the case of Lamella-forming and cylinder-forming, block copolymers under cylindrical pore confinement novel structures were reported, such as helices and concentric lamellae [21]. Different structures including stacked-disk, single-helix, gyroidal, catenoid-cylinder, stacked-circle and concentric cylindrical barrel morphologies have been obtained depending on the diameter of the confining cylindrical pores and the strengths of the surface field [7]. The volume ratio of the blocks, the immiscibility of different blocks and interaction between the confining surfaces and the blocks are important factors on which the morphology of diblock copolymer confinement in a cylindrical tube rests [9]. Block copolymers confined by cylindrical pores using Cartesian coordinates have been studied with respect to the dimensions of confinement, the diameter of the pore and domain spacings of micro-domains. There was subtle competition observed between topological constraints and chain stretching in the cylindrical phase [22]. The constrained frustration instigated by confinement, leads the system into the intricate free energy state and in addition,

confinement frustration tends to orientate microstructures perpendicular to the pore surface. Furthermore, the system of weak segregation can easily be deformable under the cylindrical confinement, the phase behaviour of such a system is more complex as compared to a rigid system and such a system may be used to produce more delicate materials [10]. The Lamella forming system confined in cylindrical tubes, the competition between the incommensurability of the diameter of the tube and the lamellae period and preference of the surface for the A segments are important for the comparable values of diameter and period [13]. Theoretical studies show that nanostructures for the development of the nano-devices can be accomplished by the self-assembly of diblock copolymers in a confined geometry [23]. Diblock copolymer melts confined to relatively narrow cylindrical pores of different diameters explored a sequence of novel structures as compared to bulk, which form with variation in pore diameter. These sequences of patterns were insensitive to the pore wall interaction [24].

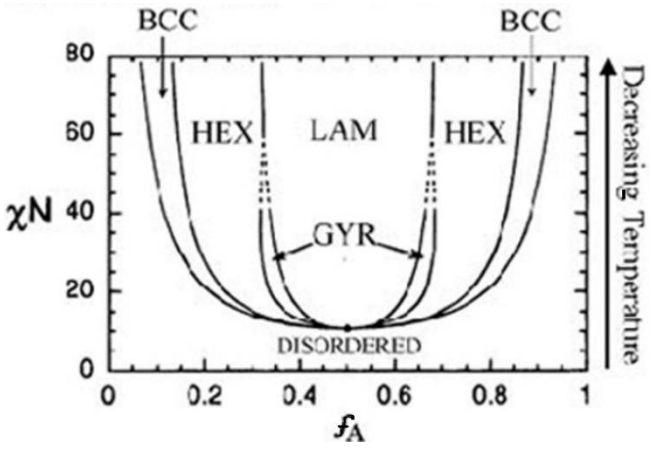

Figure 2.1: The bulk phase diagram of diblock copolymer system [25]. The horizontal axis shows volume fraction of **A** segment of polymer system, vertical axis on the left illustrates Flory-huggins interaction parameter and vertical axis on the right presents the decreasing temperature parameter. In the diagram (LAM) indicates lamella phase, (HEX) indicates hexagonal packed cylindrical phase, (BCC) is for body-centred-cubic spheres phase and (GYR) refers to the bi-continues complex gyroid phase in the bulk system.

The bulk system of diblock copolymer is a system which is large enough so that no size effect can take place in the system. Hence, based on this definition the phase behaviour

of the bulk system of **AB** diblock copolymer depends on three experimentally controllable factors volume fraction of **A** segment *f*, degree of polymerization *N* and Flory-Huggins interaction parameter χ. Note that the product χN is inversely proportional to the temperature parameter τ [26].

In the bulk system under equilibrium conditions, the minor segment segregates from the major segment of a diblock copolymer to form regular and uniformed spaced nanodomains [27]. The segregated shapes are mostly forms due the volume fraction of the minority segment of the diblock copolymer system f_A and by the chemical incompatibility of the both segments. The body-centred cubic sphere phases and hexagonally packed cylinders phases forms when the volume fraction of minority segment is in the range of $0.6 \leq f_A \leq 0.40$ in the system. The alternating lamella phases form based on the choice of the volume fraction for the minority block in the range of $0.45 < f_A < 0.60$ within the nanostructures. However, various computational [28-30] and experimental [31-33] studies fixed the value of volume fraction by tuning it at $f_A = 0.40$ for spheres and cylindrical phases. While, to obtain the lamella phases these two values $f_A = 0.48$ for asymmetric lamella and $f_A = 0.50$ for symmetric lamella are used in the melt. At low temperature spontaneous ordered nanostructures forms in the melt. The phase diagram of diblock copolymers shown in Figure 2.1 suggests that the sphere phases form on very low temperature for the values less or equal to 0.25 ($\tau \leq 0.25$), the cylindrical phases form for the values of temperature parameter $\tau \leq 0.30$ and for the alternating lamella phases the values are less than 0.35 ($\tau > 0.35$). The rest of CDS parameters are derived and fixed by tuning in the mathematical and computational studies [30, 34-36]. Note that rest of the CDS parameters are not derived from bulk phase diagram and are discussed in chapter three.

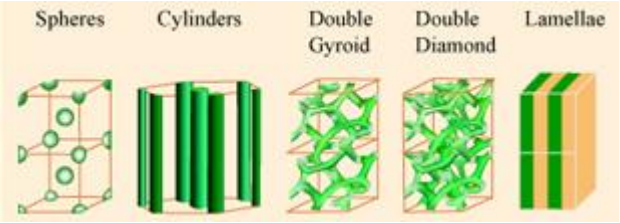

Figure 2.2: **AB** diBlock copolymers nanostructures in the bulk systems [22].

The study of soft matter is associated with the macroscopic mechanical properties of materials such as colloids, surfactants, liquid crystals, biomaterials, polymers in the melt or solution and in addition, several soft materials can be induced to flow under certain parameters [37]. Many polymer blends are highly immiscible and segregate into different phases. In many applications it is required to combine the properties of different polymers in a blend. In the polymer blends, phase separation occurs in microscopic length scale as well as macroscopic length scale. Meanwhile, AB diblock copolymers contain two blocks of different polymers interconnected linearly to each other and are less miscible on cooling; in addition phase separation occurs due to their chemical incomparability [38, 39]. The length-scale for phase separation in block copolymers is prevented by the connectivity of blocks which is about 10-100nm as a contrast with blends of polymers. The tendency of blocks to segregate on lowering temperature is called micro-phase separation. Block copolymers, due to microphase separation form variety of ordered structures in the bulk systems [37] such as lamella, hexagonally packed cylinders, body-centred cubic arrays of spheres, double gyroid, and double diamond as shown in Figure 2.2. Many smaller structural units of monomer linked covalently in any conceivable pattern form a large polymer molecule. A small molecule is said to be a monomer or “building block” if it has bonding ability (has a bonding site) with another monomer to form the polymer chain. The numbers of bonding sites are called functionality. The monomers with bi-functionality form linear molecules whereas the monomers with poly-functionality have three or more bonding

sites. The homopolymer is made up of a macromolecule which is developed by a single species of monomer, whereas, the copolymer is composed of two types of species of monomers. The scope of the topic is only limited to the polymers made up of bi-functional monomers. The architecture of copolymers can be divided into five grafting types which are A-B diblock copolymer, A-B-A triblock copolymer, Grafted A-B diblock copolymer, Star A-B-C triblock copolymer and linear A-B-C triblock copolymer, schematic diagrams of various grafting types block copolymers are shown in Figure 2.3.

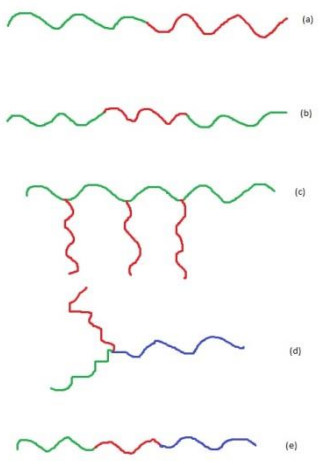

Figure 2.3: Schematic diagrams of different architectures of block copolymers. The green represents the block A, red one represents the block B and the blue one represents block C. (a) A-B diblock copolymer, (b) A-B-A triblock copolymer, (c) Grafted or branched A-B diblock copolymer, (d) Star A-B-C triblock copolymer, (e) Linear A-B-C triblock copolymer.

The self-organization property in the soft materials is a primary mechanism which leads the nanostructure formation. Soft materials with the ability of self-organization have received considerable attention in the nanotechnology over the last two decades as an efficient means of patterning surfaces on mesoscale for real applications [40, 41]. The applications include construction of high-capacity data storage devices, waveguides, quantum dot arrays, dielectric mirrors, fabrications of nanoporous membranes for advanced separation media and nanowires [12, 42]. Block copolymers are

macromolecules composed of chemically different blocks and are covalently connected to each other. They are an important class of materials with the natural ability to self-assemble into various periodic structures in the range of 10-100nm [43, 44]. At high temperatures, entropy dominates and consequently both blocks mix together homogeneously *i-e* form a disordered state and by lowering temperature and correspondingly increasing the Flory-Huggins interaction parameter, the micro-phase separation of A and B blocks may adopt different morphologies. The parameters that determine the micro-phase separation in the bulk system are the Flory-Huggins interaction parameter χ, the degree of polarization N and the volume fraction of A monomer f_A [45]. Depending on the composition of the copolymer and in the variation of χN, the micro-phase separated structure forms various patterns in the bulk systems. The Bulk phase diagram of diblock copolymers has been studied and understood on the basis of experiments and theoretical studies [46]. A number of classically ordered equilibrium phases have been identified in diblock copolymer melts such as lamellae, hexagonally packed cylinders, a body-centred array of spheres, and a bicontinuous network structure gyroid [47]. The control of long range order in structure is very important for practical applications such as the use of block copolymers in electronic and photonic applications require the production of highly ordered and defect free-structures.

2.2. Block copolymers in planar thin films

Due to its fascinating property of self-organizing, diblock copolymers are very important for fabricating materials for smart nano bioreactors and self-regulating diagnostic tools. To accomplish these goals nanostructure control is needed. Cylinder forming block copolymers are being used as templates for fabricating parallel stripes in nanotechnology [48], such as templates for nanowires [49] and polarizers [50].

Technological applications require the use of block copolymers in thin film geometries, where self-assembly is strongly influenced by surface energetics [51]. To explore new morphologies as compared to the bulk system, confinement is influential apparatus in breaking the symmetry of the nanostructure [28, 52]. The Cell Dynamic System method was employed to study diblock copolymers in planar thin films under the influence of moving walls on lamellae forming system. This study revealed that well-aligned lamellae form parallel to the walls for larger values of the surface interaction and perpendicular to the walls for a small value of the surface interaction obtained [53]. The mean-field model has also been used to study the dynamics of microphase separation and orientation of lamellae in two dimensions. In this investigation formation of lamellar structure and their stable states are discovered which depends on both periods of the lamellae and minimum of the free energy. The influence of the confining plane boundaries and interaction with block copolymers on the lamellae orientation was investigated using free energy calculations. Variation with respect to boundaries of the surface property at one boundary, the transition from preferential perpendicular to the parallel lamellar orientation was obtained [54]. Directional quenching also can influence the growth of oriented microphase-separated structures as confinement and shear flow, this observation has been verified using the CDS method applied in two dimensions in which the moving boundary resulted in ordered and disordered regions. With sufficiently slow boundary speed, well-aligned lamellae but with defects were obtained, On the other hand, with a too high boundary speed an irregular morphology which resembles with the homogeneous quench was obtained. Regular patterns of hexagonal structure are reported to be generated by low boundary speeds whereas with high speeds perpendicular lamellae to the growth front are generated subject to the small thermal fluctuation in the disordered region in the front of the boundary. Increasing both amplitudes of thermal fluctuations and boundary speeds, the formation of the hexagonal

structure was obtained [55]. The characteristic finger print morphology was obtained in planar thin films. In this study, alignment of the perpendicular lamella and reorienting the lamellae in the direction of shear was obtained by annealing the films above the glass transition temperature of the two blocks in the presence of an applied shear stress [56].

2.3. Block copolymers confined in cylindrical pores

The effect of confinement in pattern formations of copolymer systems is an area of significant importance in the polymer research. Sevink *et al* investigated the influence of pores on the pattern formation of symmetric diblock copolymers confined in the cylindrical pores, they showed under various pore sizes two types of patterns depending on the surface interactions: one is perpendicular and other is parallel patterns. Through variation of the pore radii and volume fractions, no mixed parallel/perpendicular patterns were observed in their investigations and the obtained patterns were unaffected by the pore diameter. The perpendicular pattern has slow kinetics and has a helical structure as an intermediate depending on their pore size. The kinetics of parallel pattern was observed unaffected by the pore radius for various ranges under considerations [17]. The systematic study has been carried out by confined assembly of silca-surfactant composite nanostructure in cylindrical pores with variation in pore diameter. With the same reaction conditions and precursors that were used for the production of the two-dimensional hexagonal SBA-15 nanostructured thin films, exceptionally silica nanostructured patterns with single and double helical geometries instinctively observed inside individual alumina cylindrical nanopores. In addition, by narrowing down the degree of the confinement, the transition from coiled cylindrical to the spherical cage-like geometric patterns was observed in cylindrical nanopores [16]. The lamella forming system was investigated under geometric confinements [57], results show concentric

lamellae sheets, bent lamellae pointing towards the column mantle and parallel to the pore sheets. The various patterns of symmetric A-B diblock copolymer system under geometric confinement in cylindrical channels were investigated by using Monte Carlo simulation method. The studies were carried out by considering the influence of incommensurability of the pore diameter, lamella period and volume fraction of one of the monomers of the polymer system. The simulation results reported in this study includes the formation of lamellae normal to the cylinder axis, circular lamellae, porous lamellar (mesh) pattern, lamellae parallel to the cylinder axis, single and double helixes. However, using the Monte Carlo simulation method the exact value of lamellae period cannot be obtained and commensurability of the simulation box and lamellae period was crucial to determine the exact value for lamellae period so therefore approximate value for lamellae period was used in simulations [13]. A systematical study of self-assembly of diblock copolymers confined in cylindrical channels was investigated using the simulated annealing method. Simulation results for diblock copolymers reported in cylindrical pores are 2D hexagonally packed cylinders, helices, stacked toroids. The obtained patterns of diblock copolymers were dependent on the pore diameter and the surface-polymer interaction, structural frustration and interfacial interactions. The degree of structural frustration parameterized by the ratio of pore diameter and lamellae period length is crucial for understanding the mechanism of pattern transitions and in addition they observed the transitions from helices to toroids to the sphere by imposing a tight degree of confinement [14]. The confined diblock copolymer was investigated by dissipative particle dynamics (DPD) and the results shown indicate patterns dependent on the volume fraction one of the block, the pore diameter of the cylinder, the interaction between the blocks and interaction between the wall and blocks. This study was carried out for both symmetric and none symmetric lamellae. According to the reported results perpendicular lamellae or stacked disc pattern formed in general for the

symmetric diblock copolymers under the condition that the cylindrical wall was kept uniform towards the both blocks. However, in the exceptional case of small pore diameter, a special bi-helix pattern was discovered due to the influence of entropy. In the case when the cylindrical walls kept non-uniform and pore diameter was increased transition from perpendicular-parallel-perpendicular lamellae observed, in addition, the increase in the non-uniformity of the cylindrical wall didn't respond in the shape other pattern but just only parallel lamellae formed. In the case of asymmetric lamellae multi-cylindrical micro-domains, multilayer helical phases and other complex patterns were observed [9]. The confinement of the self-assembled diblock copolymers in the cylindrical nanopores was investigated using lattice Monte Carlo simulations and the simulation results obtained by variation of pore diameter and strength of the surface field. The simulation results for diblock copolymers shown are stacked-disk, single helix, gyroidal, catenoid-cylinder, stacked-circle and concentric cylindrical barrel patterns [7]. Later Wang et al using the same method lattice Monte Carlo simulation method applied on symmetric diblock copolymer by systematic variation in pore diameter and the surface preference of the A monomer. The pore center can be either A or B monomer which depends on the size of pore diameter while the **A** segment segregates due to the strong surface preference and at neutral or weak surface preference lamellae perpendicular to the pore axis obtained regardless the size of the pore diameter, in addition, small surface preference patterns were undulated and furthermore by increasing surface preference the concentric cylinders obtained. However again it was crucial for a good estimate of the bulk period and efficient sampling of system configuration [6]. The self-assembly of asymmetric diblock copolymers were also investigated using self-consistent field theory (SCFT) under cylindrical confinement, the parameters $\chi_{AB}N = 14$ and $f_A = 0.36$ were used in the simulations [10]. A variety of nanostructures have been obtained using confinement

dimension. The system could freely achieve local free energy minimum when the pore diameter is commensurate with polymer period under surface preference and accommodation with confined pore diameter and on the other hand, the system can achieve a complex free energy landscape state due to the frustration caused by confinement in the incommensurate case. Furthermore, by tightening the degree of confinement frustration leads to orientate structures perpendicular to the pore surface and therefore study suggest that system is easily deformable at relative weak segregation under cylindrical confinement [10]. Diblock copolymer studies were investigated by using lattice simulated annealing method in cylindrical nanopores under confinement [21]. Also in this study the pore diameter and surface preference were systematically varied to investigate effects on structure formation and chain conformations. The study reveals the novel structures for lamellae forming system and cylindrical forming systems such as helices and perforated lamellae. Studies also show that the chains near the pore surfaces are compressed relative to the bulk chains which show the existence of the surfaces [21]. The real space self-consistent field theory method applied for the systemic study of diblock copolymers confined under relatively narrow cylindrical nanopores with various pores sizes. This computational study shows various structures in cylindrical forming systems obtained by increasing pore diameter including a single cylinder, stacked discs, single helix, double helix, toroid-sphere and helix-cylinder. All of these obtained patterns were sensitive to the pore wall interaction [24]. The dynamic density functional theory was employed to study confined diblock copolymers melt in cylindrical nanopores. In this study confined was two-dimensional and obtained results are general which includes catenoid, helix, the double helix and structure which resembles with experimental toroidal structure. This computational study also suggests that the patterns are sensitive to weak surface fields and small pore radii variations, in addition, these pore radii variations become responsible for interfaces

between the stable patterns and these interfaces become responsible for the transition for other patterns as well [58]. The computational study and analysis through CDS method were carried out systematically on diblock copolymer lamellae, cylindrical and spherical patterns. In this study various patterns of diblock copolymers were reported and all the structures were obtained by variation of four factors: pore diameter, affinity of pore wall to the one of the block, incommensurability of the pore lengths and domain spacing [59]. The simulated annealing technique was employed to investigate the influence of the confining geometries on self-assemblies of diblock copolymer cylindrical forming system in cylindrical, spherical and ellipsoidal nano-pores [43].

2.4. Block copolymers confined in spherical pores

Block copolymers are a splendid class of materials which are gaining scientific interest owing to their self-assembling property and potential applications [60-62]. Block copolymers can be helpful in designing smart bioreactors on mesoscale and drug delivery nano particles [63, 64]. Recently, block copolymer confinements in spherical pores have been receiving extensive consideration among the scientific community. To obtain the nano structural control, confinement is considered to be a powerful tool which is very helpful in breaking the symmetry of the nano structures and favouring materials to self-assemble into newly-ordered structures compared to the bulk [8, 31]. Furthermore, spherical confinement is a more effective confining geometry which is to be considered. Block copolymers have been studied and investigated depending on the surface field interactions and film thickness [65-67]. They reported perforated lamella, parallel, perpendicular to the surface and cylinder. In the case of block copolymers confined by the surface of the sphere, in addition to the surface field interaction, the curvature influences the morphologies. The onion-like nanostructures and hexagonally packed cylinders are prepared by variations in the block ratio and the concentration of

the solution for lamella forming systems [68]. Rider et al investigated lamella and cylindrical forming morphologies under 3D confinements by experimental work; they reported a variety of the nano structures such as onion-like lamella, complex golf ball morphologies and spheres on the curved surfaces [31]. The study and investigation of phase separation for diblock copolymer melt in a spherical geometry is a difficult problem. To study phase-separated patterns for diblock copolymers on the surface of a sphere, the study carried out using a finite volume method, study revealed stable and integral defected structures which would not occur on a planar surface [69]. The defect formation in ordered structures on curved surfaces is a hot topic, attracting growing interest. The Self-consistent field theory simulation method was applied to thin block copolymer melt films confined in spherical nano-pores. The study reveals that there is delicate competition between topological constraints and chain stretching in cylindrical phases, whereas in a lamellar phase with small sphere radii, a stable hedgehog defect configuration was observed and for larger sphere radii, competition between hedgehog and spiral defect conformation was noticed. A quasi-baseball formation with defective spiral-like nano structure was found to be metastable [22]. The CDS method in Cartesian coordinate system was used to investigate the morphology of thin block copolymer films around a nano-particle. The reported structures in spherical nano-pores for lamellae forming system are parallel, perpendicular, mixed and perforated lamellae, whereas cylindrical forming systems were parallel and perpendicular cylinders. Studies suggest that one could obtain nano-shells by using effective interplay of these parameters which are the film thickness, the block copolymer characteristics, the surface parameter and the curvature [20]. The CDS method was carried out by a systematic study on thin block copolymer films around nano-particles to investigate lamellae, cylinder and sphere morphologies. Investigations show various structures such as standing lamellae, cylinders, onions, cylinder knitting balls, golf ball, layered

spherical virus-like and mixed morphologies with T-junctions and U-type defects [8]. There was also a computational study on two-dimensional block copolymers on the surface of a sphere [70]. These computational studies were conducted by the square lattice [8, 70] and triangular lattice [69]. However, in this contribution studies were carried out on the confinement and the curvature-induced morphologies of block copolymers using spherical lattice.

CHAPTER THREE

3. Implementation of CDS method in polar, cylindrical and spherical coordinate systems

3.1. Overview

Prediction of the structure formation in copolymer melts by experiments is very difficult and time-consuming but mathematical modelling can help to understand structure formation. Molecular dynamics or Monte Carlo simulations can be used to study their behavior but due to computational demands studies have been restricted to short chains or low grafting densities. There are studies based on Self-Consistent Field Theory SCFT in one dimension for morphologies with no angular dependence and in two dimensions for morphologies with either rotational symmetry or without any radial dependence but to perform full three-dimensional calculations is still a challenge for researchers [42]. To reduce computational costs the Unit Cell Approximation (UCA) have been routinely used following SCFT to study bulk systems but accuracy was lost and the effects of packing frustration over sighted were reported, which are both important for nanoparticles [71]. However, the CDS is relatively simple Landau-Ginzburg type simulation allows for dynamic and fast simulations of very large block copolymer systems. Stiffness, architecture, polydispersity and density effects of the polymer chain can only be indirectly modeled and the modification of the coefficients can be carried out in the Landau free energy model. The CDS was originally developed to model the interface dynamics in the phase separating systems. The CDS is a coarse grained modelling in which it is possible to observe the microphase separation phenomenon in the block copolymer systems and obtained nanostructures by CDS are comparable with

experimental results [72]. The CDS is efficient and accurate in investigating often very complex dynamical behavior in a large set of systems. CDS predict the block copolymer morphologies in generic agreement with other simulation methods and experiments, in addition, some cases are in quantitative agreement. Being fast and large-scale CDS can successfully describe time evaluation of morphologies in several cases, and is capable of predicting new kinetics and the work-derivative properties of materials [12]. Pinna *et al* [59] studied diblock copolymers in cylindrical pores using CDS in the Cartesian coordinate system and they showed that a simple Ginzburg-Landau type theory can predict a tremendous rich "zoo" of diblock copolymer morphologies in cylindrical nanopores. Furthermore, CDS replicates details of a very complex collection of confinement induced nanostructures which were previously done by slow simulation techniques. In the presence of curvature and confinement, Ginzburg-Landau theory works successfully. Although many computational techniques have been developed and carried out, the field offers a large number of open questions, for some of which are addressed in the thesis. To study and analyze accurately block copolymers on curved surfaces, the computational model needs to be implemented in the curvilinear coordinate systems.

Continuous physical space discretization into a uniform orthogonal computational space is basic requirement for finite difference schemes and application of boundary conditions needs to fall on coordinate surfaces of the coordinates system. Furthermore for accuracy grid points need to be clustered in space of large gradients, whereas for computational economy grid points must be spread out in space of small gradients. For these requirements Cartesian coordinate system is incompatible [73], however, polar, cylindrical, spherical coordinates are viable. In the finite difference schemes for the partial differential equations some procedure is followed to discretise the space coordinates with time axis, regardless of the dimensionality. However, for various

realistic physical problems, the basic choice Cartesian layout with square or rectangular domains is not the natural environment. The suitable coordinate transformation of a physical problem with partial differential equations is very difficult to find in most cases [74]. The best option in this case is that to solve the partial differential equations on the geometrical irregular domains. The order parameter which represents time evaluation of block copolymers is used in CDS which varies continuously with respect to coordinate **r**. There is a Partial Differential Equation (PDE) which represents the time evaluation of order parameter with respect to each lattice point in the CDS method. The corresponding Partial Differential Equations of CDS model was solved on the lattice by taking account of each cell of the curved lattice. The discretization of Laplacian operators were carried out in polar, cylindrical and spherical coordinate systems along with appropriate boundary conditions. The lattice and weights commonly used in lattice hydrodynamics simulations are computationally efficient discrete representations of the Laplacian by means of conserving isotropy up to the leading order error. For the CDS method these Laplacians should prove beneficial, as for other problems where efficient isotropic discretization of Laplacian is required [75]. In the standard sense CDS model is not a PDE solved by numerical analysis. However its accuracy depends on time steps and spatial steps, therefore large time steps and large spatial steps cannot give accurate solutions for the initial value problem of Cahn-Hilliard-Cook (CHC) equation. The macroscopic observables are still quantitatively accurate which implies the concept of qualitative accuracy of numerical analysis. In this sense, we can say that the scheme is qualitatively accurate if the scheme can give quantitatively accurate results for the quantities which are qualitatively characteric of the system [76]. On the basis of this concept, we can say that the discretization scheme for the CDS model is a qualitatively accurate discretization method for the CHC equation. In this contribution, a computational study was carried out for diblock copolymers confined in circular annular

pores, cylindrical pores and spherical pores using curvilinear coordinate systems. The CDS method is implemented by using curvilinear coordinates systems. The CDS is a very good resolution between computational speed and physical accuracy.

3.2. CDS and its implementation in polar, cylindrical and spherical coordinate systems

In the CDS method, time dependent variations of the order parameter $\psi(t,i)$ with respect to the coordinate system *i* and it can represents the concentration of the one monomer in a binary blend. Computations of the order parameter with respect to time were carried out by the partial differential equation called Cahn-Hilliard-Cook (CHC) and this partial differential equation is given in terms of the free energy functional which controls the tendency of local diffusion motion. The discretization of Laplacian operator in curvilinear coordinates is carried out in this study. The Order Parameter $\psi(t,i)$ is determined at time *t* and in cell *i* of a discrete lattice.

In CDS method of diblock copolymers, the compositional order parameter in terms of local & global volume fractions is defined by the following relation [12]:

$$\psi(i) = \phi_A(r) - \phi_B(r) + (1-2f), \tag{3.1}$$

where ϕ_A, ϕ_B are the local volume fraction of the monomers **A** and **B** respectively. The volume fraction of monomer **A** is defined by the relation $f_A = N_A/(N_A + N_B)$, similarly, the volume fraction of monomer **B** is defined by the relation $f_B = N_B/(N_A + N_B)$, where N_A represents the number of monomers of the block A and N_B represents the number of monomers of the block **B**. $N = N_A + N_B$ is the total degree of polymerisation. The constant *f* represents here the block length ratio in the polymer system, note that if taking symmetric block ratio in this case *f=1/2* then the order parameter will take the simple form $\psi = \phi_A + \phi_B + (1-2(1/2)) = \phi_A + \phi_B$.

The change with respect to time t in the order parameter depends on the chemical potential $\mu(r,t)$ and the mass current or a flux $j(r,t)$ which is linearly related to the local chemical potential and which determines the dynamics of the order parameter through the continuity equation given below [72]:

$$\frac{\partial \psi(r,t)}{\partial t} = -\nabla j(r,t) \tag{3.2}$$

The gradient of chemical potential related to the mass current given below:

$$j(r,t) = -M\{\nabla \mu(r,t)\}, \tag{3.3}$$

where M is positive Onsager coefficient which describes the mobility of the monomer **A** with respect to the monomer **B**. The chemical potential determined by the functional derivative of free energy functional $F\{\psi\}$ with respect to order parameter is given in the following mathematical relation:

$$\mu(r,t) = \frac{\delta F\{\psi\}}{\delta \psi} \tag{3.4}$$

From equations (3.2), (3.3) and (3.4) one can easily derive the mathematical relation for the order parameter which represents the change in the order parameter with respect to time, and is called Cahn-Hilliard-cook (CHC) equation given below [77]:

$$\frac{\partial \psi}{\partial t} = M\nabla^2\left(\frac{\delta F[\psi]}{\delta \psi}\right), \tag{3.5}$$

where M the is phenomenological mobility constant and can be taken $M=1$ for simplicity and for correspondingly setting the time scale for diffusive process. In equation (3.6) $F[\psi]$ is the free energy functional, which acts as a global Lyapunov functional and tends to decrease with respect to time towards its minimum and which can be written as below by dividing it by kT [72]:

$$F[\psi(r)] = \int dr[H(\psi) + \frac{D}{2}|\nabla \psi|^2] + \frac{B}{2}\int dr \int dr' G(r-r')\psi(r)\psi(r') \tag{3.6}$$

In equation (3.6) on the right hand side, the first term represents the short range interactions whereas, the second term with double integrals represents the long-range interactions due to the connectivity of the sub-chains. In the above equation (3.6) the term $D|\nabla\psi|^2/2$, generates free energy necessary to create an interface between the segments **A** and **B** of the polymer system. The Green's function $G(r,r')$ satisfies Laplace's equation $\nabla^2 G(r,r') = -\delta(r-r')$. In the equation (3.6) D represents the diffusion constant, and B represents the chain length dependence to the free energy. The term $H(\psi)$ in the above equation (3.6) accounts the local contributions to the free energy and can be expressed in various expansions; however, in accordance with Ginzburg-Landau theory [72], following expansion was used in the current analysis:

$$H(\psi) = [-\frac{\tau}{2} + \frac{A}{2}(1-2f)^2]\psi^2 + \frac{\nu}{3}(1-2f)\psi^3 + \frac{u}{4}\psi^4, \qquad (3.7)$$

where τ represents temperature and $A, \nu, and\ u$ are phenomenological constants, these all are parameters which can be related to molecular characteristics [12]. Ohta and Kawasaki explained that $\tau' = \tau + A(1-2f)^2, D$ and B are related with the degree of polarization N, chain length b and the Flory-Huggins parameter χ. Here b is Kuhn segment length of the polymer. The mathematical relations are given by [78]:

$$\tau' = -\frac{1}{2N}\left(N_\chi - \frac{s(f)}{4f^2(1-f)^2}\right),\ D\frac{b^2}{48f(1-f)}, \text{ and } B = \frac{9}{4N^2b^2f^2(1-f)^2}\ . \qquad (3.8)$$

The Flory-Huggins parameter is inversely proportional to the temperature, if it is positive then it measures the strength of repulsion between incompatible blocks, if it has negative value it reflects the free energy which stimulates blocks towards mixing. In the set of equations (3.8), *s(f)* is an empirical fitting function of order 1. For simplicity we adopted the notations of D and B by replacing $\tilde{D}$, $\tilde{B}$ respectively. The parameters *u* and

v can be calculated by the vertex function which is given by Leibler [79]. For simplicity these very complex functions are replace by approximate constants because the phenomena under consideration is quite general so that it is permissible for choosing the parameters for equations (3.6)-(3.7) as phenomenological constants [28].

Numerical evolution of Equation (1) by means of CDS is given below.

$$\psi(i,t+1)=\psi(i,t)-\Delta t\left\{\left\langle\left\langle\Gamma(i,t)\right\rangle\right\rangle-\Gamma(i,t)\right\}, \tag{3.9}$$

where $\left\langle\left\langle\Gamma(i,t)\right\rangle\right\rangle-\Gamma(i,t)$, is the isotropic discrete Laplacian operators in polar, cylindrical or spherical coordinate system for the quantity $\Gamma(i,t)$. In the equation (3.9) i represents $i=i_r,i_\theta$ for polar coordinate system, $i=(i_r,i_\theta,i_z)$ for cylindrical coordinate system and $i=(i_r i_\theta i_\phi)$ for spherical coordinate system. In the equation (3.9) Δt shows the time steps taken in the current analysis. The following relation was used in the study for the calculations of free energy functional:

$$\Gamma(i,t)=g(\psi(i,t))-\psi(i,t)+D[\left\langle\left\langle\psi(i,t)\right\rangle\right\rangle-\psi(i,t)]+B\psi(i,t) \tag{3.10}$$

For the case when polymers were confined between two interfaces then the above equation for free energy functional was modified as following:

$$\Gamma(i,t)=g(\psi(i,t))-\psi(i,t)+D[\left\langle\left\langle\psi(i,t)\right\rangle\right\rangle-\psi(i,t)]-s_i(r), \tag{3.11}$$

where $s_i(r)=h_i\times\phi_i\times\delta_{n_r=1 or n_r=N_r}$, i denoting the attracting block (either **A** or **B**) of block copolymer system, h_i is the strength of interaction between confining walls and the blocks of polymer system and $\delta_{a=b}$ is Kronecker delta [80].

Where so-called map function is given below:

$$g(\psi)=[1+\tau-A(1-2f)^2]\psi-\upsilon(1-2f)\psi^2-u\psi^3 \tag{3.12}$$

In the next section, the Laplacian operators are discretised in the polar, cylindrical and spherical coordinate systems. The Laplacian operators were used in the computations of equations (3.9) and (3.10) where averaging of the stencil of lattice was required.

3.3. Discretisation of Laplacian in the polar coordinate system

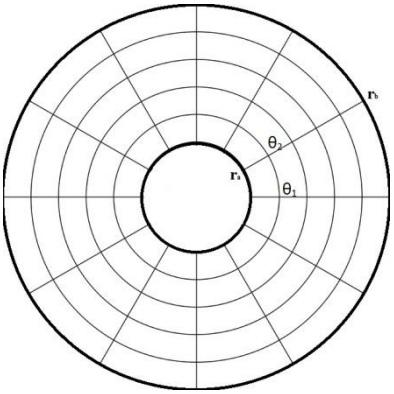

Figure 3.1: Polar mesh diagram.

The conservative form of Laplacian operator in polar coordinates is given below:

$$\nabla^2\psi = \psi_{rr} + \frac{1}{r}\psi_r + \frac{1}{r^2}\psi_{\theta\theta} \tag{3.13}$$

$$r_a \le r \le r_b \;\&\; 0 \le \theta \le 2\pi$$

For the discretisation of the Laplacian operator in polar coordinate system, Forward Time Central Space (FTCS) explicit finite differencing scheme was used in the current analysis.

$$\begin{aligned}\nabla^2\psi = {} & \frac{1}{(\Delta r)^2}(\psi_{i+1,j} - 2\psi_{i,j} + \psi_{i-1,j}) - \frac{1}{2r_i(\Delta r)}(\psi_{i+1,j} - \psi_{i-1,j}) \\ & + \frac{1}{r_i^2(\Delta\theta)^2}\left[\psi_{i,j+1} - 2\psi_{i,j} + \psi_{i,j-1}\right]\end{aligned} \tag{3.14}$$

Here domain is circular mesh contained between two circles of radii r_a and r_b, where $r_i = r_a + i\Delta r$ and $\theta_j = j\Delta\theta$ for $i = 1,2,...,N_r$, $j = 1,2,...,N_\theta$

Isolating the term $\psi_{i,j}$ get the following form:

$$\begin{aligned}\nabla^2\psi = {} & \frac{1}{(\Delta r)^2}(\psi_{i+1,j} + \psi_{i-1,j}) + \frac{1}{2r_i(\Delta r)}(\psi_{i+1,j} - \psi_{i-1,j}) \\ & + \frac{1}{r_i^2(\Delta\theta)^2}(\psi_{i,j+1} + \psi_{i,j-1}) - 2\left[\frac{r_i^2(\Delta\theta)^2 + (\Delta r)^2}{r_i^2(\Delta r)^2(\Delta\theta)^2}\right]\psi_{i,j}\end{aligned} \tag{3.15}$$

Now

$$\nabla^2 = S + O_1(h_1^n) + O_2(h_2^n) \tag{3.16}$$

Where *S* denotes a stencil in polar coordinate system and terms $O_1(h_1^n)+O_2(h_2^n)$ are the truncation errors of the order n due to finite mesh sizes h_1, h_2. The stencil must satisfy following condition [81].

$$\sum_{k=1}^{3}\sum_{l=1}^{3} S_{k,l} = 0 \tag{3.17}$$

It follows that:

$$\begin{aligned}&\frac{1}{(\Delta r)^2}(\psi_{i+1,j}+\psi_{i-1,j})+\frac{1}{2r_i(\Delta r)}(\psi_{i+1,j}-\psi_{i-1,j})\\&+\frac{1}{r_i^2(\Delta\theta)^2}(\psi_{i,j+1}+\psi_{i,j-1})-2\left[\frac{r_i^2(\Delta\theta)^2+(\Delta r)^2}{r_i^2(\Delta r)^2(\Delta\theta)^2}\right]\psi_{i,j}=0\end{aligned} \tag{3.18}$$

Multiplying both sides by of equation (3.18) by the term $\frac{r_i^2(\Delta r)^2(\Delta\theta)^2}{2(r_i^2(\Delta\theta)^2+(\Delta r)^2)}$ we have the following equation:

$$\left(\frac{r_i^2(\Delta r)^2(\Delta\theta)^2}{2(r_i^2(\Delta\theta)^2+(\Delta r)^2)}\right)\left[\begin{aligned}&\frac{1}{(\Delta r)^2}(\psi_{i+1,j}+\psi_{i-1,j})+\frac{1}{2r_i(\Delta r)}(\psi_{i+1,j}-\psi_{i-1,j})\\&+\frac{1}{r_i^2(\Delta\theta)^2}(\psi_{i,j+1}+\psi_{i,j-1})\end{aligned}\right]-\psi_{i,j}=0$$

So therefore, finally isotropised discrete five point Laplacian in polar coordinates can be written as in the following form:

$$\langle\langle\psi\rangle\rangle-\psi=\varepsilon\sum_{i=1}^{N_r}\sum_{j=1}^{N_\theta}\left[\begin{aligned}&\frac{1}{(\Delta r)^2}(\psi_{i+1,j}+\psi_{i-1,j})+\frac{1}{2r_i(\Delta r)}(\psi_{i+1,j}-\psi_{i-1,j})\\&+\frac{1}{r_i^2(\Delta\theta)^2}(\psi_{i,j+1}+\psi_{i,j-1})\end{aligned}\right]-\sum_{i=1}^{N_r}\sum_{j=1}^{N_\theta}\psi_{i,j} \tag{3.19}$$

Where $\varepsilon=\frac{r_i^2(\Delta r)^2(\Delta\theta)^2}{2(r_i^2(\Delta\theta)^2+(\Delta r)^2)}$ is weighting factor for the nearest neighbourhood points in the polar mesh system.

The following periodic boundary conditions were applied on the angular coordinate of the polar mesh for evaluation of the Laplacian operator in polar coordinates:

$\psi_{(i,N_\theta+1)}=\psi_{(i,1)}$, $\psi_{(i,0)}=\psi_{(i,N_\theta)}$, for all $i=1,2,.....,N_r$.

The following reflective boundary conditions were applied on the radial coordinate for calculations of the Laplacian in polar coordinate system:

$\psi_{(N_r+1,\ j)} = \psi_{(N_r,\ j)}$, $\psi_{(0,\ j)} = \psi_{(1,\ j)}$, for all $j = 1,2,....,N_\theta$,

where $\psi(i,j),\ i = 1,2,...,N_r,\ j = 1,2,...N_\theta$ are approximations of the order parameter function $\psi(r,\theta)$. The initial condition for the system is chosen to be the random distribution of the of the order parameter $\psi(r,\theta)_{t=0} \in (0.5,-0.5)$.

3.4. Discretisation of Laplacian in the cylindrical coordinate system

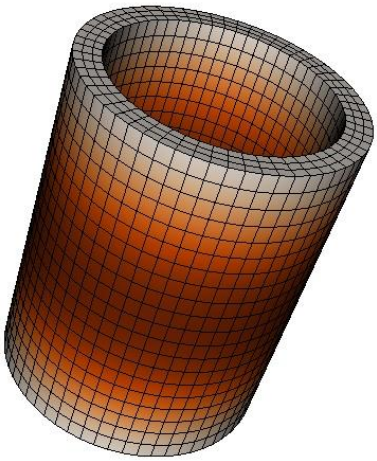

Figure 3.2: Cylindrical mesh diagram [82].

The Laplacian in cylindrical coordinates is given below.

$$\nabla^2\psi = \frac{\partial^2\psi}{\partial r^2} + \frac{1}{r}\frac{\partial\psi}{\partial r} + \frac{1}{r^2}\frac{\partial^2\psi}{\partial\theta^2} + \frac{\partial^2\psi}{\partial z^2}, \tag{3.20}$$

for boundary conditions $r_a \le r \le r_b$, $0 \le \theta \le 2\pi$ & $0 \le z \le h$. Finite difference scheme for the above Laplacian in cylindrical coordinates can be written as below:

$$\left.\begin{aligned}\nabla^2\psi = {} & \frac{1}{(\Delta r)^2}(\psi_{i+1,j,k} - 2\psi_{i,j,k} + \psi_{i-1,j,k}) - \frac{1}{2r_i(\Delta r)}(\psi_{i+1,j,k} - \psi_{i-1,j,k}) \\ & + \frac{1}{r_i^2(\Delta\theta)^2}\left[\psi_{i,j+1,k} - 2\psi_{i,j,k} + \psi_{i,j-1,k}\right] + \frac{1}{(\Delta z)^2}[\psi_{i,j,k+1} - 2\psi_{i,j,k} + \psi_{i,j,k-1}]\end{aligned}\right\} \tag{3.21}$$

Here domain is cylindrical mesh contained between two circles of radius r_a and r_b where

$r_i = r_a + i\Delta r$, $\theta_j = j\Delta\theta$ $z_k = k\Delta z$, for $i = 1,2,...,N_r$, $j = 1,2,...,N_\theta, k = 1,2,...N_z$

Isolating the term $\psi_{i,j}$ get the following form:

$$\nabla^2\psi = \frac{1}{(\Delta r)^2}(\psi_{i+1,j,k} - 2\psi_{i,j,k} + \psi_{i-1,j,k}) - \frac{1}{2r_i(\Delta r)}(\psi_{i+1,j,k} - \psi_{i-1,j,k})$$
$$+ \frac{1}{r_i^2(\Delta\theta)^2}[\psi_{i,j+1,k} - 2\psi_{i,j,k} + \psi_{i,j-1,k}] + \frac{1}{(\Delta z)^2}[\psi_{i,j,k+1} - 2\psi_{i,j,k} + \psi_{i,j,k-1}]$$
$$- \left[\frac{2}{(\Delta r)^2} + \frac{2}{r_i^2(\Delta\theta)^2} + \frac{2}{(\Delta z)^2}\right]\psi_{i,j,k}$$

or can be re-written as below:

$$\nabla^2\psi = \frac{1}{(\Delta r)^2}(\psi_{i+1,j,k} - 2\psi_{i,j,k} + \psi_{i-1,j,k}) - \frac{1}{2r_i(\Delta r)}(\psi_{i+1,j,k} - \psi_{i-1,j,k})$$
$$+ \frac{1}{r_i^2(\Delta\theta)^2}[\psi_{i,j+1,k} - 2\psi_{i,j,k} + \psi_{i,j-1,k}] + \frac{1}{(\Delta z)^2}[\psi_{i,j,k+1} - 2\psi_{i,j,k} + \psi_{i,j,k-1}]$$
$$- 2\left[\frac{r_i^2(\Delta\theta)^2(\Delta z)^2 + (\Delta r)^2(\Delta z)^2 + r_i^2(\Delta r)^2(\Delta\theta)^2}{r_i^2(\Delta r)^2(\Delta\theta)^2(\Delta z)^2}\right]\psi_{i,j,k}$$

Now

$$\nabla^2 = S + O_1(h_1^n) + O_2(h_2^n) + O_3(h_3^n) \tag{3.22}$$

Where *S* denotes a stencil in cylindrical coordinate system and terms $O_1(h_1^n) + O_2(h_2^n) + O_3(h_3^n)$ are the truncation errors of the order *n* due to finite mesh sizes h_1, h_2, h_3. The stencil must satisfy following condition [81]:

$$\sum_{k=1}^{3}\sum_{l=1}^{3}\sum_{m=1}^{3} S_{k,l,m} = 0 \tag{3.23}$$

It follows that:

$$\left.\begin{aligned}&\frac{1}{(\Delta r)^2}(\psi_{i+1,j,k}-2\psi_{i,j,k}+\psi_{i-1,j,k})-\frac{1}{2r_i(\Delta r)}(\psi_{i+1,j,k}-\psi_{i-1,j,k})\\&+\frac{1}{r_i^2(\Delta\theta)^2}\left[\psi_{i,j+1,k}-2\psi_{i,j,k}+\psi_{i,j-1,k}\right]+\frac{1}{(\Delta z)^2}[\psi_{i,j,k+1}-2\psi_{i,j,k}+\psi_{i,j,k-1}]\\&-2\left[\frac{r_i^2(\Delta\theta)^2(\Delta z)^2+(\Delta r)^2(\Delta z)^2+r_i^2(\Delta r)^2(\Delta\theta)^2}{r_i^2(\Delta r)^2(\Delta\theta)^2(\Delta z)^2}\right]\psi_{i,j,k}=0\end{aligned}\right\} \quad (3.24)$$

Multiplying Equation (3.24) both side by

$$\left[\frac{r_i^2(\Delta r)^2(\Delta\theta)^2(\Delta z)^2}{2\left\{r_i^2(\Delta\theta)^2(\Delta z)^2+(\Delta r)^2(\Delta z)^2+r_i^2(\Delta r)^2(\Delta\theta)^2\right\}}\right] \text{and let say:}$$

$$\begin{aligned}\psi^1&=\frac{1}{(\Delta r)^2}(\psi_{i+1,j,k}-2\psi_{i,j,k}+\psi_{i-1,j,k})-\frac{1}{2r_i(\Delta r)}(\psi_{i+1,j,k}-\psi_{i-1,j,k})\\&\quad+\frac{1}{r_i^2(\Delta\theta)^2}(\psi_{i,j+1,k}-2\psi_{i,j,k}+\psi_{i,j-1,k})+\frac{1}{(\Delta z)^2}(\psi_{i,j,k+1}-2\psi_{i,j,k}+\psi_{i,j,k-1})\\\psi^0&=\psi_{i,j,k}=0\end{aligned}$$

Then equation (3.24) becomes:

$$\left[\frac{r_i^2(\Delta r)^2(\Delta\theta)^2(\Delta z)^2}{2\left\{r_i^2(\Delta\theta)^2(\Delta z)^2+(\Delta r)^2(\Delta z)^2+r_i^2(\Delta r)^2(\Delta\theta)^2\right\}}\right]\psi^1-\psi^0=0 \quad (3.25)$$

Now we can write isotropic discrete Laplacian in cylindrical coordinate system as below:

$$\langle\langle\psi\rangle\rangle-\psi=\omega\sum_{NN}\psi^1-\psi^0 \quad (3.26)$$

Where $\omega=\frac{r_i^2(\Delta r)^2(\Delta\theta)^2(\Delta z)^2}{2\left\{r_i^2(\Delta\theta)^2(\Delta z)^2+(\Delta r)^2(\Delta z)^2+r_i^2(\Delta r)^2(\Delta\theta)^2\right\}}$ is weighting factor for isotropic form of the Laplacian in cylindrical coordinate system.

The following periodic boundary conditions were applied on angular coordinate in the current analysis.

$\psi_{(i,N_\theta+1,k)}=\psi_{(i,0,k)}$, $\psi_{(i,0,k)}=\psi_{(i,N_\theta,k)}$, for all $i=1,2,...,N_r, k=1,2,...,N_h$.

The following reflective boundary conditions were applied on radial coordinate in the cylindrical system.

$\psi_{(N_r+1,\,j,k)} = \psi_{(N_r,\,j,k)},\ \psi_{(0\,j,k)} = \psi_{(1,\,j,k)}$, for all $j = 1,2,...,N_\theta, k = 1,2,...,N_h$

The following periodic boundary conditions were imposed on the coordinate z in the cylindrical coordinate system.

$\psi_{(i,\,j.\,N_h+1)} = \psi_{(i,\,j,1)}, \quad \psi_{(i,\,j,0)} = \psi_{(i,\,j,N_h)}$ for all $i = 1,2,...,N_r$, $j = 1,2,...,N_\theta$.

Where $\psi(i,\,j,k)$, $i = 1,2,...,N_r$, $j = 1,2,...N_\theta, k = 1,2,...,N_h$, are approximations of the function $\psi(r,\theta,h)$. The initial conditions for order parameter were chosen to be the random distribution of the $\psi(r,\theta,z)_{t=0} \in (1,-1)$.

3.5. Discretisation of Laplacian in the spherical coordinate system

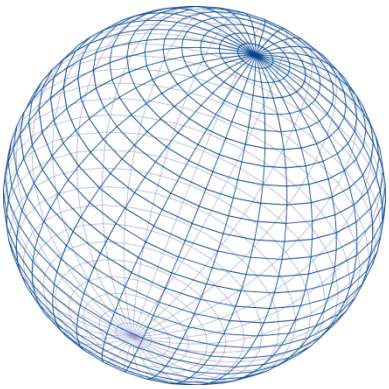

Figure 3.3: Sphere grid system diagram [83]

The Laplacian in spherical coordinates is given below.

$$\nabla^2\psi = \frac{\partial^2\psi}{\partial r^2} + \frac{2}{r}\frac{\partial\psi}{\partial r} + \frac{1}{r^2}\frac{\partial^2\psi}{\partial\theta^2} + \frac{(\cot\theta)\partial\psi}{r^2\partial\theta} + \frac{\partial^2\psi}{r^2\sin^2(\theta)\partial\phi^2} \tag{3.27}$$

Subjected to boundary conditions $r_a \le r \le r_b$, $0 \le \theta \le \pi$, $0 \le \phi \le 2\pi$, finite difference scheme for the above Laplacian is given below:

$$\left.\begin{aligned}\nabla^2\psi = &\frac{1}{(\Delta r)^2}(\psi_{i+1,j,k} - 2\psi_{i,j,k} + \psi_{i-1,j,k}) - \frac{2}{2r_i(\Delta r)}(\psi_{i+1,j,k} - \psi_{i-1,j,k}) \\ &+ \frac{1}{r_i^2(\Delta\theta)^2}\left[\psi_{i,j+1,k} - 2\psi_{i,j,k} + \psi_{i,j-1,k}\right] + \frac{\cot\theta}{2r^2(\Delta\theta)}(\psi_{i,j-1,k} - \psi_{i,j+1,k}) \\ &+ \frac{1}{(r^2\sin^2\theta)(\Delta\phi)^2}[\psi_{i,j,k+1} - 2\psi_{i,j,k} + \psi_{i,j,k-1}]\end{aligned}\right\} \quad (3.28)$$

Discretising of the spherical domain was carried by using the following conditions.

$$r_i = r_a + i\Delta r, r_a \le r \le r_b,\ \theta_j = j\Delta\theta, \phi_k = k\Delta\phi,\ \text{for}\ \ i = 1,2,...,N_r,\ \ j = 1,2,...,N_\theta, k = 1,2,...N_\phi$$

To obtain average value isolating the term $\psi_{i,j,k}$ from above equation we have.

$$\left.\begin{aligned}\nabla^2\psi = &\frac{1}{(\Delta r)^2}(\psi_{i+1,j,k} + \psi_{i-1,j,k}) - \frac{1}{r_i(\Delta r)}(\psi_{i+1,j,k} - \psi_{i-1,j,k}) \\ &+ \frac{1}{r_i^2(\Delta\theta)^2}(\psi_{i,j+1,k} + \psi_{i,j-1,k}) + \frac{\cot\theta}{2r^2(\Delta\theta)}(\psi_{i,j-1,k} - \psi_{i,j+1,k}) \\ &+ \frac{1}{(r^2\sin^2\theta)(\Delta\phi)^2}(\psi_{i,j,k+1} + \psi_{i,j,k-1}) \\ &- 2\left[\frac{1}{(\Delta r)^2} + \frac{1}{r_i^2(\Delta\theta)^2} + \frac{1}{r_i^2\sin^2\theta(\Delta\phi)^2}\right]\psi_{i,j,k}\end{aligned}\right\} \quad (3.29)$$

We can write above equation as follow:

$$\left.\begin{aligned}\nabla^2\psi = &\frac{1}{(\Delta r)^2}(\psi_{i+1,j,k} + \psi_{i-1,j,k}) - \frac{1}{r_i(\Delta r)}(\psi_{i+1,j,k} - \psi_{i-1,j,k}) \\ &+ \frac{1}{r_i^2(\Delta\theta)^2}(\psi_{i,j+1,k} + \psi_{i,j-1,k}) + \frac{\cot\theta}{2r^2(\Delta\theta)}(\psi_{i,j-1,k} - \psi_{i,j+1,k}) \\ &+ \frac{1}{(r^2\sin^2\theta)(\Delta\phi)^2}(\psi_{i,j,k+1} + \psi_{i,j,k-1}) \\ &- 2\left[\frac{r_i^2(\Delta\theta)^2(\Delta\phi)^2\sin^2\theta + (\Delta r)^2(\Delta\phi)^2\sin^2\theta + (\Delta r)^2(\Delta\theta)^2}{r_i^2(\Delta r)^2(\Delta\theta)^2(\Delta\phi)^2\sin^2\theta}\right]\psi_{i,j,k}\end{aligned}\right\} \quad (3.30)$$

Now

$$\nabla^2 = S + O_1(h_1^n) + O_2(h_2^n) + O_3(h_3^n) \quad (3.31)$$

Where *S* denotes a stencil in spherical coordinate system and terms $O_1(h_1^n) + O_2(h_2^n) + O_3(h_3^n)$ are the truncation errors of the order *n* due to finite mesh sizes h_1, h_2, h_3. The stencil must satisfy following condition [81].

$$\sum_{k=1}^{3}\sum_{l=1}^{3}\sum_{m=1}^{3} S_{k,l,m} = 0 \tag{3.32}$$

Therefore we can write above equation in the following form.

$$\left.\begin{aligned}
&\frac{1}{(\Delta r)^2}(\psi_{i+1,j,k} + \psi_{i-1,j,k}) - \frac{1}{r_i(\Delta r)}(\psi_{i+1,j,k} - \psi_{i-1,j,k}) \\
&+ \frac{1}{r_i^2(\Delta\theta)^2}(\psi_{i,j+1,k} + \psi_{i,j-1,k}) + \frac{\cot\theta}{2r^2(\Delta\theta)}(\psi_{i,j-1,k} - \psi_{i,j+1,k}) \\
&+ \frac{1}{(r^2\sin^2\theta)(\Delta\phi)^2}(\psi_{i,j,k+1} + \psi_{i,j,k-1}) \\
&- 2\left[\frac{r_i^2(\Delta\theta)^2(\Delta\phi)^2\sin^2\theta + (\Delta r)^2(\Delta\phi)^2\sin^2\theta + (\Delta r)^2(\Delta\theta)^2}{r_i^2(\Delta r)^2(\Delta\theta)^2(\Delta\phi)^2\sin^2\theta}\right]\psi_{i,j,k} = 0
\end{aligned}\right\} \tag{3.33}$$

Multiplying both sides of equation (3.31) by the following term

$$\frac{1}{2}\left[\frac{r_i^2(\Delta r)^2(\Delta\theta)^2(\Delta\phi)^2\sin^2\theta}{r_i^2(\Delta\theta)^2(\Delta\phi)^2\sin^2\theta + (\Delta r)^2(\Delta\phi)^2\sin^2\theta + (\Delta r)^2(\Delta\theta)^2}\right] \text{ and let say}$$

$$\begin{aligned}
\psi^s &= \frac{1}{(\Delta r)^2}(\psi_{i+1,j,k} + \psi_{i-1,j,k}) - \frac{1}{r_i(\Delta r)}(\psi_{i+1,j,k} - \psi_{i-1,j,k}) \\
&+ \frac{1}{r_i^2(\Delta\theta)^2}(\psi_{i,j+1,k} + \psi_{i,j-1,k}) + \frac{\cot\theta}{2r^2(\Delta\theta)}(\psi_{i,j-1,k} - \psi_{i,j+1,k}) \\
&+ \frac{1}{(r^2\sin^2\theta)(\Delta\phi)^2}(\psi_{i,j,k+1} + \psi_{i,j,k-1}) \\
\psi^0 &= \psi_{i,j,k}
\end{aligned}$$

The above equation takes the following form:

$$\frac{1}{2}\left[\frac{r_i^2(\Delta r)^2(\Delta\theta)^2(\Delta\phi)^2\sin^2\theta}{r_i^2(\Delta\theta)^2(\Delta\phi)^2\sin^2\theta + (\Delta r)^2(\Delta\phi)^2\sin^2\theta + (\Delta r)^2(\Delta\theta)^2}\right]\psi^s - \psi^0 = 0$$

Now we can write isotropic discrete Laplacian in spherical coordinates coordinates as below:

$$\langle\langle\psi\rangle\rangle - \psi = \beta\sum_{NN}\psi^s - \psi^0 \tag{3.34}$$

Where β is weighting factor for isotropic Laplacian in spherical coordinates which is given below:

$$\beta = \frac{1}{2}\left[\frac{r_i^2(\Delta r)^2(\Delta\theta)^2(\Delta\phi)^2\sin^2\theta}{r_i^2(\Delta\theta)^2(\Delta\phi)^2\sin^2\theta + (\Delta r)^2(\Delta\phi)^2\sin^2\theta + (\Delta r)^2(\Delta\theta)^2}\right]$$

The following periodic boundary conditions were applied on the angular coordinate of the spherical coordinate system.

$\psi_{(i,N_\theta+1,k)} = \psi_{(i,1,k)}$, $\psi_{(i,0,k)} = \psi_{(i,N_\theta,k)}$, for all $i = 1,2,...,N_r, k = 1,2,...,N_\phi$

The following reflective boundary conditions were applied on the radial coordinate of the spherical coordinate system.

$\psi_{(N_r+1,j,k)} = \psi_{(N_r,j,k)}$, $\psi_{(0,j,k)} = \psi_{(1,j,k)}$, for all $j = 1,2,...,N_\theta, k = 1,2,...,N_\phi$

The following periodic boundary conditions were imposed on the azimuthal coordinate ϕ of the spherical coordinate system.

$\psi_{(i,j.\,N_\phi+1)} = \psi_{(i,\,j,1)}$, $\psi_{(i,j,0)} = \psi_{(i,j,N_\phi)}$, for all $i = 1,2,...,N_r$, $j = 1,2,...,N_\theta$

Where $\psi(i,j,k)$, $i = 1,2,...,N_r$, $j = 1,2,...N_\theta, k = 1,2,...,N_\phi$, is approximation of the function $\psi(r,\theta,\phi)$. The initial condition for the system is chosen to be the random distribution of the $\psi(r,\theta,\phi)_{t=0} \in (1,-1)$.

3.6. Simulations of binary fluid

To test the method and developed CDS code, simulations of a binary fluid were carried out in the annular circular pore system. The simulation results for the binary mixture were obtained by using CDS parameter systems for lamella forming system except (*B = 0*). In this case, instead of microphase separation, a macrophase separation occurred in the pore system. This simulation setup is useful to investigate the behaviour of the mixture in the pore system. The simulation results were obtained on one million time steps to get the minimum energy level of the system.

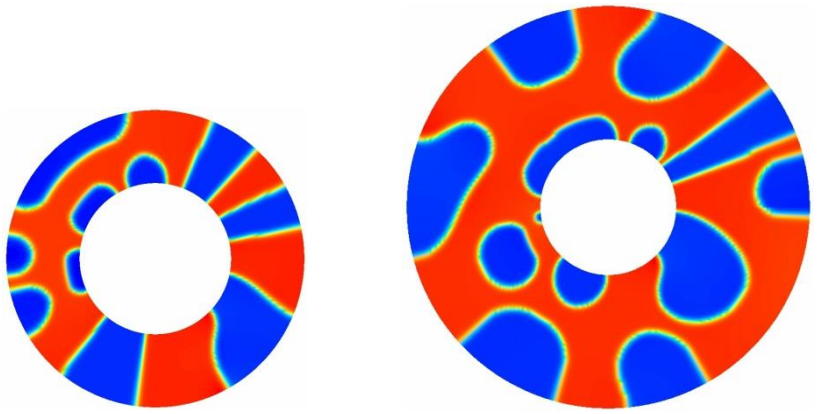

Figure 3.4: Phase separation for binary fluid were obtained on 1 million time steps, in a pore system with the interior radius of the pore system was fixed at r_a = 3.0 and the grid sizes are (a) 30x360 (b) 60x360

The simulation result shows that domain clearly divide into two rich subdomains. In the pore system shown in Figure 3.4(a), domain divided into two rich subdomains, where A-rich subdomain is blue having its minimum $\psi^+ = 0.9090243$ and B-rich subdomain having its minimum $\psi^- = -1.077136$. The pore system shown in Figure 3.4(b) also divided into two subdomains, where A-rich subdomain has its minimum $\psi^+ = 0.908395$ and B-rich domain has its minimum $\psi^- = -1.083791$.

CHAPTER FOUR

4. Block copolymer system confined in circular annular pores

4.1. Introduction

Two-dimensional studies of diblock copolymers are not sufficient to provide full information about the phase separation and structural control. However, it provides a strong background for three-dimensional studies and which can give reflections about the phase separation and structural control in three dimensions. Therefore for this reason in the first phase of the investigation, two-dimensional computational studies have been carried out in circular annular pores using the polar coordinate system. The diblock copolymer system is explored in an annular circular pore with various pore sizes in the annular circular pore. All the CDS simulations were carried out using periodic boundary conditions in the angular direction $0 \le \theta \le 2\pi$, where the angular step is taken $\Delta\theta = 2\pi / 360$, and reflective boundary conditions were applied in radial *r* direction. The pore is contained between two concentric circles where the interior radius of pore system is fixed at r_a = *3, 5, 7* in three type of pore systems and exterior radius of pore system was varied for different values of r_b to expand the pore size of the system. Therefore, circular annular pore size becomes $d = r_a - r_b$ where *d* represents pore size of the system. The simulation results were obtained on 1 million time steps. All simulations were carried out by an initial random disordered state of order parameter ψ within the range of ± *0.5*. In the CDS system, we are able to visualise simulation results by showing both blocks (**A** and **B**) of polymer system in the computational domain. Simulation results were obtained for the diblock copolymer system in computation

domain patterned in two rich domains *i-e* red rich domains represents **A** block and blue rich domain represents **B** block of the polymer system. Computational results for the diblock copolymer system are also obtained with surface preference with one of the blocks of the polymer system. In this study, the parameter α represents the strength of interaction between the wall and one of the blocks of the polymer system. Using the CDS method employed in the polar coordinates we investigated classical morphologies of lamellae, cylinder, and sphere in annular circular pores system. Lamellae forming system, cylindrical forming system, and spherical forming system are also investigated by one-dimensional confinement and two-dimensional confinements. Following table shows the computational parameters used in all simulations in polar coordinates system.

Table 1: Computational parameters used in the simulation results

Radial step Δr	Angular step $\Delta\theta$	Time step Δt	Total time steps
0.1	0.017453292	0.1	1 Million

4.2. Results and discussions

In this section, the results for the diblock copolymers system confined in the circular annular pores are presented and discussed. The results for diblock copolymers shown in this section were obtained in the pore geometry with various film thicknesses and the pore radii of the pore system. The results are also presented which were obtained with interfacial circular walls having the affinity with both the majority segment and the minority segment of the polymer system.

4.2.1. Asymmetric lamellae forming system confined in circular annular pores

In CDS system, lamellae morphology can be obtained using different global volume fractions of $f = 0.50$ in the symmetric case and $f = 0.48$ in the asymmetric case with same temperature parameter $\tau = 0.36$. The global volume fraction play an important role

in morphology formation, therefore simulation results were obtained for the lamellae forming system against both values of global volume fraction *i-e f = 0.50* (symmetric) and *f = 0.48* (asymmetric). However, the rest of the CDS parameters were also tested and modified accordingly. In the following section asymmetric lamellae forming system is investigated in annular circular pore system.

I. Asymmetric lamellae forming system confined in neutral circular annular pores

The simulation results for diblock copolymer lamellae morphology for asymmetric global volume fractions (*f = 0.48*), in the circular annulus pore systems with various pore sizes and pore radii were obtained and discussed. The results were obtained on 1 million time steps. The CDS simulations were performed with CDS parameter for asymmetric lamellae system given in table (2).

Table 2: CDS Parameters for asymmetric lamella forming system

τ	f	u	v	B	D	A
0.36	0.48	0.38	2.30	0.02	0.70	1.50

The pore domains were contained between two concentric circles for which the interior radius r_a of the pore systems was fixed, while the pore sizes were expanded by increasing the exterior radius r_b of the pore system. The interior radius of the pore system was fixed at $r_a = 3.0$ in all the following simulation results, however the exterior radius of pore systems were varied by expanding exterior radii of pore systems for different sizes $r_b = 4, 5, 6, 7, 8, 9, 11, 13$ hence film thicknesses under investigation were *d=1, 2, 3, 4, 5, 6, 8, 10.*

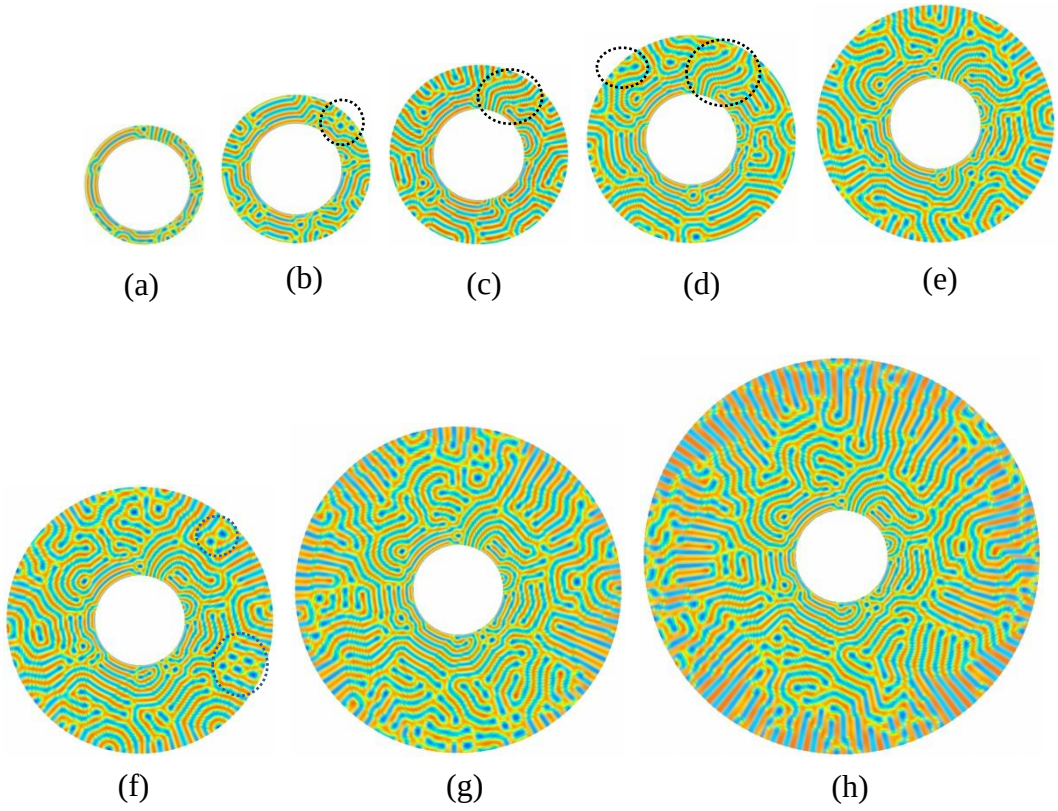

Figure 4.1: Evolutions of asymmetric lamellae system on 1 million time steps confined in various circular annular pore sizes with the interior radius of the pore was fixed at $r_a = 3.0$ and the exterior radius of pore was expanded to obtain various pore sizes: (a) evolution of asymmetric lamella in the pore system size *d = 1*, pore system induces alternating lamella strips (b) evolution of asymmetric lamella in the pore system size *d = 2*, system patterned into Y-shaped, U-shaped and perforated holes morphologies (c) evolution of asymmetric lamella in the pore system size *d = 3*, pore shows Y-shaped or tilted Y-shaped star shaped and W-shaped patterns (d) evolution of asymmetric lamella in the pore system size *d = 4*, system induces Y-shaped, W-shaped U-shaped and a few perforated holes (e) evolution of asymmetric lamella in the pore system size *d = 5*, patterns are two arm stars and single arm star with a perforated hole at the centre of the star (f) evolution of asymmetric lamella in the pore system size *d = 6*, induced nanostructures include perforated holes morphology (g) evolution of asymmetric lamella in the pore system size *d = 8*, mixed morphologies (h) evolution of asymmetric lamella in the pore system size *d = 10*, alternating lamella strips normal to the exterior circular boundary.

The lamellae system in circular annular pore system shows a mixed orientation of strip lamella, parallel to the pore system, perpendicular to the pore system and oblique. Lamella forming systems confined in circular annular pore induces a few perforated holes into the lamella morphology. Grain boundaries are induced into the Y-shape, U-shape, W-shape, V-shape and star shape in the circular annular pores. The lamella confined in the circular annular pore show straight lamellae strips and curved lamella. In

the narrow pore size system *d = 1,* shown in Figure 4.1(a) there are three lamellae on left half of the pore system, wrapping around (concentric lamellae) the pore system. In the same pore system, on the upper half of the pore system, there are six straight lamellae strips normal to the circumference of the boundaries of the pore system. Between the parallel strips and concentric lamellae, there is one perforated hole induced in the pore system. Concentric alternating lamellae were conformed due to the curvature effect in the circular annular pore geometry. In the pore size *d = 2,* as shown in Figure 4.1(b) a major part of concentric lamellae that was formed in previously sized system deformed into U-shape and Y-shape lamellae due to the decrease in the curvature. Furthermore, parallel strips normal to the circumference also disappeared in the circular annular pore. In this pore size system, five perforated holes adjacent to each other are displayed in the first quadrant of the pore system shown in Figure 4.1(b) by dashed lines. Increasing the pore size of the system *d = 3* these perforated holes disappeared and replaced by the curved lamellae which are normal to the circumference of exterior as well as the interior circular boundary of the pore system as shown in Figure 4.1(c) by dashed lines. If we compare the system Figure 4.1(b) and Figure 4.1(c) left half of the pore system then we can observe that concentric lamellae have a tendency to deform into Y-shape and W-shape with respect to the increase in the pore size. This shows that microdomains are changing orientation, from parallel to the pore to normal to the pore system with respect to the increase in the pore size. In this pore size grain boundaries induced in the pore system are in Y-shape or tilted Y-shape star shape and W-shape. For the pore system *d = 4,* we observed the four perforated holes adjacent to each other on the top of the left half of the pore system as we observed similar perforated holes in the pore system with the pore size *d = 2* on the top of right half of the pore system. The rest of the domains were patterned with nanodomains in the Y-shape, W-shape U-shape and a few perforated holes. Furthermore, increasing the size of the pore system *d = 5* as

shown in Figure 4.1(e) we observed the star lamellae with a perforated hole at the centre of the star are displayed on the top right half of the pore system as shown inside the dashed lines. There are similar star lamellae connected with near the interior circular boundary as well in the pore system. The pore system also displays lamellae in the form of the two arm stars and single arm stars with a perforated hole at the centre of the star. In the rest of the pore system grain boundaries are induced in the form of Y-shape, W-shape and U-shape. In the pore size $d = 6$ again we observed the perforated holes adjacent to each other but in this size system, there are six arrays of perforated holes appeared at the bottom of the right half of the pore system and two perforated holes adjacent to each other displayed at top right half of the pore system as shown in Figure 4.1(f). However, in the rest of the circular annular pore system microdomains were induced in Y-shape, W-shape, U-shape and star shape with a perforated hole at the centre of the star. Furthermore increasing the size of the pore system, grain boundaries are becoming straight strips at the exterior circular boundary of the pore system and oriented normal to the pore system as shown in Figure 4.1(g) and Figure 4.1(h). Both systems are enriched with grain boundaries patterned in Y-shape, W-shape, U-shape, star shape with a perforated hole at the centre of the star. Y-shape, W-shape, U-shape and star lamellae are induced in the circular annular pore system due to the curvature effect of the pore geometry. However, the perforated holes are appearing in the circular pore geometry due the competition between incompatible blocks and entropy. Furthermore, spiral morphology did not appear in the pore geometry due to the size effect as a computational domain under investigation is far away from the centre of the pore system, where the curvature of the pore geometry has a maximum value. Simulations results obtained with asymmetric volume fractions for lamella forming systems are stable and consistent with the experimental and computational studies in the field; however we predicted some novel morphologies such as star lamellae with a

perforated hole at the centre of the star and W-shape lamellae which are to be confirmed by the experimental studies. The results of this study can be compared with the experimental work [56], the fingerprints lamella achieved in the planar thin films. In the planar thin films, lamella mostly forms Y-shape and U-shape patterns, however, here under geometric confinement results predict perforated holes, star shape and W-shape strip patterns. The results show bent lamella with openings in the direction of outer circumference, these patterns are consistent with the results obtained for lamella under cylindrical confinement where results show bent lamellae pointing towards the column mantle of the pore Figure 3(c) shown in therein [57]. Fingerprints morphologies were also observed in planar thin films, microdomains were observed perpendicular to the substrate and coexistence of fingerprint morphology with perforated holes was observed in Figure 2(a) therein [84].

In the second case, the interior radius of the annular pore systems was fixed at $r_a = 5.0$ and the pore size of systems increased by the exterior radius r_b of pore systems. The exterior radius of pore systems were increased for different values $r_b =$ *7, 8, 9, 11*, hence the film thicknesses under investigation were $d = 2, 3, 4, 6$.

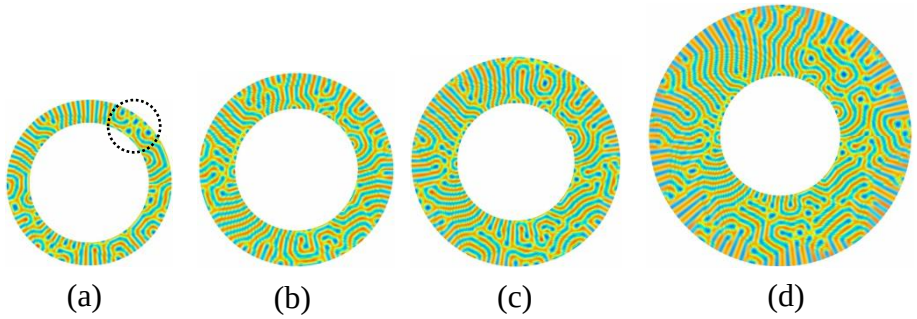

Figure 4.2: Evolution of asymmetric lamellae system on 1 million time steps in the pore system with the interior radius of pore system was fixed at $r_a = 5.0$ and the exterior radius r_b of the pore system was expanded to obtain various pore sizes, pore size of the systems: (a) evolution of nanodomains in the pore size $d = 2$, system show alternating lamella strips normal to the circular boundaries, perforated holes and Y-shaped defects (b) evolution of lamella patterns in the pore system size $d = 3$ system induces lamella strips and Y-shaped defects (c) evolution of the asymmetric lamella system in the pore size $d = 4$ induced morphologies are Y-shape, U-shape, W-shape and star shape lamellae with a perforated hole at the centre of the star (d) nanostructure evolution in the pore size $d = 5$ induces diverse lamella patterns.

The simulation results for the expanded interior radius show that lamellae are induced normal to pore walls in the pore geometry. In the system size $d = 2$, shown in Figure 4.2(a) there are lamellae strips normal to the pore walls and there are perforated holes adjacent to each other found at top inside right half of the pore system. In the pore system, Y-shape micro domains are deformed into straight strip or U-shape micro domains due to the size effect in the geometry. Expanding the pore size of the system $d = 3$ lamellae straight strips taking back into Y-shape lamellae in the pore geometry as shown in Figure 4.2(b). Therefore, it can be argued that morphological transition between straight strips lamellae and Y-shape lamellae are due the size effect of the pore geometry. In this system size no perfect perforated holes appeared in the pore system. Furthermore, expanding the pore system $d = 4$ we can observe Y-shape, U-shape, W-shape and star shape lamellae with a perforated hole at the centre of the star appearing in the pore geometry as shown in Figure 4.2(c). As we go further by expanding the pore size of the system $d = 6$ we can observe diversity of lamellae morphological patterns in the form of Y-shape, U-shape and star lamellae with single arm, double arm, triple arm, and 4 armed star with perforated hole at centre of the star as shown in Figure 4.2(d).

The simulation results show that the narrow pore sized system induces the parallel strips of grain boundaries whereas in the expanded pore system these parallel grain boundaries transform into Y-shape grain boundaries due to the size effect of the pore geometry. Furthermore, the grain boundaries in the expanded pore system were induced normal to the pore system.

In the third case, we expanded the pore system furthermore by increasing interior radius of the annular pore system by keeping it fixed at $r_a = 7.0$ and pore size of the system was enlarged by increasing exterior radius r_b of the pore systems. The exterior radius of the pore systems was increased by expanding the exterior radius of the pore systems for different sizes $r_b = 9, 10$, hence film thicknesses under investigation was $d = 2, 3$.

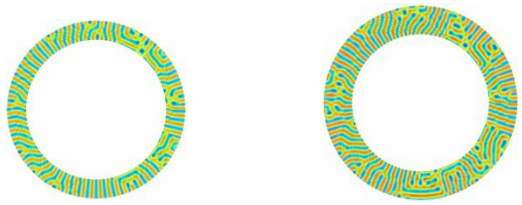

(a) (b)

Figure 4.3: The asymmetric lamellae system in the expanded pore size with the interior radius of pore system was fixed at $r_a = 7$: (a) the system size $d = 2$, system induces alternating parallel lamella strips normal to the circular boundaries, Y-shaped, W-shaped and star shaped patterns (b) the system size $d = 3$, induced patterns including a few alternating lamella strips normal to the circular boundaries, Y-shaped, W-shaped and star shaped defects.

The simulation results with expanded pore system show parallel lamellae strips normal to the pore system. In the pore size $d = 2$, system shows more parallel strips of lamellae normal to the pore geometry system. Including parallel strips there are Y-shape and W-shape and star lamellae with perforated hole at the centre of the star also observed in the pore system as shown in Figure 4.3(a). Increasing the pore size of the pore system $d = 3$, parallel lamellae strips normal to the system taking the form of Y-shape boundary grains but there are still few parallel strips normal to the pore system in the pore geometry as shown in Figure 4.3(b). While rest of the domain in the pore geometry,

patterned into W-shape and double arm star, triple arm star lamellae with perforated hole at the centre of the star.

II. Asymmetric lamella system with interfacial circular walls

The simulation results for diblock copolymer lamellae forming system with asymmetric volume fractions in circular annular nano pores system were obtained by applying preferential attractive walls for the **A** monomer as well as for the **B** monomer. In the circular annular pore geometry, simulation results are obtained by CDS parameter system for asymmetric lamellae system. Simulation parameters are taken same as in previous sections for the pore geometry. Periodic boundary conditions were imposed on the angular coordinates, whereas reflective boundary conditions were imposed on the radial coordinate in the pore systems. The symmetric boundary conditions were applied for confining polymer system between two circular walls which carry equal preference for one of the block of the polymer system throughout the surface. All the simulations were carried out on 1 million time steps for the pore system. The parameter α denotes the interaction strength between the one of the segment of the polymer system and confining walls of the pore system.

In the first case of one dimensional confinement, boundary conditions were imposed on radial axis parallel to the pore system and attractive circular boundary wall with affinity of **A** monomer, applied with strength of interaction α for various values. The interior radius of the pore system was fixed at $r_a = 3$, whereas the pore system was expanded by increasing the exterior radius r_b of the pore system. In this analysis *d* denotes the pore size of the system which shows the difference between the exterior radius of the pore systems and the interior radius of the pore systems.

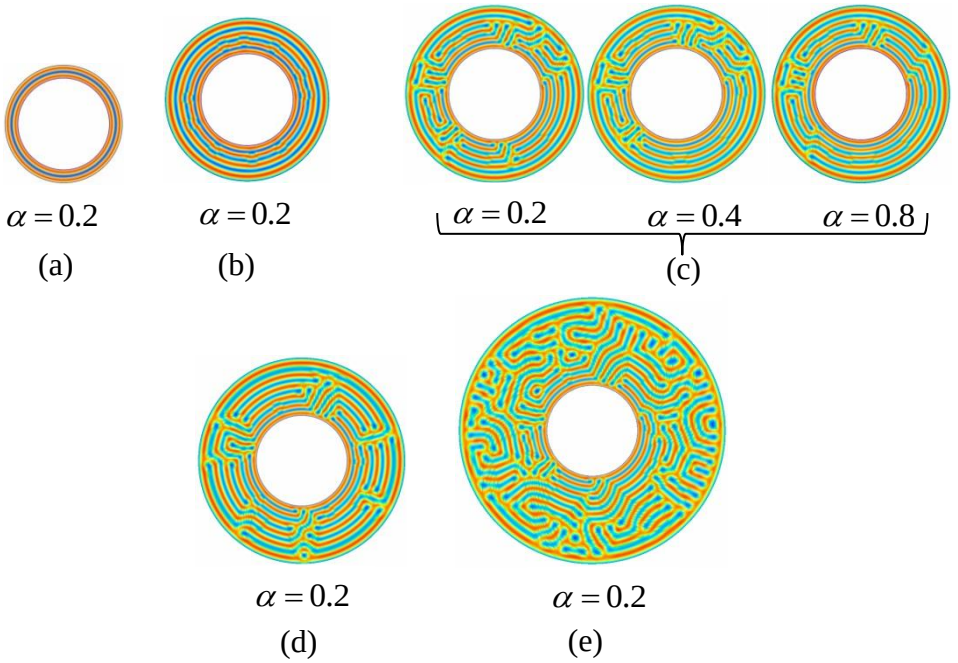

Figure 4.4: Asymmetric lamellae system under one dimensional confinement obtained on 1 million time steps, the interior radius of the pore system was fixed at r_a=3.0 and the pore sizes of systems are (a) *d = 1*, pore system induces three alternating concentric lamella rings (b) *d = 2.5*, pore system induces seven alternating concentric lamella rings (c) *d = 3*, system induced concentric lamella and strip lamella (d) *d = 4*, system induced concentric lamella and dislocations (e) *d = 6*, system patterned with mixed lamella morphologies.

The simulation results in the annular circular pore system under geometric confinement show that the confinement influences the microdomains into concentric lamellae parallel to the pore system. In the pore size *d = 1* with weak interaction applied $\alpha = 0.2$ for the pore system as shown in Figure 4.4(a) the system shows perfect concentric parallel to the pore lamellae in the pore geometry. There is only one circular lamella with two boundary lamellae appeared in the pore geometry system. The concentric lamellae parallel to the pore system induced in the pore geometry due to the interplay of both curvature and confinement effect. The pore system size *d* = 2 does not show concentric circular lamellae in the pore geometry not shown here. Furthermore, in the expanded pore system *d = 2.5*, perfect concentric circular lamellae were induced in the pore system as shown in Figure 4.4(b). Between the confining circular walls, it can be observed that there are seven alternating lamellae induced in circular ring shape in the pore geometry. As moving further, by expanding the size of the pore system *d = 3*,

system shows that lamellae are tending to wrapping around the centre of the pore system, however in these sizes system perfect concentric circular lamellae are not induced as shown in Figure 4.4(c). For this system interaction strength between **A** segment of the polymer system and boundary walls were increased from $\alpha = 0.2$ to $\alpha = 0.4$ and $\alpha = 0.8$, the system shows Y-shape lamellae are converting into concentric circular lamellae gradually with respect to the size of the system, the system is shown in three wheels in Figure 4.4(c). For the system size *d = 4* as shown in Figure 4.4(d), it can be observe the Y-shape lamellae are being converting into the concentric lamellae in the pore system. However, the system with size *d = 6* shows mixed orientation of the lamellae and diverse patterns which shows that in the large systems confining effect is minimal.

For the similar pore system, simulation results are also obtained by putting interacting circular walls around the pore system having affinity with **B** segment of the polymer system in the pore geometry. The pore system for having affinity of circular walls to **B** segment of the polymer system is similar as was designed for counterpart segment **A** of the polymer system in the pore geometry.

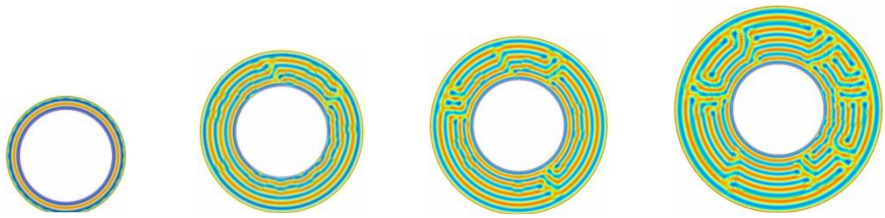

Figure 4.5: Evolution of asymmetric lamellae system on 1 million time steps under geometric confinement, interacting circular walls has affinity with the **B** segment of polymer system, interaction strength was applied $\alpha = 0.2$, the interior radius of the pore system was fixed at r_a = *3*, whereas system was expanded by the exterior radius of the pore system and pore system size are (a) *d = 1*, system patterned into concentric lamella (b) *d = 2.5*, system induces concentric lamella with very few dislocations (c) *d = 3*, concentric lamella, perforated holes and dislocations (d) *d = 4*, mixed patterns.

The pore system confined by putting affinity of the circular walls for **B** segment of the polymer system is more effective than the counterpart **A** segment in the pore geometry.

Figure 4.5 shows the results obtained by confining polymer system by circular walls around the pore geometry having affinity for **B** segment of the polymer system. The pore system size $d = 1$ shown in Figure 4.5(a) show single perfect circular lamella of **B** segment of the polymer system enfolded around the pore. In the second system with pore size $d = 2.5$ there are five concentric alternating circular lamellae system induced in the pore system with defects at two points where circular lamellae were not properly connected to each other in the pore geometry as shown in Figure 4.5(b). The pore system having size of the pore $d = 3$ also shows two concentric perfect circular rings of lamellae and inside the rings mainly lamellae are circular parallel to the pore system as shown in Figure 4.5(c). Similarly the system with pore size $d = 4$ shown in Figure 4.5(d) also shows similar behaviour of the two concentric perfect circular rings inside the rings lamellae with mixed patterns found in the pore system. The simulation results predict a confinement effect more effective with having affinity to the circular walls for B segment of the polymer system in the pore geometry as compared to the counterpart **A** segment of the polymer system.

For the expanded pore system with interior radius set fixed at $r_a = 5$ and exterior radius of system increased to obtained various sizes of the pore system, simulation results have been obtained by preferential affinity of the surface between circular walls and **A** segment of the polymer system. One dimensional confinement is imposed on the radial coordinate of the pore system, where **A** segment have preferential affinity to the circular walls around the pore system. The interior radius of the pore system was kept fixed at $r_a = 5$ whereas the pore systems were expanded by increasing the exterior radius r_b of the pore systems. Here d denotes the pore size of the system which is the difference of the exterior and the interior radii of the pore systems.

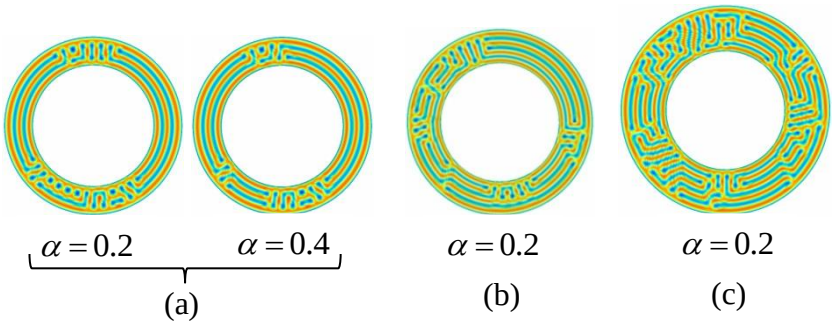

Figure 4.6: Asymmetric lamellae system under one dimensional confinement into expanded pore system with the interior radius was fixed at r_a = *5* and the pore size of the systems are (a) *d = 2.5* (b) *d = 3* (c) *d = 4.*

The simulation results under geometric confinement in the expanded pore systems with interior radius fixed at r_a = *5* show parallel concentric circular lamellae and Y-shape lamellae in the pore systems. In the system size *d = 2.5* shown in Figure 4.6(a) with interaction strength $\alpha = 0.2$ system shows concentric circular lamellae parallel to the pore system and a few packs of perforated holes, however system with increased interaction strength $\alpha = 0.4$ most of the packs of perforated holes disappeared and pore system induces circular lamellae parallel to the pore system. The pore system with size *d = 3* shown in Figure 4.6(b) shows mostly concentric circular lamellae parallel to the system under geometric confinement subjected to interaction strength applied $\alpha = 0.2$. However, in this system there are still lamellae normal to the pore system with a few perforated holes in the pore system. The pore system with size *d = 4* shows mixed lamellae system induced in the Y-shape parallel to the pore system and lamellae normal to the pore system as shown in Figure 4.6(c).

For the similar pore system, pore walls activated for having affinity to **B** segment of the polymer system in the pore geometry. The strength of interaction between the polymer segment **B** and the circular walls are applied $\alpha = 0.2$.

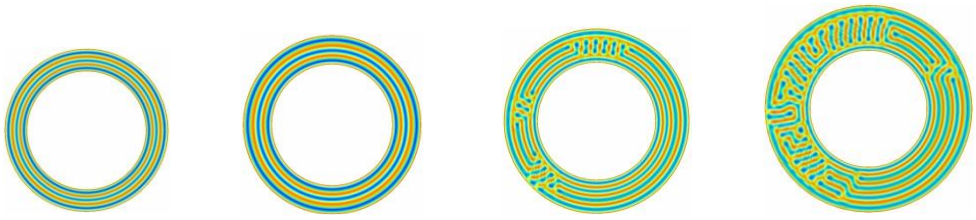

(a) (b) (c) (d)

Figure 4.7: Asymmetric lamellae system under geometric confinement, circular walls have affinity to the **B** segment of the polymer system, the interior radius of the pore systems was fixed at $r_a = 5$, and the pore sizes are (a) $d = 2$ (b) $d = 2.5$ (c) $d = 3$ (d) $d = 4$.

The simulation results obtained with changing preference of the interacting walls for **B** segment of the polymers system show concentric circular rings of the grain boundaries. There are three concentric perfect circular rings of micro domains apart from circular boundary walls in the system having size $d = 2$ as shown in Figure 4.7(a). The pore system having pore size $d = 2.5$ also shows three concentric circular rings of boundary grains induced in the pore geometry as shown in Figure 4.7(b). Both the systems show same number of micro domains due the size effect of the polar grid system. It can easily be observed that lamellae in the pore system shown in Figure 4.7(a) are thicker than the system shown in Figure 4.7(a). The similar structure of concentric alternating lamellae can be observed in experimental study [15] there in Figure 1(A). This type of morphology is also called dartboard morphology. Using moderate surface interaction Sevink *et al* computationally obtained dartboard morphologies in various pore sizes [17] Figure 4 therein but these observed alternating concentric were not perfectly circular. These onion-like concentric alternating layered lamella were also obtained by the preparing lamella in the spherical pores [85], see Figure 1 therein.

The pore system with size $d = 3$ as shown in Figure 4.7(c) shows concentric circular lamellae with a few packs of the perforated holes displayed inside the pore system. The pore system having size of the system $d = 4$ displays in one half of the pore system concentric circular lamellae and other half of the circle mixed behaviour of lamellae in the pore system as shown in Figure 4.7(d). The simulation results show that changing

preference from **A** segment to **B** segment of the polymer system influence more to form periodic patterns of concentric circular lamellae ring in the pore geometry.

Furthermore, expanding the pore system through the interior radius of the pore system by keeping it fixed at $r_a = 7$ and the exterior radius of the system was increased to obtained various sizes of the pore geometry, simulation results were obtained in the pore system by preferential affinity of the surface between circular walls and **A** segment of the polymer system. One dimensional confinement is imposed with symmetric boundary conditions on the radial coordinate of the pore system, where **A** segment have preferential affinity to the circular walls around the pore system. The interior radius of the pore systems was kept fixed at $r_a = 7$, whereas the pore systems were expanded by increasing the exterior radius r_b of the pore system. Here *d* denotes the pore size of the system which is the difference of the exterior and the interior radii of the pore system.

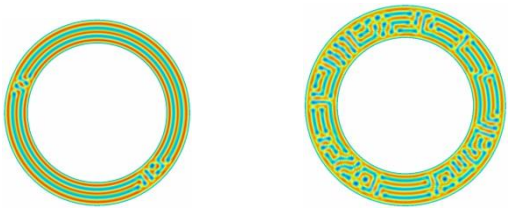

(a) (b)

Figure 4.8: Asymmetric lamellae system under geometric confinement, the interaction strength was applied $\alpha = 0.2$, the expanded pore system with the interior radius of the pores were fixed at $r_a = 7$ and pore sizes of the systems are (a) $d = 2.5$ (b) $d = 3.5$.

The simulations results under geometric 1-D confinement into expanded pore system show perforated holes and lamellae normal to the pore system. The interior radius of the pore systems were fixed at $r_a = 7$, whereas the exterior radius of the pore systems were expanded as $r_b = 9.5, 10.5$ hence results were obtained in the pore sizes $d = 2.5, 3.5$. Due to the large system impact of the curvature in the pore geometry on microdomains is nominal. The pore system under one dimensional confinements are shown in Figure 4.8(a) with the size of the system $d = 2.5$ and in Figure 4.8(b) with size $d = 3.5$. The

pore system having pore size $d = 2.5$ induces three alternating circular lamellae with defects at two sections of the pore system where circular lamellae are not properly connected to each other. However, the pore system with size $d = 3.5$ did not show perfect circular lamellae in the pore geometry. This system size show mixed behaviour of lamellae in the pore geometry where lamellae are in parallel to the pore, normal to the pore and perforated holes are induced in the pore system. This shows that due to the size effect there is nominal inclination of grain boundaries to reorient themselves into parallel to the pore system.

For the similar pore systems simulation results are also obtained by changing preference to the circular walls from **A** segment to **B** segment of the polymer system in the pore geometry. The interaction strength between the circular walls and the **B** segment of the polymer system is set at $\alpha = 0.2$ in the pore geometry.

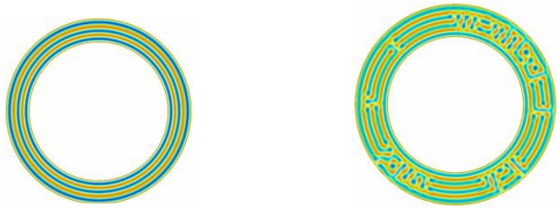

(a) (b)

Figure 4.9: Lamellae system under geometric confinement, circular walls have affinity to the **B** segment of the polymer system, the interior radius of the pore system was fixed at $r_a = 7$, the pore size expanded by the exterior radius of the pore system, pore sizes are (a) $d = 2.5$ (b) $d = 3.5$.

The pore system with changing preference for monomer **B** shows lamellae in the form of circular ring in the pore geometry. For the system having pore size $d = 2.5$ displays three perfect circular rings of alternating lamellae induced in the pore system as shown in Figure 4.9(a). The system with pore size $d = 3.5$ shows two concentric circular rings of lamellae and inside the rings there is mixed behaviour of lamellae system where some packs of circular lamellae and some packs of lamellae are normal to the pore system as shown in Figure 4.9(b).

The concentric lamella (onion-like) structure are obtained here are very much consistent with the results obtained for lamella system confined in cylindrical pore by the experimental work [57] shown in Figure 3(a) therein.

4.2.2. Symmetric lamella forming system confined in circular annular pores

The simulation results for diblock copolymer lamellae morphology for symmetric volume fractions in circular annular pores with variations in diameter obtained on one million time steps by using CDS method employed in polar coordinate system. Volume fractions play a vital role in nano fabrications of block copolymer systems. The simulation results were obtained with the symmetric volume fraction of CDS parameter system to investigate the influence of volume ratio on diblock copolymer lamellae forming system in the pore geometry. For the simulation results of lamellae system with symmetric volume fractions CDS parameters u and D also changed along with f. Following table (3) shows CDS parameters system used in the simulations; however the simulation parameters used were same as in previous section.

Table 3: CDS parameters for symmetric lamella system

τ	f	u	v	B	D	A
0.36	0.50	0.50	2.30	0.02	0.50	1.50

The interior radius of pore system was fixed at $r_a = 3$, however, the exterior radius of pore systems was varied to expand the pore size of the systems as $r_b = 5,7,9$, hence domain sizes of pore under consideration were $d=2, 4, 6$. The Snapshots of CDS simulation results are shown in following Figure 4.10.

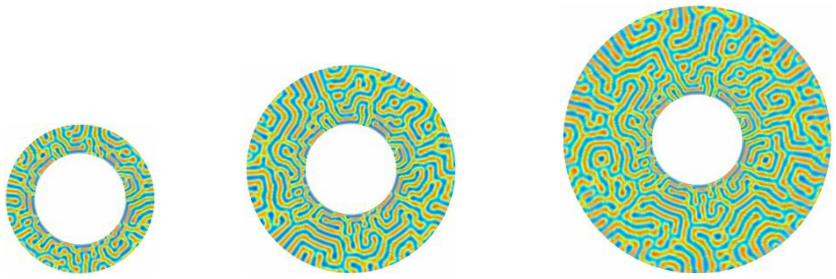

(a) (b) (c)

Figure 4.10: Symmetric lamellae forming system confined in circular annular pores with the interior radius of the pore system was fixed at r_a = 3.0 and the pore sizes are (a) 2 (b) 4 (c) 6.

The computational results for diblock copolymer lamellae forming system in circular annular nano pores with using equal volume fractions of both monomers were obtained. The results show more defect lamellae as compared to previous sections results obtained with asymmetric volume fractions in annular circular pore system. In the simulation results shown in Figure 4.10, it can be observed that they are more diagonal as compared to the simulation results obtained with non-symmetric volume fractions parameter system. It can also be noted here that they are discontinuous as compared to the asymmetric volume fraction case. Similarly, the like behaviour of lamellae normal to the circumference of the exterior circle can be observed in symmetric case but in this case normal lamellae to circumference of exterior circular boundary of pore are small in length and discontinuous. In the middle of the domain of hollow disk lamellae shows mix behaviour like normal to the pore system and parallel to to the pore system and shows more diagonal shapes. Therefore the important thing observed by comparing both results of asymmetric case and asymmetric case is that asymmetric lamellae are more curved and continuous whereas in symmetric case lamellae are more diagonal and discontinuous.

For the similar pore system, simulation results were obtained by one dimensional geometric confinement by giving preference to the circular walls for **A** segment of the

polymer system. The interaction strength between circular walls and **A** segment of the polymer system was set at $\alpha = 0.2$.

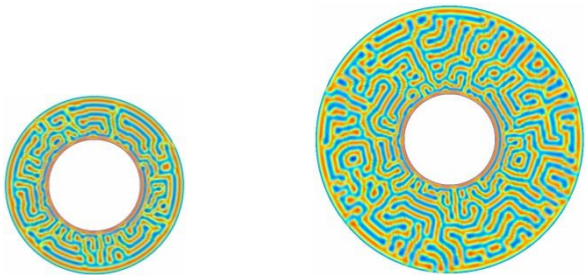

(a) (b)

Figure 4.11: Symmetric lamellae system under geometric confinement with the interior radius of the pore system was fixed at r_a = 3.0 and pore sizes of the system are (a) *d = 3* (b) *d = 6.*

Symmetric lamellae system under one dimensional geometric confinement in annular pore system shows grain boundaries in mixed orientation between confined walls in the pore geometry. The pore system having size *d = 3* shows that few micro domains are parallel to the circular wall and others are normal to the circular walls in the pore geometry as shown in Figure 4.11(a). The pore system with size *d = 6* shown in Figure 4.11(b) also shows mixed behaviour of the boundary grains with few perforated holes inside the pore system. This shows that symmetric lamellae parameter system in CDS is not efficient to study lamellae forming system in the pore geometry.

4.2.3. Cylindrical forming system confined in circular annulus pores

Cylindrical morphology of diblock copolymer investigated in circular annular nano channels without confinement's walls and with geometric confinements in one dimension as well as two dimensions. The cylindrical forming system can be achieved by using CDS parameters system for volume fraction *f = 0.40* and temperature parameter τ = 0.30. The simulation results were obtained in circular annular pore with keeping interior radius of the pore system fixed and expanding exterior radius of the system on various sizes of pore. In the pore geometry simulation results were obtained on one million time steps.

I. Cylindrical forming system confined in neutral circular annular pores

The computational results for cylinder forming in circular annulus pores were obtained by keeping the interior radius of the pore fixed and expanding exterior radius of pore system for various values of radius. The simulation results were obtained on 1 million time steps in annular circular pore system. The CDS Simulations were performed using CDS parameters for cylindrical forming system shown in following table (4).

Table 4: CDS parameter system for cylindrical forming system

τ	f	u	v	**B**	**D**	**A**
0.30	0.40	0.50	1.50	0.02	0.50	1.50

The simulation results were obtained in a pore system which is contained by concentric circles of radius r_a and r_b, where r_a represents interior radius of the pore system and r_b represents the exterior radius of the pore system. The interior radius of pore systems were fixed at $r_a = 3.0$ and the pore systems were extended by increasing the exterior radius of pore systems as $r_b = 4, 5, 6, 7, 9$. The size of the pore system is represented here by $d = r_b - r_a$. The simulation results were obtained with various pore sizes are shown in Figure 4.12.

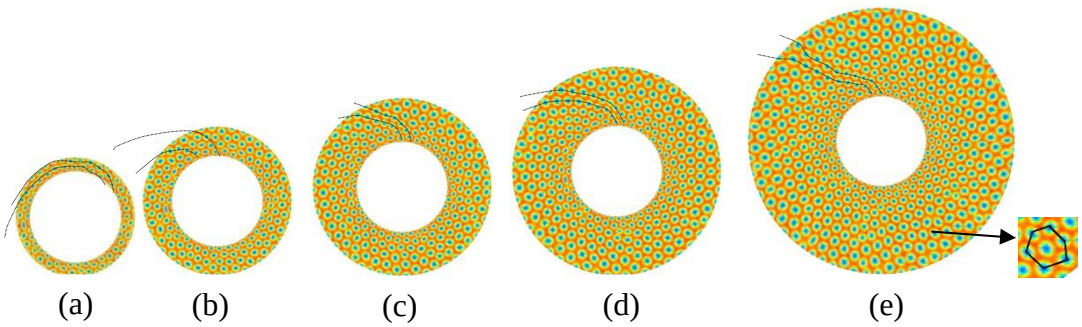

Figure 4.12: Cylindrical system in the pore geometry with pore sizes (a) $d = 1$ (b) $d = 2$ (c) $d = 3$ (e) $d = 4$ (f) $d = 6$

Cylindrical system in the pore geometry shows that microdomains make alignment on the logarithmic spiral lines in the pore system. Microdomains also show the hexagonal packing arrangements in the pore geometry. In Figure 4.12(a) the system is shown with pore size $d = 1$ cylinders lie on the logarithmic spiral lines where spiral line are shown by dashed lines. In this system spiral rays are narrowed or spiral lines have short distances from the origin. The pore system with size $d = 2$ also shows that the cylinders are aligned on the logarithmic spiral lines where spiral lines are shown by the dashed lines as shown in Figure 4.12(b). In this system spiral rays are bit wider or have a more distance from the centre of the pore system as compared to previous sized pore system. The pore system having pore size $d = 3$ as in Figure 4.12(c) shows micro domains lie on the spiral lines having almost same spiral rays distance from the origin of the pore system. However, the pore system with size of the pore $d = 4$ shows cylinders on the spiral lines having spiral rays wider due the size effect of the pore geometry. Furthermore, pore system with size $d = 6$ shows micro domains on the spiral lines with spiral rays very much wider due the size effect of the pore geometry as shown in Figure 4.12(d). The cylinders in the pore system are also hexagonally packed as shown in Figure 4.12(d) along with zoomed snapshot of the image. This shows that in the pore geometry cylinders align on the spiral rays and spiral arms becomes wider with respect to increase in the pore size of the system. The experimental study shows that the frustration caused by the confinement distorts the natural packing of hexagonal arrangements of the microdomains [86, 87].

The pore system is also expended by the increasing interior radius of the pore system at two fixed values $r_a = 5$ and $r_a = 7$ and the exterior radius of the pore system was increased at different values to expand the pore system. In both pore systems we obtained similar patterns of the cylindrical forming system in the pore geometry. The cylindrical forming systems were observed packed along the spiral lines in the pore

geometry due to curvature influence. Hexagonal packing of the micro domains was also observed inside the pore geometry.

II. Cylindrical system with interfacial circular walls

Diblock copolymer cylindrical forming system was studied in circular annulus pore system using preferential attractive circular walls having interaction strength $\alpha = 0.2$ between the walls and one of the segments of the polymer system. In one dimensional confinement attractive circular wall interaction with one of the segments of the polymer system applied in radial *r* direction in annular pore system. The simulation results were obtained in a pore system by keeping fixed the interior radius of the pore system $r_a = 3$ and pore size was expanded by increasing exterior radius r_b of the pore system. The parameter $d = r_b - r_a$ represents the pore size of the pore geometry.

In the first case, attractive wall for interaction with monomer **A** was applied in one dimension in the pore system.

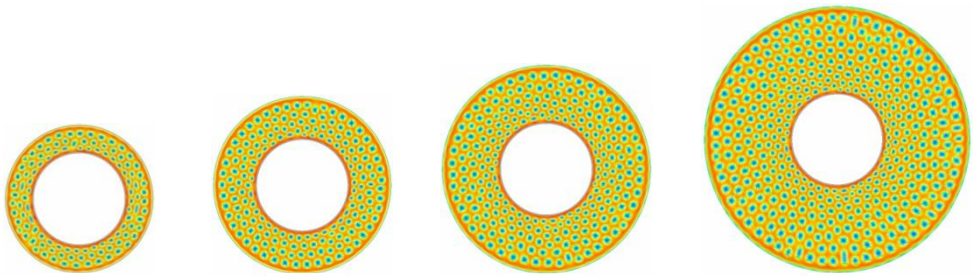

Figure 4.13: Cylindrical systems confined under interfacial circular walls having affinity to **A** block and the pore size of systems are (a) *d = 2* (b) *d = 3* (c) *d = 4* (d) *d = 6.*

The simulation results obtained in one dimensional circular confinement show that the surface preference influences the micro domains to form circular alignment in concentric circles around the centre of the pore system. Surface affinity to **A** segment of the polymer system distort the spiral alignment of the micro domains pack them in the concentric circles in the pore geometry. However, there are still micro domains packed on the rough spiral lines inside the pore system. Micro domains which had been

distorted from both spiral and circular packing were due to the packing frustration caused by interplay of both curvature and confinement effects. In pore system having pore size *d = 2* as shown in Figure 4.13(a) the cylinders were packed in three concentric circles in the pore system. The pore system with size of the pore *d = 3,* micro domains were packed in four concentric circle in the pore geometry. The pore size *d = 4,* contains cylinders packed in six concentric circles in the pore system. In this sized system micro domains are not well packed in the in circular lines due the size effect. The pore size *d = 6,* contains eight circular lines of the micro domains in the pore system. In this sized system micro domains are also not well packed in the circular lines due to the size effect.

The simulation results for diblock copolymer cylindrical system with preferential attractive circular wall with interaction between circular walls and monomer **B** were obtained in circular annular pore system. Interaction strength $\alpha = 0.6$ applied between the circular walls of the pore system and **B** segment of the polymer system in the pore geometry. Similarly, the simulation results were obtained in a pore system whose interior radius r_a *= 3* of the pore system was fixed and the pore size was extended by exterior radius r_b of the pore system, where *d* defined the pore size of the pore system.

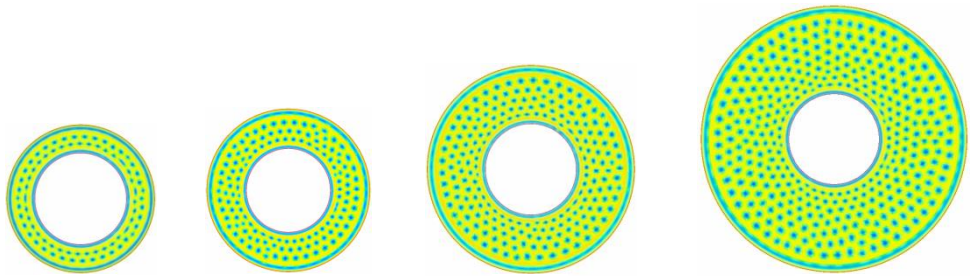

(a) (b) (c) (d)

Figure 4.14: Cylindrical systems with interfacial affinity to **B** block and the pore size of the systems are (a) *d = 2* (b) *d = 3* (c) *d = 4* (d) *d = 6.0.*

The cylindrical forming system under geometric confinement with circular walls having affinity with **B** monomer shows similar patterns as was in the case when walls had affinity with **A** monomer in the pore geometry. Microdomains are packed along the

concentric circles inside the pore system. The pore system of size $d = 2$ shows micro domains packed into two concentric circles in the pore geometry as shown in Figure 4.14(a). However, similar sized system pore walls having affinity with the **A** monomer showed micro domains are packed into three concentric circles in the pore system which is due to the incompatibility of segments of the polymer system. Incompatibility of both segments squeeze down the micro domains because the **A** segment remains outside of the micro domains and when the **B** segment was placed on the circular walls. The pore system $d = 3$ shows cylinders are packed in three concentric circles in the pore system as shown in Figure 4.14(b). Similarly the pore system $d = 4$ shows micro domains are aligned in five concentric circles in the pore geometry as shown in Figure 4.14(c). Finally the pore system $d = 6$ shows micro domains are packed in seven concentric circles in the pore system as shown in Figure 4.14(d).Simulation results show that the spiral packing of micro domains is influenced by the curvature effect whereas the micro domains packed into concentric circles due the confinement effect in the pore geometry.

4.2.4. Spherical forming system confined in circular annular pores

AB Diblock copolymer spherical forming systems is explored in circular annular pore with various sizes of pore system. Spherical morphology is investigated without interacting walls in the pore geometry as well as with interacting walls (circular walls) with one of the segment of the polymer system in the pore system. Refinement of CDS parameters were also carried for better choice of phenomenological constants.

I. Sphere forming system confined in the neutral circular annular pores

The Simulation results were obtained for spherical forming system in circular annulus pore systems with various pore sizes, by keeping interior radius of pore system fixed at $r_a = 3$ and pore size was expanded by increasing exterior radius of the pore system. Simulation results were obtained on 1 million time steps. In the pore geometry simulation results were obtained without confining circular walls. The Simulations

results for the sphere forming system were obtained by initializing the order parameters in the range $\Psi = \pm 0.5$ in the annular pore system. The following table 5 shows CDS parameter system for sphere system with higher temperature entered in the simulation.

Table 5: CDS parameters on higher temperature for sphere system

τ	f	u	v	B	D	A
0.20	0.40	0.38	2.30	0.01	0.50	1.50

The pore system is contained between two concentric circles of radii r_a and r_b, where r_a represents the interior radius of the pore system and r_b represents the exterior radius of the pore system. The interior radius of the pore systems $r_a = 3$ was fixed. The size of the pore systems was increased by increasing the exterior radius of pore systems as $r_b = 5, 6, 7, 9$. The pore sizes of the circular annular system is denoted by $d = r_b - r_a$ which shows the difference between the interior radius and the exterior radius of the pore systems.

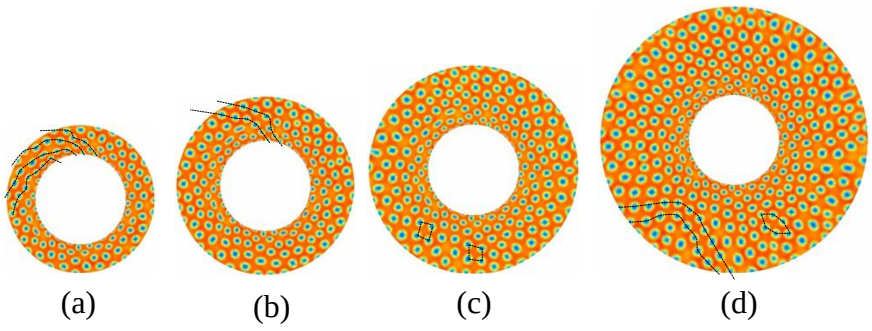

Figure 4.15: Sphere system in the circular annular pore geometry and the pore sizes are (a) $d = 2$ (b) $d = 3$ (c) $d = 4$ (d) $d = 6$.

The simulation results for sphere forming system show various arrangements in the pore system. Figure 4.15(a) shows the system with size $d = 2$, micro domains are packed along the spiral lines in the pore system. Figure 4.15(b) shows the system size $d = 3$, which also show that spheres are induced in the system along the spiral rays and spiral rays are very wide in the pore system. This shows the size effect of the system due to

the curvature in the pore geometry. However, the pore system $d = 4$, show rhombohedral arrangements of the sphere in the pore system as shown in Figure 4.15(c) by dashed lines. Furthermore, the pore system $d = 6$ show spheres are packed along the hyperbolic lines as well as hexagonal arrangements in the pore system as shown in Figure 4.15(d) by dashed lines.

The CDS parameters were investigated by the different choice of values for phenomenological constants including the high temperature parameter value. Following table shows the CDS parameters chosen for sphere forming system in circular annular pore system. The simulation results were obtained in similar pore system as above in which interior radius of the pore systems were fixed at $r_a = 3$ and pore size of the systems was extended by increasing the exterior radius of the pore systems.

Table 4 Modified CDS parameters for sphere forming system

τ	f	u	v	B	D	A
0.25	0.40	0.50	1.5	0.02	0.50	1.50

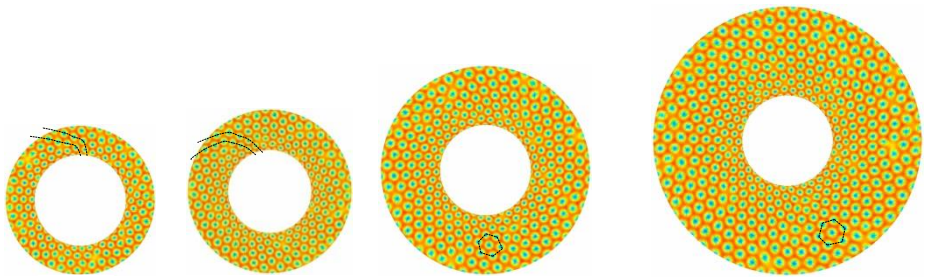

(a) (b) (c) (d)

Figure 4.16: Sphere forming system with modified CDS parameter system and pore system sizes are (a) $d = 2$ (b) $d = 3$ (c) $d = 4$ (d) $d = 6$.

The simulation results were obtained with the modified CDS parameters for sphere forming system in circular annular pore system. In the pore system with modified CDS parameter system sphere system is more ordered as compared to the previous Parameter system. Sphere systems are induced in hexagonal arrangement in the pore systems. The pore system $d = 2$ show spheres are induced along the spiral lines in the pore geometry

as shown in Figure 4.16(a). In this sized system, hexagonal arrangements of the sphere forming system in the pore geometry can be observed. The pore system *d = 3* also shows spheres are packed along the spiral lines and hexagonal arrangements of the sphere system in the pore geometry as shown in Figure 4.16(b). As pore size increase the sphere system induced along the spiral lines vanish but the sphere system remains in the hexagonal packing in the pore, the system pore system *d = 4* is shown in Figure 4.16(c). The pore system *d = 6* also shows hexagonal arrangements of the sphere forming system in the pore geometry as shown in the Figure 4.16(d).

II. Sphere system with interfacial circular walls

The simulation results were obtained for the sphere forming system in circular annulus nano pores using one dimensional confinement by placing affinity of the circular walls to the one of the segments of the polymer system. One dimensional confinement boundary conditions were applied by interior and exterior circular walls of pore system with interaction strength $\alpha = 0.2$. The CDS parameters system with low temperature as shown in table 5 is used for sphere forming system. Similar pore system was used in the simulations as was in the previous section. In the first case, the simulation results were obtained with confining interacting circular walls having affinity to the **A** monomer of the polymer system in the pore geometry.

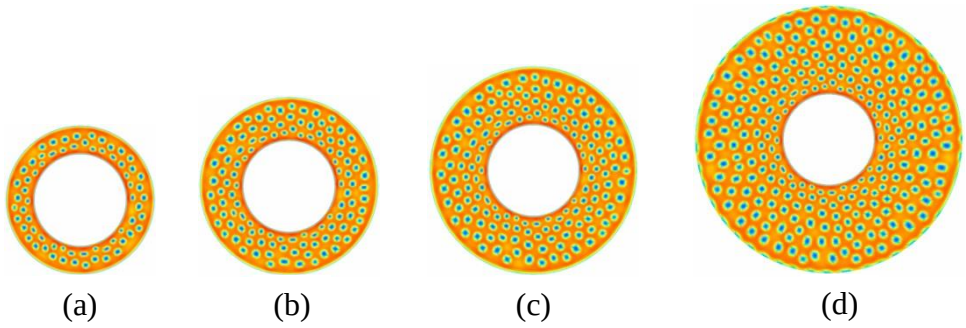

Figure 4.17: sphere forming system with system subject to the affinity of interacting walls to **A** block and system size (a) *d = 2* (b) *d = 3* (c) *d = 4* (d) *d = 6.*

The simulation results were obtained under geometric confinement in the pore geometry and show alignment in the concentric circles and rhombus arrangements. The pore system $d = 2$ show sphere aligned along two concentric circles in the pore system as shown in Figure 4.17(a). Similarly the pore system $d = 3$, show micro domains aligned along the three concentric circles in the pore system as shown in Figure 4.17(b). However, the pore system $d = 4$ show sphere packing along five concentric circles in the pore system as shown by Figure 4.17(c). Similarly the pore system $d = 6$ show micro domains are packed along seven concentric circles in the pore system as shown by Figure 4.17(d). In all system sizes spheres are also arranged in rhombus packing as well which was predicted in the unconfined system as well in previous section.

The simulation results were also obtained for sphere forming system under geometric confinement where circular walls have affinity to the **B** segment of the polymer system in the pore geometry. The interaction between the circular walls and the **B** segment of the polymer system was applied $\alpha = 0.2$ in the pore system.

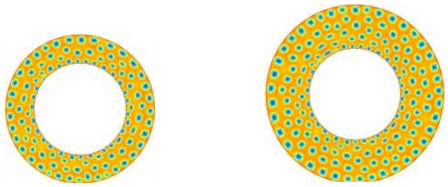

(a) (b)

Figure 4.18: Sphere system with preferential attractive wall for monomer **B** and the pore system size are (a) $d = 2$ (b) $d = 3$.

The simulation results show that the B block is not properly forming the circular walls around the pore system due to the low temperature and minority segment of the polymer system as shown in Figure 4.18. Locations of the circular walls spheres are induced in the system that shows that there is minimal impact of confinement on the polymer system in the pore geometry. The simulation results were also obtained by increasing the interaction strength between the circular walls and the **B** segment of the polymer

system but proper circular walls could not arise in the form of **B** segment around the pore system.

In the pore system simulation results were also obtained by modified CDS parameter system with high temperature, CDS parameters are shown in table 8. Similar pore system is used in the simulation results where interior radius of the pore system is fixed at $r_a = 3$ and pore size expanded by the exterior radius r_b of the pore system.

In the first case interacting circular walls applied around the pore system having affinity to **A** segments of the polymer system in the pore geometry. Interaction strength between the circular walls and **A** segment of the polymer system set at $\alpha = 0.2$ in the pore geometry.

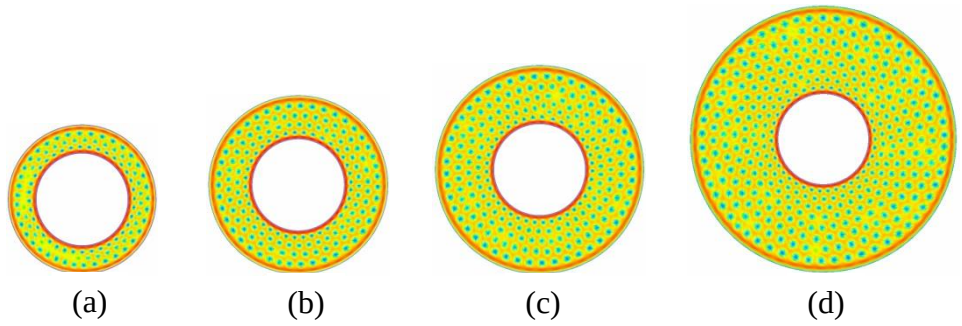

Figure 4.19: Sphere forming system with modified CDS parameter system subject to the affinity of interacting walls to A block and system sizes are (a) *d = 2* (b) *d = 3* (c) *d = 4* (d) *d = 6.*

The sphere forming system obtained by modified CDS parameter system under confinement having affinity of circular walls to the **A** segment of the polymer system show micro domains are packed along perfect concentric circles in the pore geometry. In this system micro domains are squeezed down under geometric confinement in the pore geometry. The pore system *d = 2* show spheres packed in three concentric circles as shown in Figure 4.19(a). Due to the squeezing down the micro domains we observed one extra circular line of the sphere system as compared to previous confined results with CDS parameter system with low temperature in the pore system. The pore system *d = 3*, shows micro domains are packed in four concentric circles in the pore system as

shown by the Figure 4.19(b). Similarly the pore system *d = 4,* displays five rings packed with sphere system in the pore geometry as shown in Figure 4.19(c). The pore system *d = 6,* shows spheres are induced into eight rings of concentric circles in the pore geometry. This shows that under geometric confinement sphere system induces into the rings in the pore geometry. It can be easily observed that spheres are also arranged in hexagonal packing in the pore geometry under geometric confinements.

The simulation results were also obtained for sphere forming system by modified CDS parameter system using interacting walls having the affinity to the **B** segment of the polymer system in the pore geometry. The interaction strength between the circular walls around the pore system and the **B** segment of the polymer system applied is $\alpha = 0.6$ in the pore system. The pore system is similar with the interior radius of the system is fixed at r_a *= 3* and the pore size is extended by the increasing the exterior radius r_b of the pore systems.

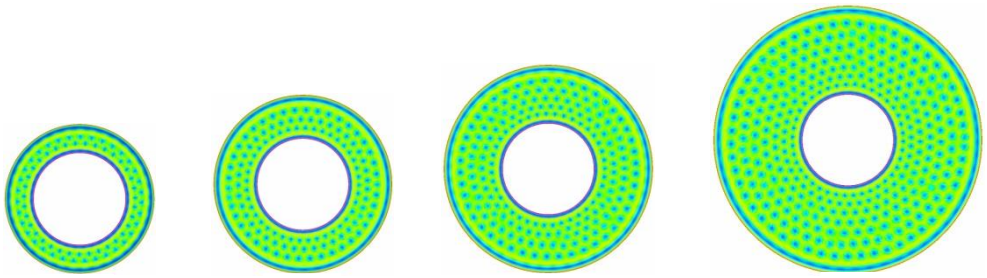

(a) (b) (c) (d)

Figure 4.20: Sphere forming system with modified CDS parameter system subject to the affinity of interacting walls to **A** block and system size (a) *d = 2* (b) *d = 3* (c) *d = 4* (d) *d = 6.*

The simulations results were obtained by placing interacting walls having affinity to the **B** monomer of the polymer system in the pore system. The simulation results show circular alignment in the concentric circles around the pore system in the pore geometry as shown in Figure 4.20. Microdomains in this case squeezed down their size due the frustration caused by the preference of the minority segment on the boundary walls in the pore system. Microdomains are also packed in rhombus arrangements in the pore system. Figure 4.20(a) show the pore system with size *d = 2* micro domains are induced

into two concentric circles between the circular walls occupied by the **B** segment of the polymer system in the pore geometry. The pore system with size *d = 3,* in Figure 4.20(b) show spheres are packed in three concentric circles in the pore geometry surrounded by the circular walls occupied by the **B** segment of the polymer system. Similarly the pore system having size of the pore *d = 4,* show microdomains are induced into the four concentric circles in the pore system surrounded by the **B** segment of the polymer system in the pore geometry as shown in Figure 4.20(c). The pore size system *d = 6,* shows spheres packed into seven concentric circles surrounded by the circular walls containing **B** segment of the polymer system in the pore geometry. The experimental studies [86, 87] show that the confinement distorts the natural packing arrangements of the microdomains.

4.3. Summary

Using CDS method employed in polar coordinate system we obtained novel nanostructures in the circular pore geometry for lamella, cylinder and sphere forming systems. Asymmetric lamella forming system in the neutral film interfaces shows perpendicular to the exterior circumference and parallel to the interior circumference tendency in the circular pore system. Grain boundaries confined in the circular pore geometry show various formations of lamella including Y-shape, U-shape, W-shape, V-shape and T-junctions. Fingerprint morphology confined in the neutral circular pore with various pore thicknesses induced clusters of perforated holes, isolated perforated holes and star lamella with perforated hole at the centre of star. Close to the exterior pore boundary, lamellae conforms concentric parabolic patterns having openings in the direction of outer boundary, however for larger system sizes these parabolic patterns evolve into the parallel lamella strips normal to the outer circular boundary. The pore system with large the interior radii shows parallel strips lamellae normal to the circular

pore boundaries. The interplay of both interfacial circular walls and curvature influence induces lamella into the concentric circular rings in the circular pore geometry. In the presence of interfacial circular walls, concentric alternating lamella (onion-like) nanostructure were obtained in the circular pores which are strongly consistent with experimental results. Results show that under the influence of curvature and interfacial circular walls, the microdomains tend to form concentric lamella in the pore geometry. Symmetric lamella system induces defective nanostructures in the circular pore geometry.

Cylindrical forming system in the neutral circular annular pore system shows, the novel packing arrangements along the spiral lines. However, in the larger pore systems spiral packing arrangements alters and system regains in the classical hexagonal packing arrangements in the circular pore system. While, in the presence of interacting circular walls microdomains induces packing arrangements in the concentric circular rings in the pore geometry.

Similarly, sphere forming systems show, packing arrangements along the spiral lines, parabolic lines with opening along the outer boundary and hexagonal packing arrangements in the pore system. A new set of CDS parameters for sphere forming system were also introduced in the study. Results obtained with modified CDS parameters show that small system size induces sphere along the spiral curve, while large circular pore system induces sphere in the classical hexagonal packing arrangements. In the presence of interfacial circular walls, the sphere system with modified CDS parameters was squeezed down in size and shape. The sphere system under geometric confinement of annular circular pores with the interfacial circular walls shows, packing arrangements in the concentric circular rings. The results show that under the influence of the curvature nanodomains show spiral packing arrangements,

while, due to the interplay of both curvature and interfacial circular walls microdomains forms packing arrangements in the concentric circular rings in the pore geometry.

CHAPTER FIVE

5. Block copolymers confined in cylindrical pores

5.1. Introduction

Block copolymer were investigated under the geometric confinements of hollow cylindrical pores using the CDS method employed in the cylindrical coordinate system. Lamella, cylinder and sphere forming systems are obtained in the cylindrical pore geometry. Formations of lamella, cylinder and sphere morphologies were obtained in cylindrical surfaces with various pore radii and pore lengths. The results were obtained for block copolymers confined in neutral cylinders pores and with interfacial surfaces. In the case of interfacial surfaces, symmetric boundary conditions were applied on the pore interfaces. The interaction strength between the pore walls and the majority segment of the polymer system is represented by parameter α. The results for block copolymers confined in the cylindrical pore were obtained with various interaction strengths in the pore geometry. In the case of interfacial cylindrical surfaces results were also obtained by applying two dimensional interfacial surfaces. Two dimensional interfacial surfaces were applied by parallel to the pore surface circular walls and perpendicular to the pore surface covering top and bottom of the cylindrical pores. For the parallel interfaces boundary conditions were applied on the radial coordinate of the lattice, while, for perpendicular interfaces boundary conditions were applied on the length coordinate *z* of the pore lattice. In the cylindrical pores, results were obtained by keeping the interior radius r_a fixed, while, the pore size was expanded by increasing the exterior radius r_b of the pore surface. The results were obtained for block copolymers confined in cylindrical surfaces by applying periodic boundary conditions on the

angular coordinate θ and pore length coordinate *z*. In addition, results were obtained by applying reflective boundary conditions on the radial coordinate *r*.

5.2. Results and discussions

The **AB** diblock copolymer lamella forming system, cylindrical forming system and spherical forming patterns were investigated in hollow cylindrical nano channels using the CDS method employed in the cylindrical coordinate system. Study and analysis were carried out for diblock copolymers with neutral surfaces and with confining interacting walls. The simulation results in cylindrical pore system were obtained under one-dimensional geometric confinement as well as two-dimensional geometric confinements are presented. The simulation results were obtained using an initial random disordered state for order parameter (ψ) which was a random number within the range $\Psi = \pm 1$. All the simulations were carried out on 1 million time steps using CDS method employed in cylindrical coordinate system.

5.2.1. Lamella forming system confined in cylindrical pores

The AB diblock copolymer asymmetric lamella forming system was investigated in cylindrical nano channels. The CDS simulation results for lamella forming system were obtained by applying asymmetric volume fraction parameter system. The asymmetric volume fraction is used with $f = 0.48$ which is different from the case $f = 0.50$ as shown in results of circular annular pore system in chapter 3 that asymmetric parameter system works well as compared to symmetric lamellae system in the pore geometry.

I. Lamella system confined in neutral cylindrical pores

In the first case, the simulation results were obtained in a pore system without applying preferential interacting walls around pore system. The simulation results were obtained with various pores sizes and pore radii of the pore geometry.

Table 5: CDS parameter system for asymmetric lamella forming system

τ	f	u	v	B	D	A
0.36	0.48	0.38	2.30	0.02	0.70	1.50

In the first case simulations results are obtained for asymmetric lamellae system in the cylindrical pore system where the interior pore radius was fixed at $r_a = 3$ and the pore size were varied by the exterior pore radius r_b. The pore size is defined by $d = r_b - r_a$, where r_a represents interior radius of the pore system and r_b represents the exterior radius of pore system. The length of the pore system was kept fixed $h = 4$ and angular coordinate was varied $0 \leq \theta \leq 2\pi$ in all simulation results.

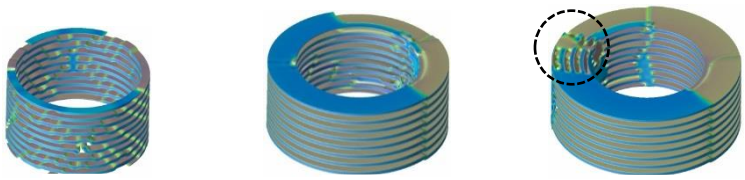

(a) (b) (c)

Figure 5.1: Lamella system confined in neutral cylindrical pores, with pore system where interior radius was fixed at $r_a = 3$ and the pore size (a) $d = 0.5$ (b) $d = 1.5$ (c) $d = 2$.

The simulation results in the pore system with the interior radius fixed at $r_a = 3$ show helical morphology of lamellae system in the pore geometry. The pore size $d = 0.5$ system show single helix of patchy lamella in the pore system as shown in Figure 5.1(a). However, the pore system with size $d = 1.5$, show single helix of flat lamella in the pore system as shown in Figure 5.1(b). Furthermore increasing the size of the pore system $d = 2.0$ we get single helix of lamella with defect in the section where lamellae becomes parallel to the pore walls as shown by dashed lines in the Figure 5.1(c).

In the second case, the simulation results are obtained in a pore system with interior pore radius was fixed as $r_a = 5$ and pore size were varied by the exterior pore radius r_b. The pore size is defined by $d = r_b - r_a$, where r_a represents the interior radius of the pore

system and r_b represents the exterior radius of pore system. The length of the pore system was fixed at $h = 4$ and angular coordinate was varied $0 \le \theta \le 2\pi$ in all the following simulation results.

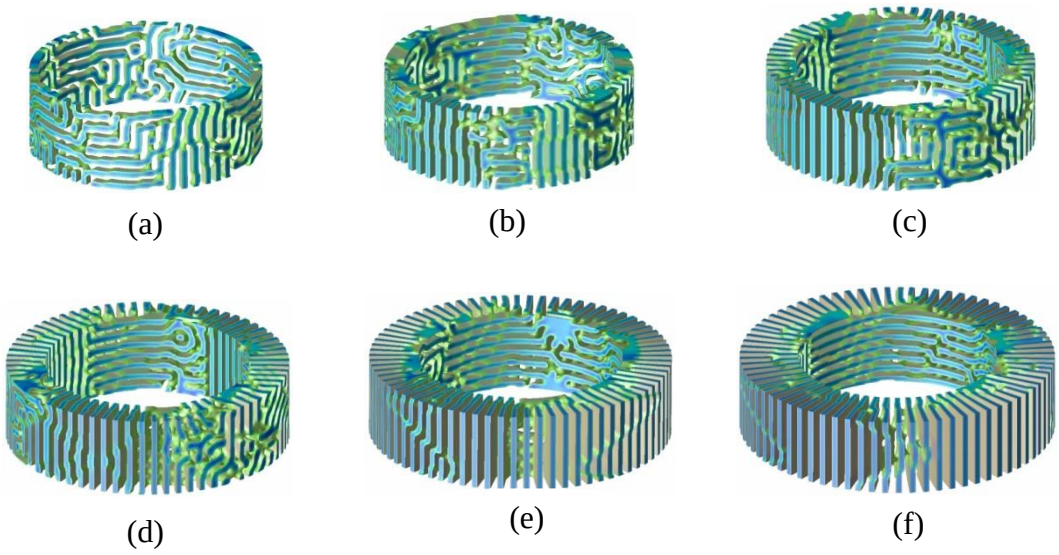

Figure 5.2: Lamellae system confined in the neutral cylindrical pores, interior radius of pore system fixed at $r_a = 5$ and pore size (a) $d = 0.5$ (b) pore size $d = 1$ (c) $d = 1.5$ (d) $d = 2$ (e) $d = 2.5$ (f) $d = 3$.

The simulation results of the lamella system confined in neutral surfaces shows sequences of lamellae sheets flaked in circular alignment mostly perpendicular to the pore system. In narrow pore system (pore size $d = 0.5$), long curved strings of lamellae were found which are parallel to the pore as shown in Figure 5.2(a). Parallel to the pore patterns of lamellae system forms due to the size effect. Increasing the size of pore system ($d = 1.0$) result is shown in Figure 5.2(b) these lamellae strings adapt sheets structure parallel to the pore system and perpendicular to the pore system. Further increasing the size of the pore ($d = 1.5$), most these lamellae sheets became perpendicular to the pore system. This shows that increase in the pore size of the system lamellae sheets tends to perpendicular to the pore system. The pore system shows that micro domains on the interior boundary of the pore system tend to become parallel to the pore system while rest of the micro domains tend to perpendicular to the pore system in the pore geometry. The simulation results show that increasing the pore size of the pore system lamellae tend to become perpendicular to the pore system in the pore

geometry. The pore system with size *d = 3,* show perpendicular to the pore lamellae system in the pore geometry as shown in Figure 5.2(f).

I. Lamella system with interfacial surfaces

Computational results were obtained in the cylindrical pore system with applying preferential attractive walls around polymer system. The strength of interaction between circular walls and one of the blocks of polymer system is defined by the parameter α in the pore system. In first case, preferential affinity to the pore surface for one of the blocks set at $\alpha = 0.2$. Simulation results were obtained by one-dimensional confinement in radial direction so that polymers are confined between two concentric circular walls parallel to the pore system.

In the first case, interior radius of the pore system was fixed at $r_a = 3$ and exterior radius r_b of the pore system increased to expand the pore system.

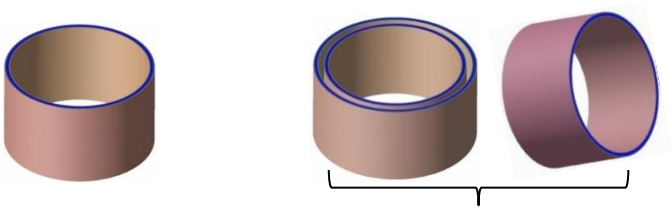

(a) (b)

Figure 5.3: Lamella system with interfacial surfaces, the pore system with interior radius fixed at $r_a = 3$ and the pore sizes are (a) *d = 1.0* (b) *d = 1.5.*

The simulation results under geometric confinement show concentric lamellae cylindrical sheets in the pore geometry system. In the pore system *d = 1* show single lamella cylindrical sheet under the influence of the geometric confinement in the pore system as shown in Figure 5.3(a). However, in the pore system with pore size *d = 1.5,* we observed two concentric lamellae sheets in the pore system under the influence of geometric confinements by circular parallel walls as shown in Figure 5.3(b) along with interior layer of the pore system.

In the next case, the interior radius of the pore system was fixed at $r_a = 5$ and exterior radius r_b of the pore system increased to expand the pore system.

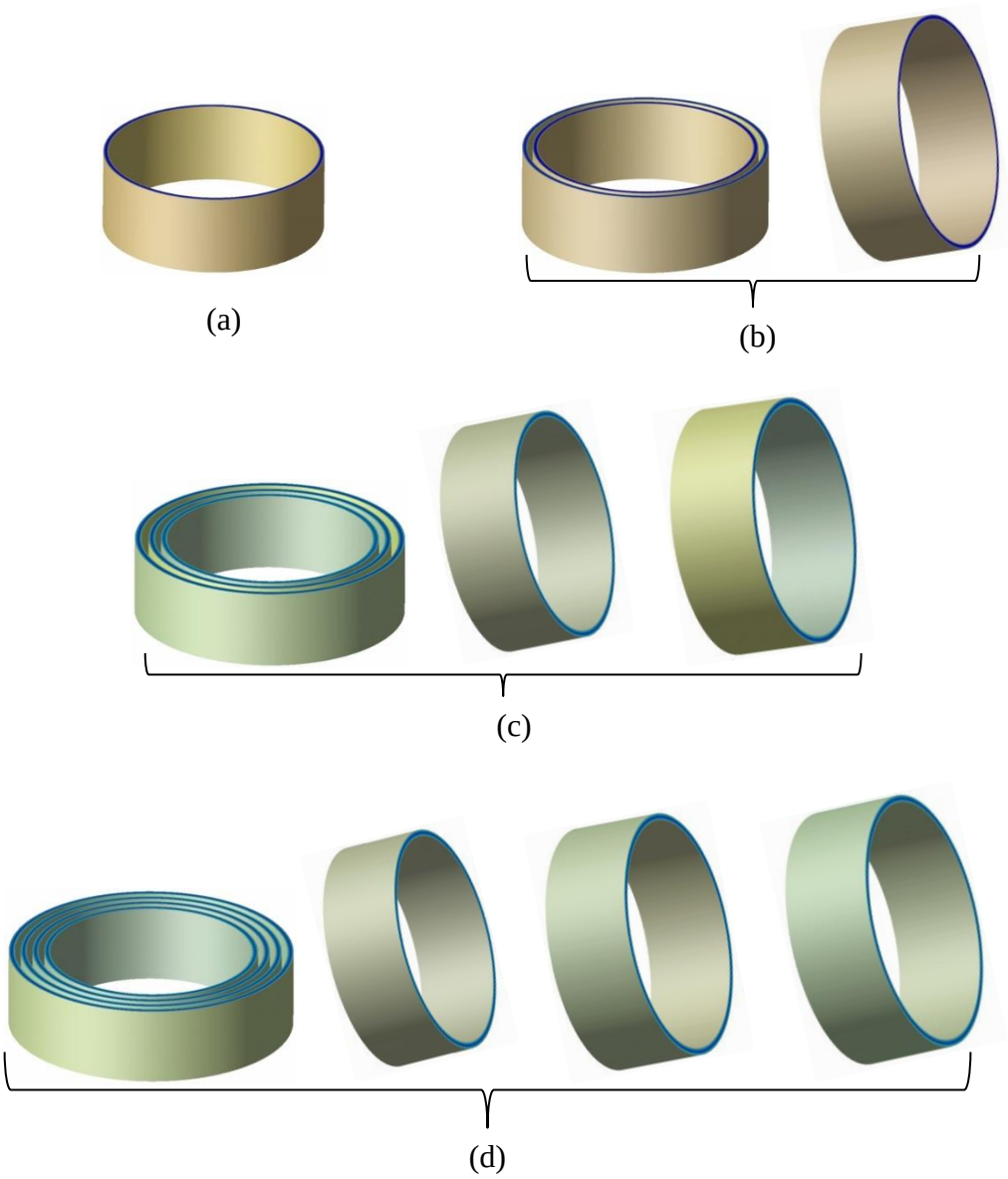

Figure 5.4: Lamella system with interfacial surfaces, interior radius of the pore surface was fixed at $r_a = 5$ and the pore sizes are (a) *d = 1.0* (b) *d = 1.5*(c) *d = 2.5* (d) *d = 3.0.*

Under geometrical confinement diblock copolymer lamellae forming system in cylindrical pores displays concentric lamellae cylindrical sheets for preferential affinity of surface to one of the monomer of the polymers system. It shows that lamellae plates appeared in the unconfined system shown in previous section results transformed into cylindrical sheets under geometrical confinement in the pore system. These results show

consistency with what we have achieved in simulation results obtained in annular circular pore system with one-dimensional confinement. Perfect parallel cylindrical sheets of lamellae system is a results of both curvature and confinements. In the system with dimensions (*d = 1.0)* have appeared with single-layer of cylindrical sheet of lamella parallel to the pore system as shown in Figure 5.4(a). The Pore system with size and length (*d = 1.5),* displays two layers of lamellae sheets parallel to the pore system as shown in Figure 5.4(b) with interior layer of lamellae sheet adjacent to the image. For pore size and length (*d = 2.5),* the obtained results show three lamellae layers of cylindrical sheets parallel to the pore system shown in Figure 5.4(c) with both interior layers adjacent to the main image. The cylindrical pore system with size and length (*d = 3.0),* shows four lamellae layers of cylindrical sheets parallel to the pore system as shown in Figure 5.4(d). In the pore system strong interaction strength $\alpha = 0.4$ also applied between the majority segment of the polymer system and surface walls but in this case, similar results were observed in the pore geometry. The concentric lamella (onion-like) structure were obtained here are very much consistent with the results obtained for lamella system confined in cylindrical pore by the experimental work [57] shown in Figure 3(a) therein.

Subsequently, results were obtained by applied interfacial surfaces to the majority segment of the polymer system in *z* direction covering top and bottom of the cylindrical pore system through cross sections. The strength of interaction between microdomains and surface walls was same $\alpha = 0.2$ and was applied in perpendicular to the pore system. In the experimental study of PS-*b*-PBD lamella confined in the cylindrical pores concentric cylinder morphology formed within the cylindrical pores, in addition, study show the number of cylinders depends on the ratio of the pore diameter to the equilibrium period of the copolymer [87]. The concentric-layered morphology of lamella system was also obtained in cylindrical pore by the experimental study [15].

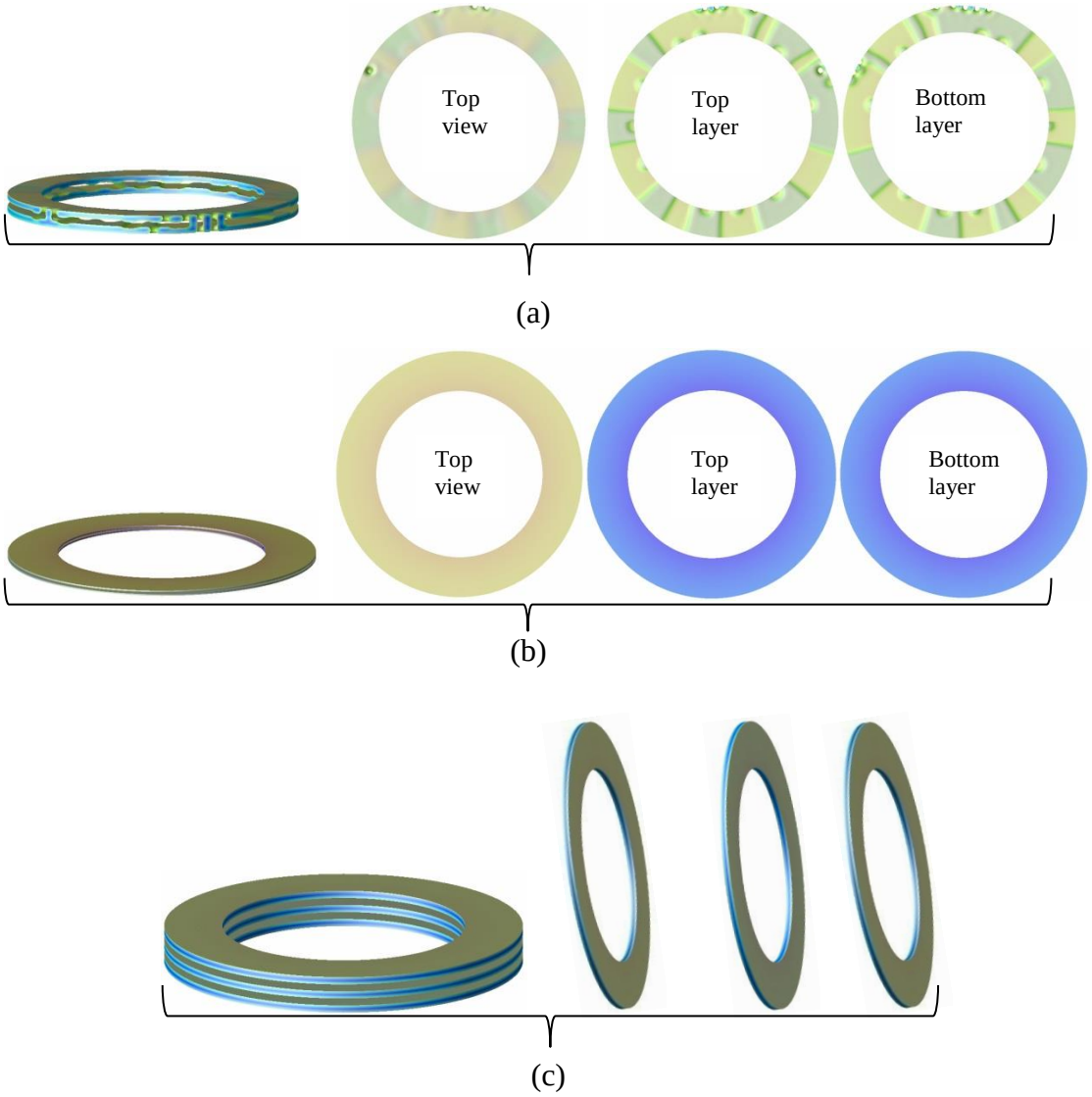

Figure 5.5: Cylindrical system confined by interfacial surfaces perpendicular to the pore system and the pore size and pore lengths are (a) $d = 1.6$ and $h = 1.6$ (b) $d = 2.5$ and $h = 1.0$ (c) $d = 2.5$ and $h = 2.5$.

In the system with interacting boundary walls applied in z direction system shows circular disks perpendicular to the pore system. Lamellae cylindrical sheets parallel to the pore system in parallel confinement transformed into disks perpendicular to the pore system in perpendicular confinement due to preferential affinity of the surface changed from parallel walls to perpendicular walls. In the pore system shown in Figure 5.5(a) there are two disks in the system one on top of each other. The top view of the system with top layer and bottom layer of the system also shows adjacent to the image Figure 5.5(a). The obtained disks are not flat from inside and are connected with each other at four points at the exterior boundary of the pore system. Inside the disks there are thick

layers patterned on the interior surface of disks and the outer surface of disks is flat. This is due the interaction of polymer blocks with each other. Subsequently squeezing domain size (*d = 2.5* and *h = 1*) system shown in Figure 5.5(b) two very thin layered disks appeared in the pore system. The image of the system shown in Figure 5.5(b) is followed by the top view of pore system and top and bottom layers of the pore system. The surface of the disks is quite flat and very thin. Both blocks of polymer system segregated well so that both blocks are clearly visible. Both blocks of the polymer system segregated in the form of plate layers where one block is on top of the layer whereas second is on bottom of layer of the disk. Despite of squeezes the domain size both disks are not connected to each other and there is very narrow space between the disks. However, in the system of equal size and length (*d = 2.5* and *h = 2.5*) three parallel flat disks appeared in the pore system perpendicular to the pore system as shown in Figure 5.5(c) along with the interior-layers. It shows quite good agreement with the result of parallel confinement, in which there were three cylindrical parallel sheets of cylinders, the pore system shown in Figure 5.4(c). This shows that in cylindrical confinements parallel confinement induces parallel cylindrical sheets of lamellae and perpendicular confinement induces perpendicular lamellae sheets.

The last, two dimensional confinements' results were investigated in cylindrical pore geometry. In two dimensional confinements one of the monomer of polymer system has preferential affinity to the pore surface and the pore system was confined between parallel walls and perpendicular walls around the pore system. For two-dimensional confinements here boundary conditions are applied in the radial direction and height *z* direction. The interaction between walls and one of the blocks of the polymer system was applied $\alpha = 0.2$ in the pore system.

(a) (b)

Figure 5.6: Two dimensional confinement of cylindrical system with the pore sizes and the pore lengths are (a) $d = 1.0$ and $h = 1$ (b) $d = 1.0$ and $h = 1.6$.

The simulation results were obtained under two-dimensional confinements show perfect circular rings. The pore system shown in Figure 5.6(a) under two-dimensional confinements a perfect circular cylindrical ring parallel to the pore system appeared. The pore system with the increased size of pore also shows circular ring but here in this pore system circular ring consists of two cylinder one on other. This shows that, under the effect of two-dimensional confinements and the narrow size cylindrical pore, lamellae segregated into cylindrical system in the pore geometry.

5.2.2. Cylindrical forming system confined in cylindrical pores

In this section, the diblock copolymer cylindrical forming system was investigated with various cylindrical dimensions of pore system, pore radii and pore length by using the CDS method functional in cylindrical coordinates. The polymer system was investigated without confining surfaces (neutral surfaces) as well as preferential attractive circular walls having affinity to the majority segment of the polymer system. The results were also obtained by one-dimensional confinement and two-dimensional confinements.

I. Cylindrical forming system confined in neutral surfaces

In this section, the results of diblock copolymer cylindrical forming system confined in cylindrical pores are presented and discussed. The CDS parameters were used in the computation are $\tau = 0.30$, $f = 0.40$, $u = 0.50$, $v = 1.5$, $B = 0.02$, $D = 0.50$ $A = 1.5$. Simulation results were obtained in various pore sizes by keeping the interior radius r_a fixed and the pore size of system was expanded by the increasing the exterior radius r_b

of the pore system. The length of the pore system was fixed at $h = 4$ and angular coordinate varied $0 \le \theta \le 2\pi$ in the pore system. The pore size of the system is defined by $d = r_b - r_a$, where r_a denote the interior radius of pore system and r_b denote the exterior radius of the pore system. All the simulation results were carried out without confining walls (neutral pores) around the pore system and were carried out on one million time steps.

In the first case, the simulation results were obtained for cylindrical forming system in a pore system in which the interior radius was fixed at $r_a = 3$ and the exterior radius r_b of the pore system were increased to expand the pore size of the system.

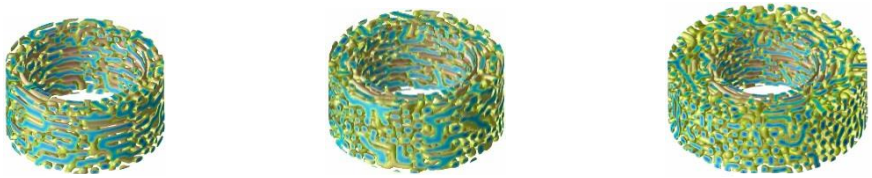

(a) (b) (c)

Figure 5.7: Cylindrical forming system confined in neutral surfaces, in a pore system with the interior radius fixed at $r_a = 3$, the pore sizes of the system are (a) $d = 1$ (b) $d = 1.5$ (c) $d = 3$.

The simulation results for cylindrical forming system in the pore system are oriented parallel to the pore system in a small sized system. However, with increasing size of the pore system the cylinders change their orientation perpendicular to the pore system. The pore system $d = 1$ show cylinders parallel to the pore system in the pore geometry as shown in Figure 5.7(a). While, increasing the size of the pore system $d = 1.5$ cylinders became perpendicular to the pore geometry as shown in Figure 5.7(b). The bigger size pore system $d = 3$ show most of the cylinder are perpendicular to the pore system as shown by Figure 5.7(c). This shows that cylinder under the influence of the curvature turn to be parallel to the pore system in smaller sized systems, while, in larger sizes system due to nominal curvature they reorient themselves perpendicular to the pore system. Furthermore, in the larger sized systems cylinders are still observed parallel to

the pore system due the effect of the curvature. Cylindrical forming system in the pore geometry also shows a few defects in the form of spheres. Cylinders in the pore system show rhombus packing arrangement and Y-shape formation under the influence of the curvature.

In the second case, the interior radius of pore was fixed at $r_a = 5$ in all simulation results, while, the pore size of the system was increased by using various values of the exterior radius r_b of the pore system. The cylindrical morphology was obtained without interacting wall (neutral pores) and shows short straight cylinders and curved cylinders, most of cylinders are perpendicular to the pore axis in the pore geometry. Short straight cylinders which are perpendicular to the pore system form in the pore geometry due to the minimal curvature effect. In the Figure 5.8(a), cylindrical system obtained in narrow cylindrical channel (pore size $d = 0.5$), where short straight cylinders can be observed oriented perpendicular the cylindrical axis. Short straight cylinders are hexagonally packed as shown in zoom snapshot below the Figure 5.8(a). Increasing the pore size of the system ($d = 1$) and decreasing length ($h = 2.8$) of the pore system we get similar cylindrical system, however some short cylinders showed mixed orientation as shown in Figure 5.8(b). In this system very few defects in the form of spheres were also observed. The system shows parallel, perpendicular and oblique cylinders. For the pore system obtained for dimensions of the pore ($d = 1.5$ and pore length $h=4$) shown in Figure 5.8(c) results shows the mobbed of short cylinders mostly oriented perpendicular to the pore axis. This system also shows very few spheres and few cylinders with mixed orientation. In this system a very few long cylinders observed with oblique orientation. Micro domains vary in size, shape and orientation in the pore system.

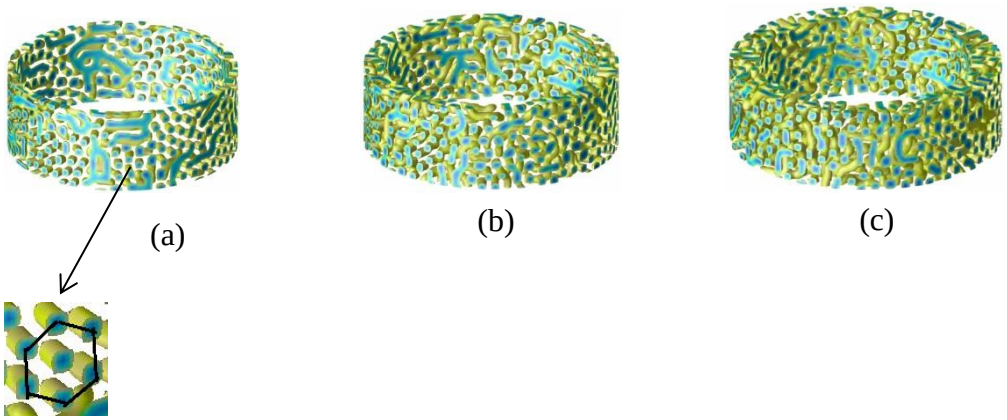

Figure 5.8: Cylindrical morphology in the neutral cylindrical pores with a pore system whose the interior radius was fixed at $r_a = 5$ and the pore size of systems are (a) *d = 0.5* (b) *d = 1.0* (c) *d = 1.5.*

I. Cylindrical system with interfacial surfaces

The value of α at the boundary describes the preference of one copolymer block to the surface of the pore system. For the interaction between wall and copolymer, we set the strength of interaction between surface wall and one of polymer block at $\alpha = 0.2$. The simulation results are obtained in different pore systems using one dimensional confinement of parallel circular walls around the pore system.

In the first case simulation results were obtained in a pore system whose interior radius was fixed at $r_a = 3$ and the exterior radius r_b of the pore system was increased different values to expand the pore size of the system. Surface interaction strength to the majority segment of the polymers system was applied with $\alpha = 0.2$ in the pore system.

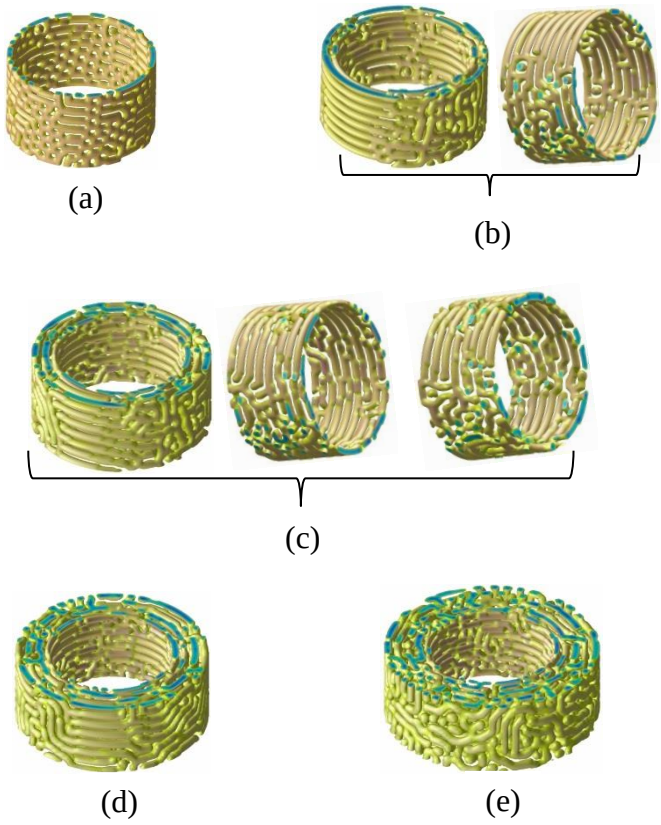

Figure 5.9: Cylinder system under interfacial surfaces in a pore system with the interior radius fixed at $r_a = 3$ and the pore sizes of system are (a) *d = 1* (b) *d = 1.5* (c) *d = 2* (d) *d = 2.5* (e) *d = 3*.

The cylinder forming systems under influence of surface interaction in a pore system which has the interior radius fixed at $r_a = 3$ show cylinders are wrapped around the pore system and perforated morphology in the pore system. In the narrow channel size pore system with pore size *d = 1* pore system displays single layer of polymer system with perforated morphology as shown in Figure 5.9(a). The pore size *d = 1.5,* system show two-layered system where straight cylinders wrapped around the pore system as shown in Figure 5.9(b) with interior layer of the system. This pore system also displays few defects in the form of perforated holes, short cylinders and spheres in the pore geometry. The pore system with pore size *d = 2,* show three layered system where straight cylinders are wrapped around in the pore system and having similar defects of perforated holes and spheres in the pore geometry as shown in Figure 5.9(c) along with interior layers of the system. Wrapped cylinders forms due to the curvature effect in the pore system. Similarly the pore system *d =2.5,* show four layers of the micro domains

in which cylinders are also wrapped around the pore system and this system is less defective as compare to other systems, pore system is shown in Figure 5.9(d). As we increased the size of the pore system to *d = 3*, we observed cylinders with mixed orientation including parallel to the pore system and more defective system as shown in Figure 5.9(e). Simulation results show that due to the interplay of both curvature and confinement cylinders are wrapped around the pore system in the pore geometry.

In the second case, the pore system was designed by keeping the interior radius fixed at $r_a = 5$ and pore size was increased by taking different valued of the exterior radius r_b of the pore system. The simulation results were obtained for characteristic case in which the pore wall is attractive to the majority of the block of the polymer system in the pore geometry.

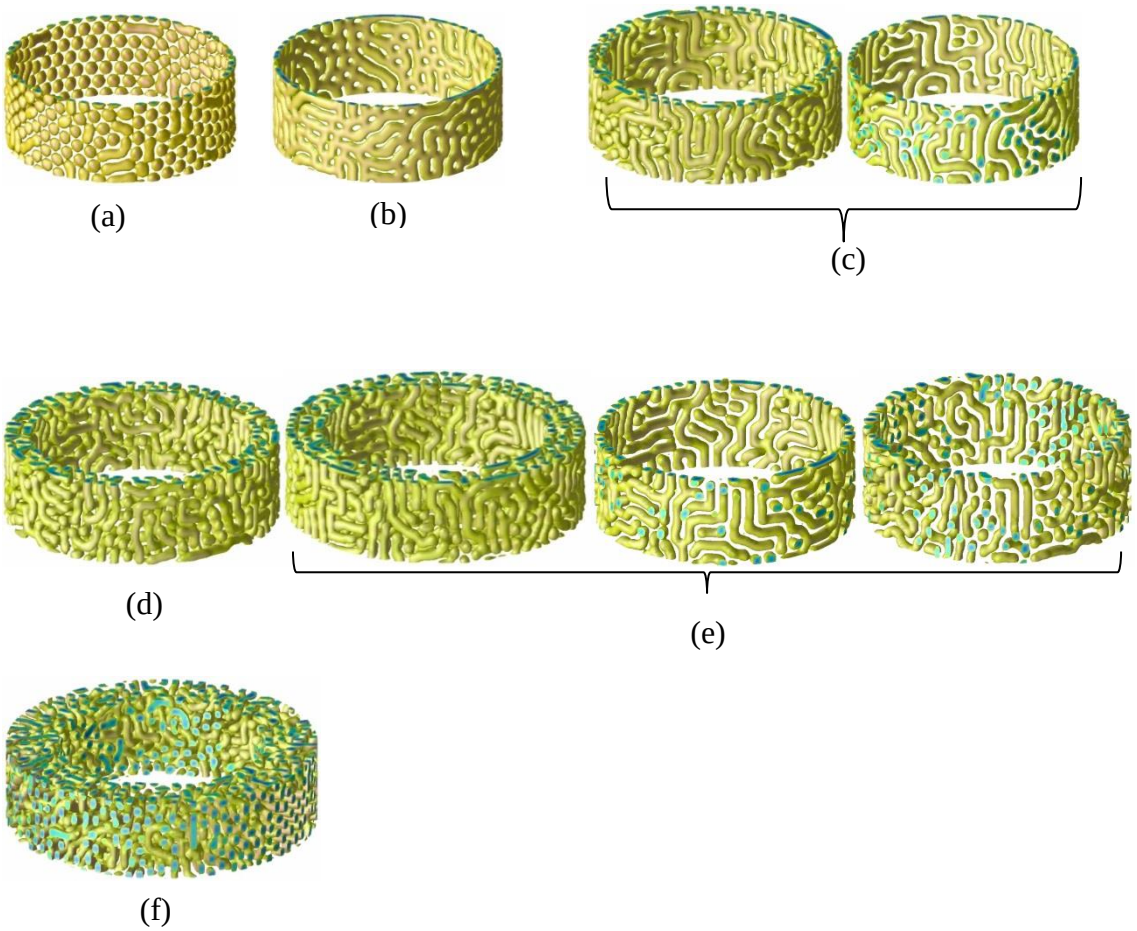

Figure 5.10: Cylindrical forming system under surface interacting parameter $\alpha = 2$, the interior radius of pore system is fixed at $r_a = 5$, the length of pore was fixed at $h = 6, 0 \le \theta \le 2\pi$ and the pore sizes are (a) *d = 0.9* (b) *d= 1.0* (c) *d = 1.5* with the interior layer (d) *d = 2* (e) *d = 2.5* (f) *d = 3.*

The results under geometrical confinement show that under the influence of preferential attractive circular walls cylinders show mixed behaviour. The curved cylinders form different formations under confinement U-shape cylinders, Y-shape cylinders and W-shape cylinders. Perforated lamellae PL morphology observed here in the system for the case when pore size was $d = 1$ under geometrical confinement.

In the narrow cylindrical pore size system ($d = 0.9$), we get the system in single-layer and micro domains became compressed and loosed their structural formation only very few micro domains able survive in their structural morphology in the pore system as shown in Figure 5.10(a). With pore size (pore size $d = 1.0$) system turned into perforated morphology with few cylinders oriented parallel to the pore system and oblique Figure 5.10(b) shows the results. In this case also we get a single layered system. Increasing the pore size of the system by expanding the exterior radius of pore ($d = 1.5$), we get bi-layered system inside the pore system. In this system a very few perforated holes are observed and rest of the system displays curved cylinders. Microdomains are oriented parallel to the pore axis and oblique. Figure 5.10(c) shows the system with interior layer adjacent. The microdomains were observed are long cylinders with few defects of spheres in the pore geometry. There are also some cross sectional cylinders apparent in interior layer of the system. Increasing further size of the system ($d = 2.0$) shown in Figure 5.10(d) system is more defective as compared to previous one in the proe system. The cylinders in the pore system are diversely oriented. For the pore size ($d = 2.5$) system shows three layers of cylinder system with mixed orientation in the pore system as shown in Figure 5.10(e) along with two interior layers. In this system orientation of curved cylinders remained diverse this mean that preferential attractive wall effect is weak in the pore system. Increasing the pore size bit more ($d = 3$) system show cylinders oriented perpendicular to the pore system in the

pore geometry as shown in Figure 5.10(f). This shows that long sized pore system curvature and confinement influence is nominal.

The cylindrical forming system investigated in narrow channels keeping the fixed pore size $d = 1$ by keeping the interior radius of pore fixed at $r_a = 5$, the exterior radius of pore at fixed at $r_b = 6$, while angular coordinate varied $0 \le \theta \le 2\pi$ however, length of pore varied from $h=1$ to different values ranging from $h=1$ to $h=4.0$ are shown in Figure 5.11. Simulation results are obtained on one million time steps with preferential attractive walls. Length of cylindrical pore was varied to check influence of confinement on different layers of cylinders. The circular wall interaction with one of block was set at $\alpha = 0.2$ in the pore system. The cylindrical system was investigated by one dimensional confinement and two dimensional confinements. In one dimensional confinement circular walls were placed parallel to the pore axis and two dimensional confinements in addition to the parallel to the pore walls the top and bottom covering walls were placed confining the pore surface perpendicularly through cross sections of the pore system. Figure 5.11 shows the results obtained with various lengths of pore.

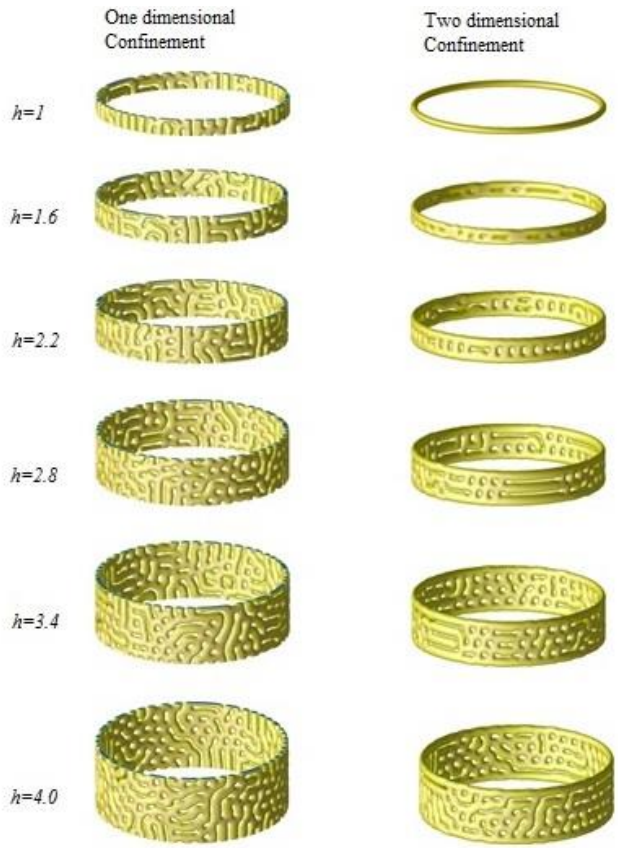

Figure 5.11: Cylindrical forming system with fixed pore size *d =5*, whereas, the height was varied for different values of lattice.

In the first case when was *h=1* simulation results under one dimensional confinement show most of the cylinders are oriented parallel to the cylinder axis due to the wall interaction. In one dimensionally confined system very few perforated holes can be observed. Interestingly with two dimensional confinements we obtained just one cylinder perfectly in the circular ring shape. Perfectly a circular ring cylinder obtained due to the two factors one is curvature effect and other is due to the interacting circular walls. Further height of pore increased *h=1.6* to study bi-layered cylinder with one dimensional cylinder oriented parallel to the axis of cylinder, parallel to the circumference of cylinder and oblique. However with two dimensional confinements we obtained the ring containing two circular cylinders one on other and between these cylinders perforation morphology observed. For the *h=2.2* system three layers of cylinders not observed in two dimensional confinement which shows third cylinder in between the two cylinder is distorted by internal energies and due to this perforated

morphology is developed between the cylinders.. As we moved forwarded by increasing height, we find more perforated morphology appeared in one dimensional confinement and in two dimensional confinements perforated morphology is observed between parallel to the pore cylinders. Perforated morphology was also observed in planer and cylindrical confinement [10]. Similar patterns of parallel cylinders to the axis of pore and perforated morphology under two dimensional confinements can be observed in [87] where you can see there in Figure 3(b) and furthermore, confinement distorts hexagonal packing of the cylinders. Similar nanostructure were obtained in nanotubes, Chen *et al* [88] explained these nanostructures shown in Figure 2 therein, as uniform wormlike nanostructures entangled each other to form perforated holes morphology.

The simulation results for the cylindrical forming system were also obtained by increasing interaction strength $\alpha = 0.4$ between the surface walls and majority of the block of the polymer system in the pore geometry. One-dimensional confinement is used in this system to investigate the effect of preferential attractive circular wall parallel to the pore. Simulation results are carried out on one million time steps. The simulation results for the cylinder system are obtained in a pore system with interior radius fixed at $r_a = 5$ and exterior radius r_b of the pore system varied to expand the pore size of the system. The length of the pore system is also fixed at $h = 4$ however, in one system it is changed which is mentioned in the figure below. Snapshots of the simulation results are shown in figure 5.12.

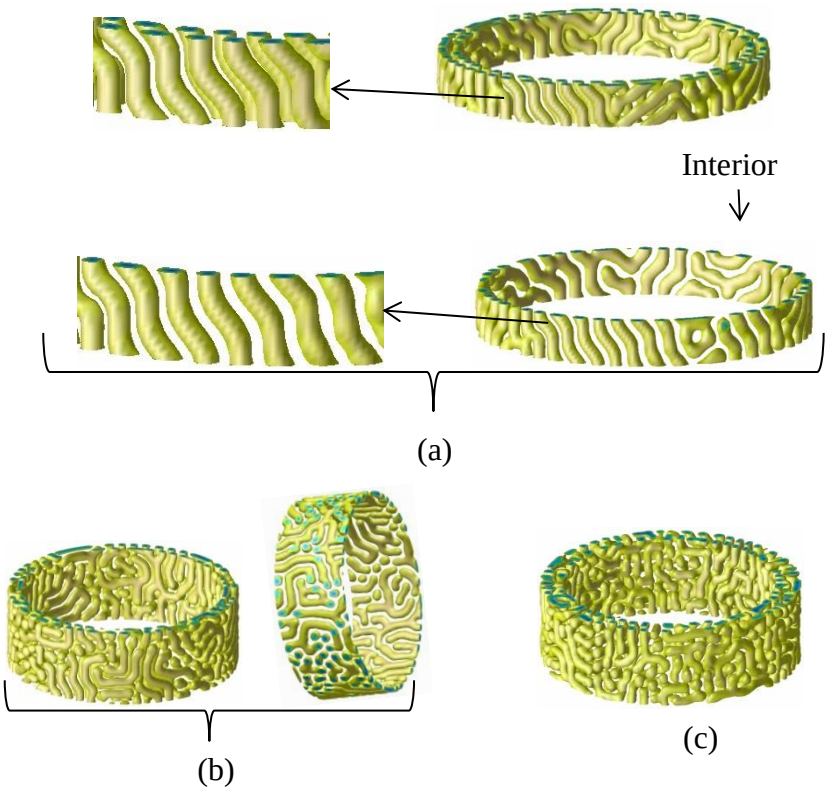

Figure 5.12: cylindrical system obtained with interaction parameter $\alpha = 0.4$, the pore size and the pore lengths respectively are (a) d = 1.6 and *h* = 1.6 (b) d = 1.5 and *h* = 4 (c) d = 2 and *h*=4.

The first system obtained with pore size *d = 1.6* and pore length *h = 1.6* shown in Figure 5.12(a) with zoomed snapshots adjacent to the image and the interior layer of the system. System shows mostly perpendicular to the pore tilted cylinders in circular alignment with very few parallel to the pore cylinders. Perpendicular to the pore cylinders are due the influence of preferential attractive wall in the pore system. Parallel to the pore cylinders are tilted cylinders emerged due to the strong circular wall interaction $\alpha = 0.4$ and in previous simulation results with week wall interaction we observed curved cylinders in the pore system. These tilted cylinders appeared in both layers of the pore system. For the pore system size *d = 1.5* and pore length *h = 4* system there are curved cylinders appear in the pore system as shown in Figure 5.12(b). Furthermore increasing the size of the pore system diversely oriented cylinders appear in the pore system as shown in Figure 5.9(c). The experimental study [86] shows that in the cylinder forming system under the preferential wetting of the pore walls microdomains align along the pore axis in cylindrical confinements.

5.2.3. Spherical forming system confined in cylindrical pores

In this section, a study was carried out on spherical forming system in cylindrical pores using CDS method in cylindrical coordinates system. The Spherical polymer system was investigated using various cylindrical pore dimensions without confinements (neutral surfaces) and with preferential affinity to the surface of the pore system of one of the monomer of the polymer system. All the simulations were carried out on one million time steps.

I. Sphere forming system confined in neutral pores

First of all, the sphere forming system was obtained without confinement of the pore walls in the pore system. The sphere morphology of diblock copolymer system were obtained in a hollow cylindrical pore system. In the first case simulation results are obtained by using following CDS parameter system with low temperature parameter in the pore system.

Table 6: CDS parameter system with low temperature for sphere forming system

τ	f	u	v	B	D	A
0.20	0.40	0.38	2.3	0.01	0.50	1.50

In the first case for neutral pore system, the interior radius of the pore system was fixed at $r_a = 3$ whereas the exterior radius r_b were increased by five grid points to expand the pore system. In the pore system d describes the pore size of the system which is the difference of the interior and the exterior radius of the pore system.

(a) (b)

Figure 5.13: Sphere forming system in neutral cylindrical pore systems with low temperature CDS parameter system, the interior radius of pore system was fixed at $r_a = 3$ and the pore sizes are (a) $d = 2.5$ (b) $d = 3.0$.

The results in the pore system show a lot of defects arising in the form of short cylinders in the pore system as shown in Figure 5.13. There are spheres which vary in size throughout the pore system. This may be due to the influence of the curvature because in the outer layer system is less destabilized as compare to the interior layer where system is almost destabilized in the pore system.

In the second case, simulation results were obtained using the CDS parameter system with low temperature for sphere system in the pore system whose interior radius is fixed at $r_a = 5$ and exterior radius r_b varied to expand the pore system. Similarly $d = r_b - r_a$ defines the pore size of the pore system.

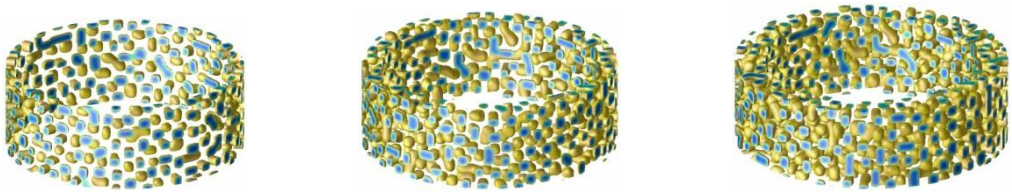

(a) (b) (c)

Figure 5.14: Sphere system obtained by low temperature CDS parameter system, the pore system has the interior radius fixed at $r_a = 5$ and pore sizes in the images are (a) $d = 0.5$ (b) $d = 1$ (c) $d = 1.5$.

The sphere forming system obtained in the pore system with the interior radius fixed at $r_a = 5$ also show defects in the form of short cylinders in the pore system as shown in Figure 5.14. Two spheres merge to gather to form short cylinders in the pore system. Short cylinders formed by the merging two spheres are look like double dumbbell in the pore system and the long cylinders are formed by the merging of three or more than

three spheres in the pore geometry. There are also observed defects in the form of long curved cylinders and straight cylinders in the pore geometry. However, system show better stabilized sphere system in the pore geometry as compared to the pore system whose interior radius was fixed at $r_a = 3$. This further strengthening the argument that defects arising in the sphere system with low temperature was due to the curvature influence in the pore system. The spheres which maintain their structural morphology do not vary too much in shape and size as compared to previous pore system with interior radius fixed at $r_a = 3$. We can observe some perfect sphere system in the pore geometry.

I. Sphere system with modified CDS parameter system in cylindrical pores

The sphere forming system is also achieved in the pore geometry by using modified CDS parameter system with higher temperature. The modified CDS parameter system for sphere forming system is achieved by extensive simulation work, while searching for modification of cylindrical forming system. The search started by taking different variations around the temperature parameter $\tau = 0.30$ which was fixed for the cylinder system. The temperature parameter τ is chosen for modification because mainly the temperature parameter τ and volume fraction *f* play important role in the morphology formation of diblock copolymers systems. The volume fraction $f = 40$ is fixed for both cylinder system and sphere system. The search domain was $\tau = 0.30 \pm 5$ with fixed change in each time given to $\tau = 0.30$ be the fixed number ± 0.1, so there are 100 simulations were carried out in the search of modification of CDS of parameters system. Unfortunately, we couldn't find any best CDS parameter system for cylindrical system but we did find a CDS parameter system for sphere forming system. The modified CDS parameter system for sphere system is shown in table 7. Note that values for CDS parameters *u*, *v* and *B* were the same as used for cylinders system because we were

looking for modification of cylinder system and using CDS parameters for cylindrical system in the mean time we arrived at the sphere morphology on $\tau = 0.25$.

Table 7: Modified CDS parameter system for sphere forming system

τ	f	u	v	B	D	A
0.25	0.40	0.50	1.5	0.02	0.50	1.50

In the first case, simulations results are obtained with neutral surface in a pore system with the interior radius fixed at $r_a = 3$ while, the exterior radius r_b of the pore system increased by *0.5* grid points to expand the pore size of the system.

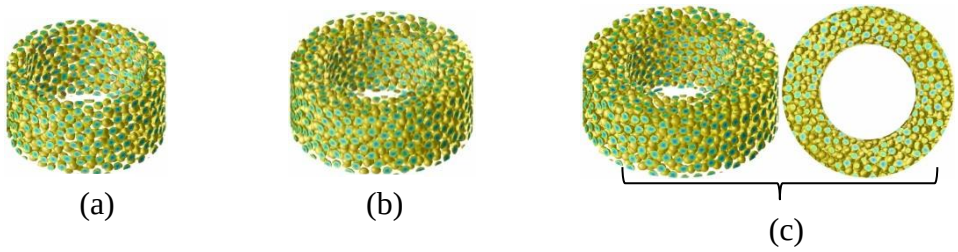

Figure 5.15: Sphere system obtained by modified CDS parameters system with high temperature in a pore system with the interior radius fixed at $r_a = 3$ and the pore sizes are (a) $d = 1$ (b) $d = 2$ (c) $d = 2.5$.

The simulation results were obtained by modified CDS parameters for sphere systems in a pore system with interior radius fixed at $r_a = 3$ show perfect sphere system packed in cylindrical pores as shown in Figure 5.15. There is no any defect in the form of short cylinders and all micro domains are perfect spheres having similar size and shape in the pore system. There are various packing arrangement of spheres observed in the pore system like rhombus, pentagon and quadrilateral. Simulation results are very well ordered and stabilized as compare to simulation results obtained with low temperature CDS parameter system for sphere forming system shown in previous section. This shows that increasing temperature parameter τ and B which defines the chain length dependence of free energy functional played a role in stabilizing the sphere forming

system. This modification of CDS parameter system for sphere forming system will further pave the way for predicting new morphologies in the future.

In the second case, sphere system obtained with modified parameter system in apore system having interior radius fixed at $r_a = 5.0$ and exterior radius r_b of the pore system varied to expand the size of the system, therefore pore size of the system becomes $d = r_b - r_a$. The length of the pore system represented here by the $h = 4$ which is fixed as well in the pore system, whereas angular coordinate of the pore system varied $0 \le \theta \le 2\pi$ throughout the pore system.

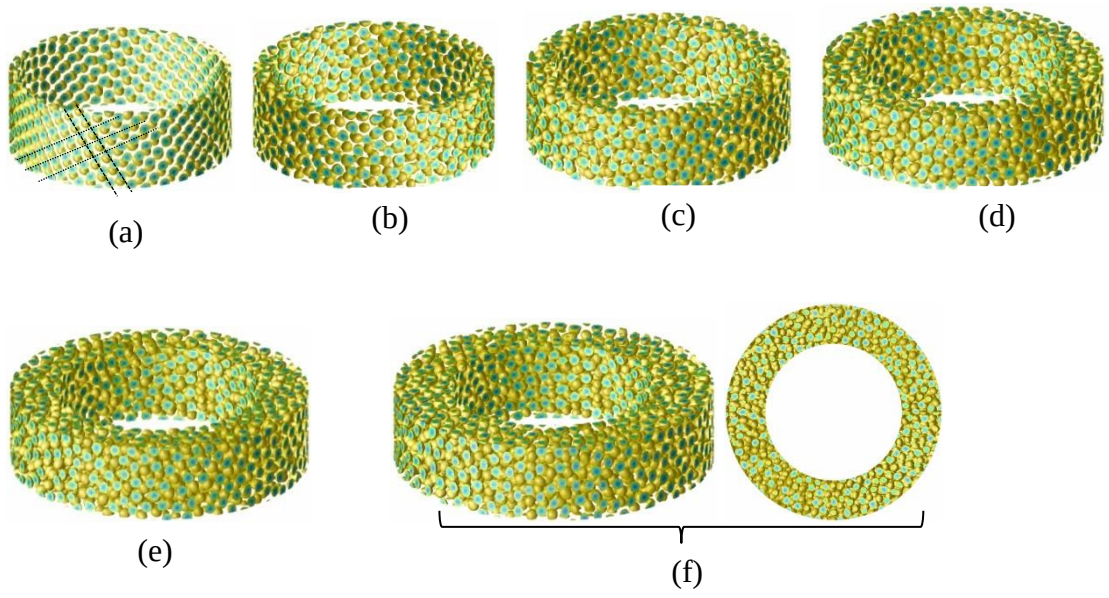

Figure 5.16: Sphere system obtained with modified CDS parameter system in a pore system whose interior radius were fixed at $r_a = 0.5$and the pore sizes of the systems are (a) $d = 0.5$ (b) $d = 1$ (c) $d = 1.5$ (d) $d = 2$ (e) $d = 2.5$ (f) $d = 3$.

The simulation results for sphere forming systems obtained by modified CDS parameter system in a pore system with interior radius fixed at $r_a = 5.0$ also show perfect spheres packed into cylindrical pore system without any single defects of the short cylinders as shown in Figure 5.16. The pore system with size $d = 0.5$ show spheres are perfectly packed in the diagonal strips and anti-diagonal strips in the pore surface as shown in Figure 5.16(a) by dashed lines. Sphere system due to the packing along diagonal and anti-diagonal packing also show square packing arrangements in the pore geometry. On

the other hand spheres packing can be seen as along the vertices of the concentric squares in the cylindrical pore surface. The spheres in the outer layer (cut off in half) are shifted slightly with respect to the spheres in the interior layer of the nanostructure. However, by increasing the pore size of the system this diagonal packing of spheres disappeared in the pore system due to the size effect. This shows that except the narrow channel size system $d = 0.5$, curvature does not influence on the spheres system in the pore system as remaining system shown in Figure 5.16 did not show any significant change in the pore system. The sphere system under modified CDS parameter system achieves its minimum energy rapidly as compared to the low temperature CDS parameter system for sphere forming system. The sphere system in cylindrical pores shows micro domains are jam-packed as shown in Figure 5.16(b-f). This shows that, there is no size effect and curvature effect on the system. The system shows no alignment of the micro domains in the cylindrical pore system. All the spheres are packed in single layered cylindrical pore system. This system of modified parameters also works very well for CDS system in Cartesian coordinate system.

II. Sphere system with interfacial surfaces

The sphere forming system was obtained in cylindrical pore system by applying preferential affinity to the surface for one of the monomer of the polymer system. The modified CDS parameter system for the sphere forming system are not working under geometric confinements because under geometric confinement micro domains in the system becomes squeezed down, lose their structure and get close to each other. This may be due to the high temperature and interaction of surface. Therefore for confinement case we inserted the Previous CDS parameter system with low temperature shown in table 8.

Table 8: CDS parameter system for sphere forming system for low temperature

τ	f	u	v	B	D	A
0.20	0.40	0.50	2.30	0.01	0.50	1.50

In the first case, preferential attractive circular walls parallel to the pore system applied in a pore system with the interior radius fixed at $r_a = 3$ and the exterior radius r_a of the pore system increased by 5 grid points to expand the pore system. The interaction strength set was at $\alpha = 0.2$ between the pore walls and the majority segment of the polymer system in the pore geometry.

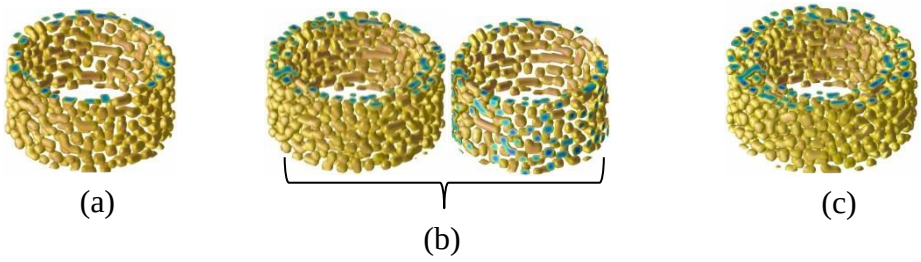

Figure 5.17: Sphere system with interacting parallel circular walls having preferential affinity with majority segment of the polymer system, in a pore system with interior radius of the pore were fixed at $r_a = 3$ and the pore sizes of the system are (a) $d = 1.5$ (b) $d = 2$ (c) $d = 2.5$.

The sphere system confined by circular parallel walls in a pore system with interior radius fixed at $r_a = 3$ show sphere packed in the pore system with defects in the form of cylinders formed by merger of two or more spheres in the pore geometry as shown in Figure 5.17. The pore system with pore size $d = 1.5$ show single layer packed with sphere along with defective cylinder in the pore system as shown in Figure 5.17(a). However, the pore system having size $d = 2$ show two layers of pore system packed with spheres in the pore geometry as shown by the Figure 5.17(b) along with interior layer of the system. This pore system shows that interior layer of the pore is more defective as compared to outer layer of the pore system which shows that interior layer of the system is more defective due the influence of the curvature on the sphere forming system. The pore system with pore size $d = 2.5$ also shows defective sphere system as

shown in Figure 5.17(c). This pore system is a less defective compared to the previous pore size system which shows that increasing the size of the system we get a less defective system.

In the second case, simulation results were obtained with preferential attractive walls parallel to the pore system having affinity to the majority of the block of the polymer system in the pore geometry. The interior radius of the pore system kept fixed at $r_a = 5$ and the exterior radius r_b of the pore system varied to expand the pore size of the system. The interaction strength between the circular walls and majority segment of the polymer system applied $\alpha = 0.2$ in the pore system.

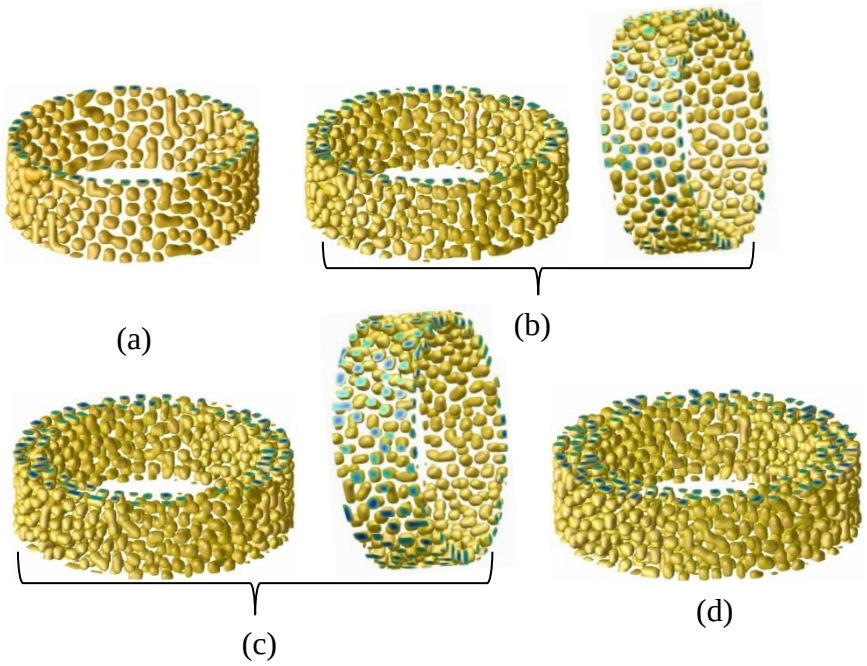

Figure 5.18: Sphere system under interfacial cylindrical surfaces and size of pore systems are (a) *d = 1.5* (b) *d = 2* (c) *d = 2.5* (d) *d = 0.3.*

Under geometric confinements, micro domains show circular alignment around the centre of the pore. However, the structure shows some defects in the form of short cylinders formed by merger of two spheres. For the pore size *d = 1.5*, pore system shows single layered system and micro domains are packed in the pore as shown in Figure 5.18(a). The pore system with pore size *d* = 2, shown in Figure 5.18(b) display spheres packed in concentric circular rings parallel to the pore system. In this two

layered system we observed very few defects in the form of short cylinders. The pore system with size *d = 2.5*, shows micro domains are packed in three layers of concentric circles parallel to the pore system. This system also shows very few defects in the form short cylinders. This shows that under geometrical confinement sphere forming systems tend to form circular alignments in concentric circles parallel to pore system. Results are also obtained by applying interaction strength $\alpha = 0.4$ between the majority segment of the polymers system and cylindrical walls in the pore system but we observed no significant change in the results.

For the second case, interacting walls were applied perpendicular to the pore through cross section of cylindrical pore. In this system polymer is confined in cylindrical pore and interacting walls covering the top and bottom of the pore system. Strength of interaction between walls and one of the polymer blocks set at $\alpha = 0.2$.

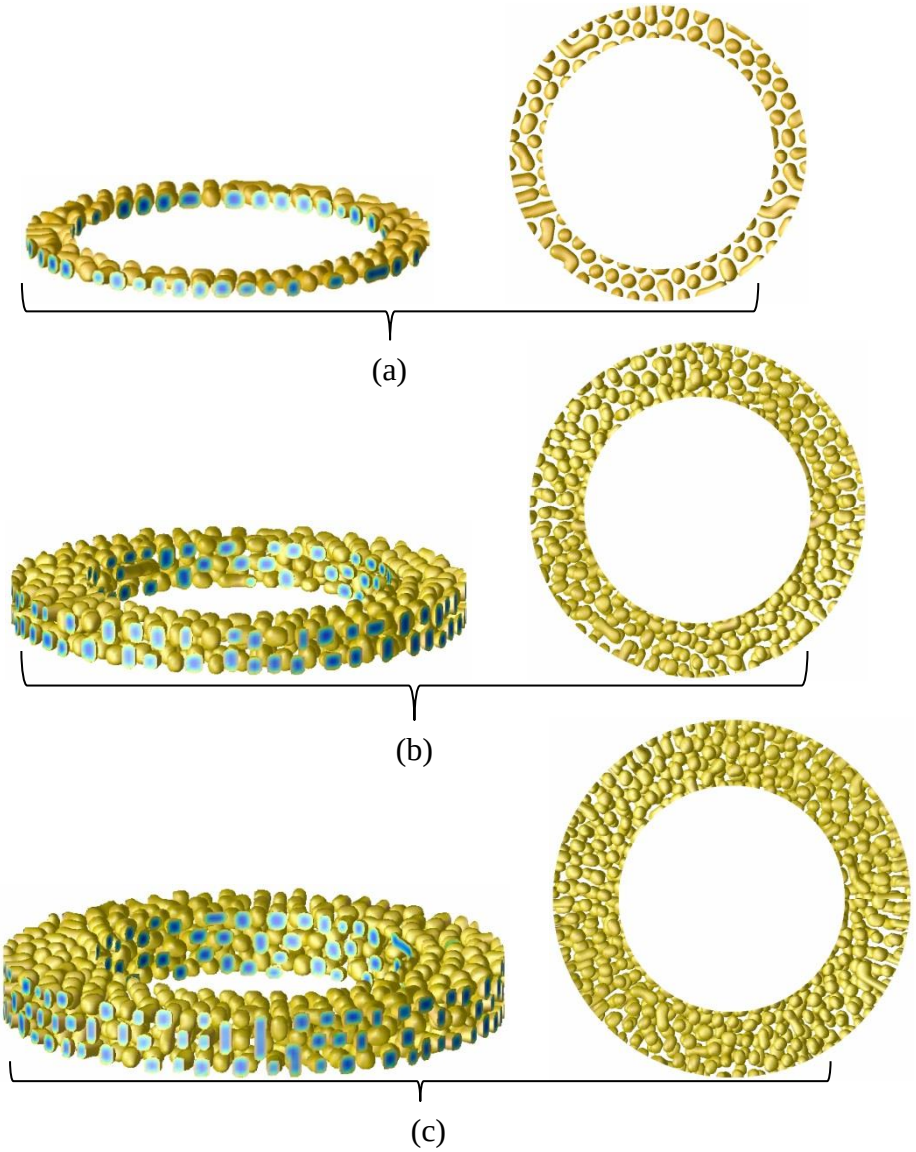

Figure 5.19: Sphere system under geometric confinement applied through cross sections of cylindrical pore system with the pore size and the pore length are respectively (a) *d = 1.5, h = 1.2* (b) *d = 2.5, h = 2.5* (c) *d = 3.0, h = 3.0.*

Under perpendicular confinement applied through the top and bottom cross sections of cylindrical pore system micro domains show perpendicular packing to the pore system. For the system with pore size and length respectively *d = 1.5, h = 1.5,* display spheres packed in a single layer perpendicular to the pore system as shown in Figure 5.19(a) along with top view of the image. There are some defects as well in the form of short cylinders. Increasing size and length respectively *d = 2.5, h = 2.*5 of the system, pore system shows spheres packed in bi-layered system perpendicular to the pore system as shown in Figure 5.19(b). For this size and length of the pore system some defects are

observed in the pore system. Similarly, for the system size and length respectively *d = 3.0, h = 3.0,* spheres are packed in three layers perpendicular to the pore system, pore system shown in Figure 5.19(c). This shows that geometric confinement perpendicular to the pore system induces the packing of micro domains in layers perpendicular to the pore system. Increasing the strength of interaction between walls and polymer blocks we get more defective system. The simulation results were also obtained with the very strong interaction parameter was set at $\alpha = 0.4$, we get the pore system with very few more defects in the system not shown here.

The simulation results for sphere forming system were also obtained with two dimensional confinements applied on the cylindrical pore system. Two dimensional confinement was applied by the parallel walls and perpendicular walls around the pore system. Parallel walls are imposed on the cylindrical pore system by applying the boundary conditions on the radial coordinate of the cylindrical coordinate system. Perpendicular walls are imposed on the pore system by the applying the boundary conditions on the *z* coordinate system of cylindrical coordinate system. The pore system is confined between parallel circular walls and pore system is capped by top and bottom interacting walls. The strength of interaction between surface and one of the blocks of polymer system used in simulation was set at $\alpha = 0.2$.

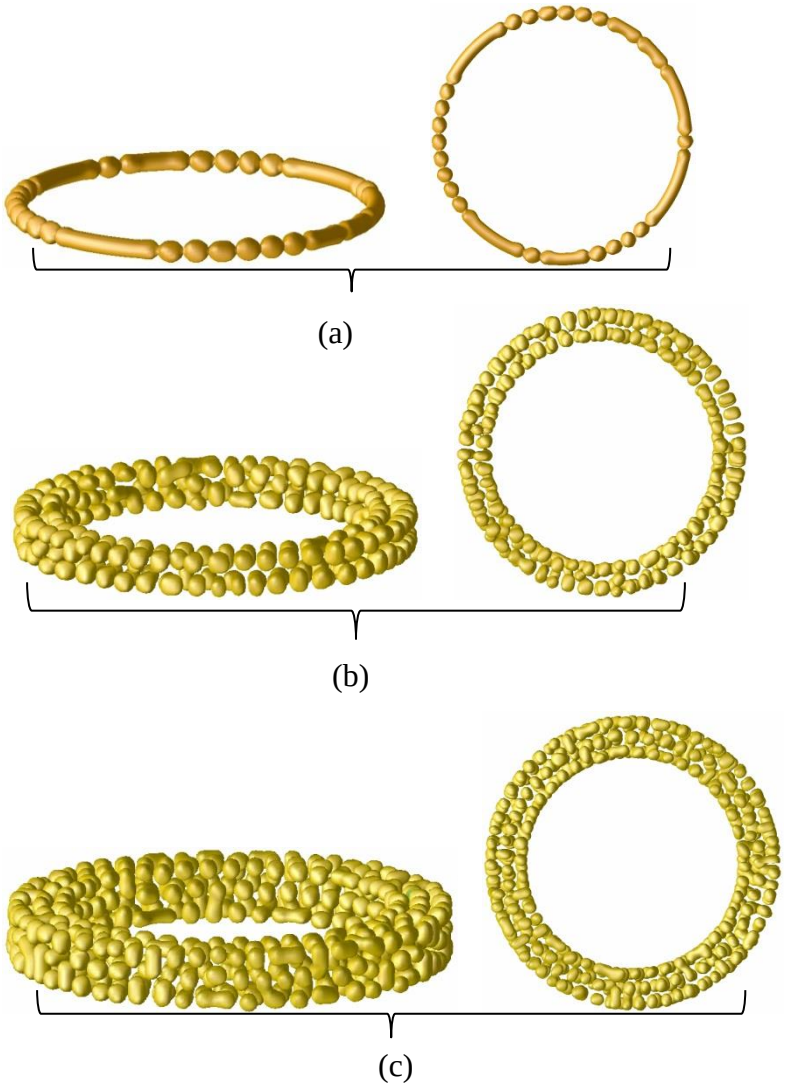

Figure 5.20: Sphere system under two dimensional confinements with system size and length are respectively (a) $d = h = 1.5$ (b) $d = h = 2.5$ (c) $d = h = 3.0$.

The results obtained under two dimensional geometric confinements shows that spheres are induced in circular alignments in the cylindrical pore system. In the first case, two dimensional confinements applied on the narrow system with size and length respectively $d = h = 1.5$ as shown in Figure 5.20(a). In this system due to the confining effect some spheres merged to gather and formed cylinders. There are seven cylinders formed by merging two or more spheres. There are two short cylinders formed by merging two spheres, however there are five medium cylinders formed by the merging of three or more spheres. The remaining survived spheres are in a perfect circular alignment with cylinders around the centre of the pore system. However, the surviving spheres are interconnected to each other in the pore system. The story of the pore

cylindrical pore system under two dimensional confinements is much different than the narrow sized pore system. The pore system with size and length respectively $d = h = 2.5$, show that the spheres are in perfect circular alignment in concentric circles and circles one upon each other as shown in Figure 5.20(b). The microdomains are induced in pore system by four circular layers parallel to the pore system as well as perpendicular to the pore system due to the two dimensional confinements. The cylindrical pore system of size and length $d = h = 3.0$ under two dimensional confinements also shows spheres are induced in the cylindrical pore system in circular rings parallel to the pore system as well as perpendicular to the pore system as shown in Figure 5.20(c). This system size also shows very few defects under two dimensional confinements as compared to system with same size under one dimensional confinement. There are in total nine circular rings induced spheres in the cylindrical pore system. However, there are also very few defects of short cylinders formed due to the merger of two spheres. Under two dimensional confinements we obtained less defected and more ordered system in the cylindrical pore system due to the interplay of surface interaction and curvature effect. Two dimensional confinements are working well in the cylindrical pores for the sphere forming system as compared to cylindrical and lamella.

5.3. Summary

Lamella foming system confined in the neutral cylindrical pore show mixed orientations like helical, strip lamella and lamella sheets perpendicular to the pore surface. However, in the presence of the interacting surfaces concentric lamella were induced in the pore geometry. Results show that under the influence of the both curvature and interfacial surfaces lamella tends to form concentric layers. Cylinder forming system under geometric confinements of the neutral cylindrical pore show mixed orientations of

microdomains, perpendicular to pore surface and parallel to the pore surface. However, in the presence of interfacial cylindrical surfaces microdomains show parallel to pore surface orientation and wrapped around the pore system. In the narrow pore size system perforated morphology and parallel to the pore cylinders were observed in the pore geometry. In the short length pore surface we obtained standing cylinders which were packed in the concentric circles in the pore system. The sphere forming systems were obtained with a new set of CDS parameters with high temperature. In this case we obtained a perfect sphere system in the cylindrical pores without any defective cylinders. Sphere forming system confined in the cylindrical pore with interfacial surfaces show concentric circles packing arrangements.

CHAPTER SIX

6. Diblock copolymer system confined in spherical pores

6.1. Introduction

This study investigates the nonstructural formation of block copolymers on the surface of a sphere in the spherical coordinate system. In this study, investigations were carried out for classical morphologies of diblock copolymer systems lamella, cylindrical and spherical forming systems in the hemispherical pore shell. Lamella, cylindrical and spherical morphologies are investigated under geometric confinement of spherical pores with neutral surfaces and with interacting surface walls having affinity with the majority segment of the polymer system. In the case of interfacial surfaces, symmetric boundary conditions (each interface has same preference for the selected segment of the polymer system) were applied on the pore interfaces. The results were obtained in the pore surfaces with the interior radius r_a fixed and the exterior radius r_b was varied to expand the pore size of the surfaces. In the pore shell, the simulations were carried out by radial step $\Delta r = 0.1$, with polar angular step $\Delta\theta = 2\pi/360$, with azimuthal angular step $\Delta\phi = \pi/180$. The CDS simulations are carried out with time step $\Delta t = 0.1$. In order to obtain results in the hemispherical shell by avoiding singularities, the radial coordinates are restricted by $r_a \le r \le r_b$, similarly angular and azimuthal coordinates are also restricted by $0 < \theta < \pi$, and $0 < \phi \le \pi$ respectively. The pore size of the surface is defined by the relation $d = r_b - r_a$, which is the difference between the exterior radius of the pore system and the interior radius of the pore system. All simulations are carried out for one million time steps. All the CDS simulations were carried out by initializing the order parameter Ψ in the range of values ± 1.

6.2. Results and discussion

Using CDS simulations employed in spherical coordinate system, investigations were carried out for lamella, cylinder and sphere forming block copolymers with various pore radii of hemispherical shells. The confinement induced and curvature influenced nanostructures were obtained with neutral spherical surfaces as well as with interfacial spherical surfaces. In the interfacial results, the majority segment of the polymer system is chosen to have affinity with the pore walls. In order to investigate the curvature influence, results were obtained with various pore thicknesses of the pore surfaces in the pore geometry.

6.2.1. Lamella forming system confined in spherical pores

In this section, lamella forming system is investigated in the spherical pores. The results were obtained with the different pore sizes of the surface by keeping the interior radius r_a fixed and by varying the exterior radius r_b to expand the pore surface are shown and discussed.

I. Lamella forming system with neutral surfaces of the spherical pores

The results were obtained and discussed for asymmetric lamella forming system with neutral surfaces in the spherical pores using the CDS parameter system and these parameters are shown in table (9).

Table 9: CDS parameter system for asymmetric lamella forming system

τ	f	u	v	B	D	A
0.36	0.48	0.38	2.30	0.02	0.70	1.50

In the first part, the simulation results were obtained in a pore surface with the interior radius were fixed at $r_a = 3$ and the exterior radius r_b of the pore surface varied to expand the pore size of the system.

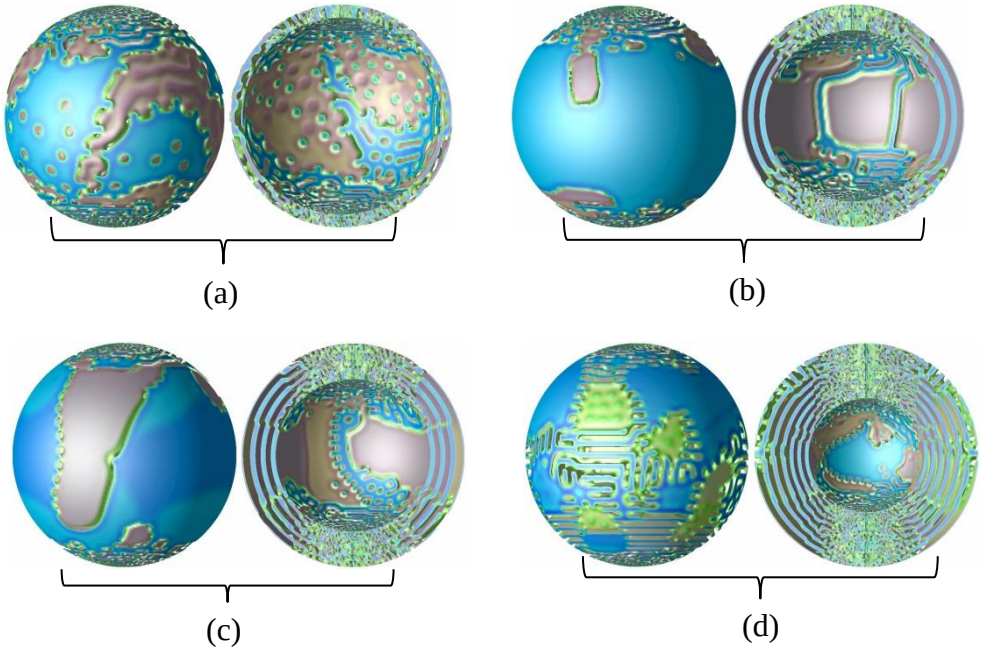

Figure 6.1: Asymmetric lamellae system in spherical pores with neutral surfaces, the interior radius of the pores were fixed at $r_a = 3$ and the pore sizes of the systems are (a) *d = 0.5* (b) *d = 1* (c) *d = 1.5* (d) *d = 3.*

Asymmetric lamella confined in spherical shells having the interior radius fixed at $r_a = 3$ shows concentric lamellae sheets with perforated holes. In the sphere shell size *d* = 0.5, there is single a parallel lamellar sheet with perforated holes as shown in Figure 6.1(a). The pore surface *d* = 1 displays onion-like structure of lamella with standing lamella packed in the interior sheet of the structure as shown in Figure 6.1(b). There are three parallel concentric lamellar sheets in the pore surface. As we increasing thickness of the pore surface *d* = 1.5, sphere shell induces four concentric lamellar sheets with few standing lamella packed in the interior sheet of the pore surface as shown by the Figure 6.1(c). As the thickness of the pore surface is increased, concentric lamellae sheets tend to deform into a stacked lamella system. The pore system having the size of pore *d* = 3, shows mixed concentric lamellar sheets and stacked lamella as shown in Figure 6.1(d). The pore system displays seven layers of microdomains. However, stacked lamella were observed only on the outer layer of the pore surface. This shows that by increasing the size of the spherical shell concentric lamella switch to the stacked lamella morphology. Recently, onions-like structures were also obtained by

experimental study [89]. Similar Onion-like structures had also been observed by the experimental work conducted by transmission electron microscopy [31] as shown in Figure 7 there in and [68] shown in Figure 1(c) there in. However, this onion-like morphology was achieved by the confinement of the pore surface but here we obtained the results with neutral surfaces. There are also similar, parallel to the pore lamella in the planar thin films were obtained in the experimental work [90]. These onions-like structures were also reported by the simulated annealing Monte Carlo simulations [91] by applying strong surface preference Figure 1(a) there in. The study was also conducted by using the CDS computational method, where block copolymers were grown in planar surfaces and shown on spherical pores [8]; they also observed onion-like nanostructures in the spherical pore shell with one-dimensional confinement. The onion-like concentric alternating layered lamella morphology was obtained by preparing nanoparticles confined in the spherical surfaces from PS-b-PI diblock copolymer [85], where results are shown by Figure 1 and Figure 3(b) are clearly consistent with the results obtained in this study as shown in Figure 6.1.

In the second case, results for lamella system are obtained and discussed by keeping the interior radius of the pore surface fixed at $r_a = 5$ and the thickness of the pore surface expanded by the increasing the exterior radius r_b of the hemispherical shell.

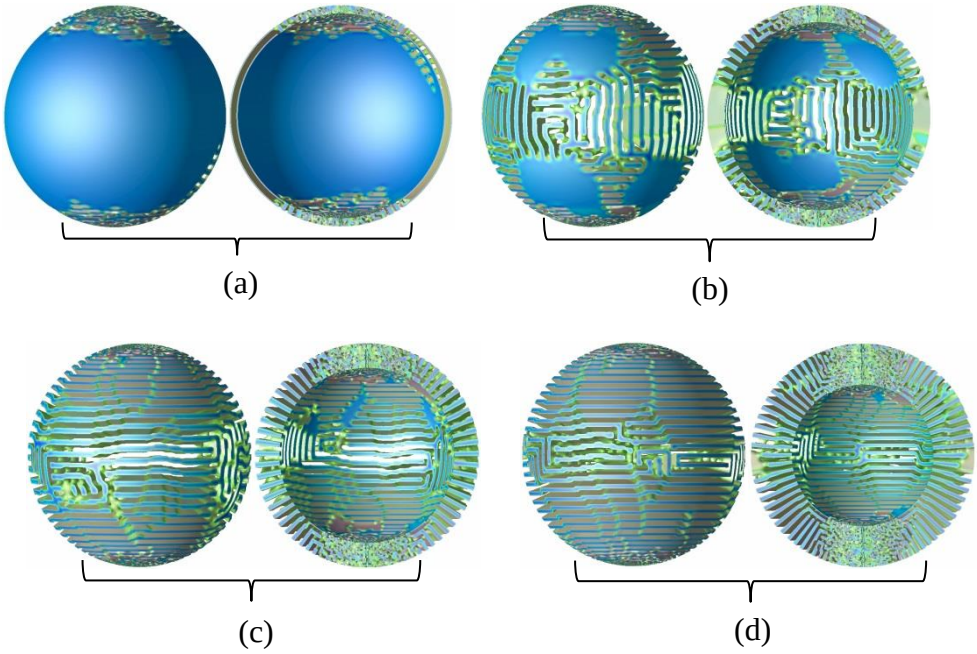

Figure 6.2: Asymmetric lamella system in the pore surface with the interior radius fixed at $r_a = 5$ and shell sizes are (a) *d = 0.5* (b) *d = 1* (c) *d = 1.5* (d) *d = 3.*

The asymmetric lamella confined in the spherical shell with the interior radius of the pore surface fixed at $r_a = 5$ shows nanostructure evolution of the lamella system from the concentric lamella to the stacked lamella morphologies with respect to the pore size of the system. The spherical pore shell with a thickness of the pore surface of *d = 0.5,* displays two concentric lamellae sheets with the smooth surface as shown in Figure 6.2(a). However, the spherical shell with pore size *d =1* shows a mixed structure of standing lamella, stacked lamellae and a few clusters of lamellar sheets as shown in Figure 6.2(b). The pore surface *d = 1.5,* shows fully evolved stacked lamella morphology as shown in Figure 6.2(c). Increasing the thickness of the pore system *d = 3,* it can be observed stacked morphology of the lamella system as shown in Figure 6.2(d). Results show that under the influence of the curvature, the lamella system forms concentric parallel sheets and under the weak curvature effect lamella evolves into the stacked morphology. These stacked lamellar systems obtained here, are consistent with the stacked lamellar system which were obtained by the experimental work [68] shown in Figure 1(a) there in, whereas, concentric lamella or onion-likes structures are also

consistent see Figure 1(c) there in. The stacked lamellar system were also reported by the computational work [91] as in Figure 1(a) there in.

In the following, results were obtained with the interior radius of the spherical pore surface was fixed at $r_a = 7$ and the size of the spherical shells extended by the exterior radius r_b of the pore surface geometry.

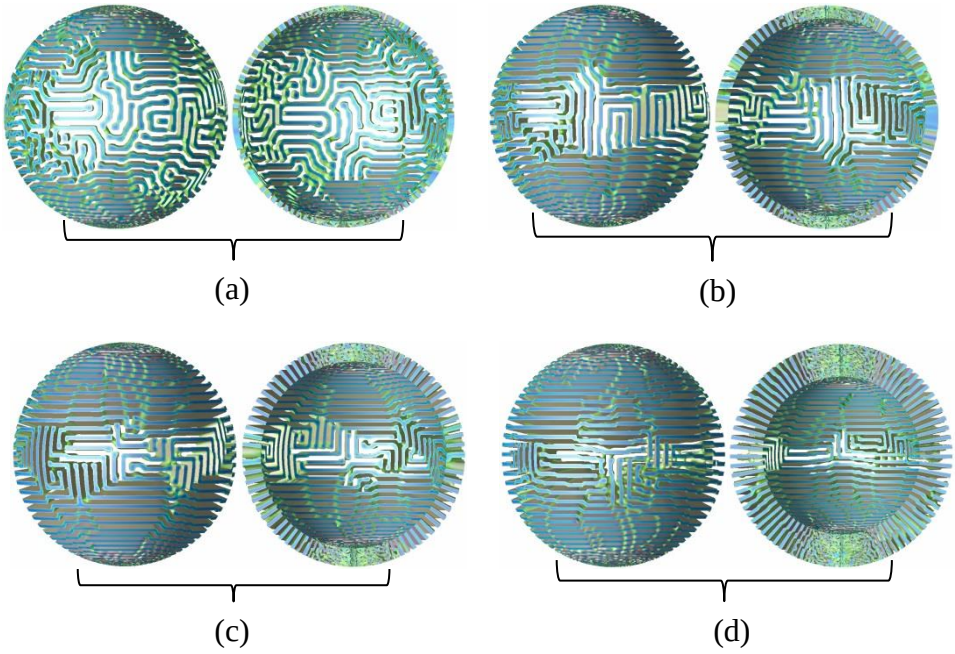

Figure 6.3: Asymmetric lamella system in spherical pore with the interior radius of the pore system fixed at $r_a = 7$ and the spherical pore sizes are (a) *d = 0.5* (b) *d = 1* (c) *d = 1.5* (d) *d = 3*.

The lamella system in the spherical surface with the interior radius fixed at $r_a = 7$ shows formation of the nanostructure from mixed morphology to stacked morphology. The narrow pore surface *d =0.5* shows a so called standing-up lamella system with mixed curved patterns in the pore surface as shown in Figure 6.3(a). By increasing the surface size *d =1*, the pore surface displays stacked lamella morphology on the top and bottom of the pore surface, while in the middle of the pore surface, there are standing-up lamella with parallel and perpendicular orientation as shown in Figure 6.3(b). The pore systems shown in Figure 6.3(c,d) show stacked lamella morphology developed under weaker curvature influence in the pore system. Results show that lamella in the

spherical pore geometry evolves from mixed morphology to the stacked morphology in the pore surface system with respect to the size.

II. Asymmetric lamella system with interfacial surfaces

In this section, we consider the asymmetric lamella forming system confined by similar interfaces with preferential affinity to the majority segment of the polymer system in the spherical pore surface. The interaction strength between the pore interfaces and majority block of the polymer system which was applied is $\alpha = 0.2$.

In the first case, we consider pore surface with the interior radius fixed at $r_a = 3$ and the pore surface extended by the exterior radius r_b of the pore system.

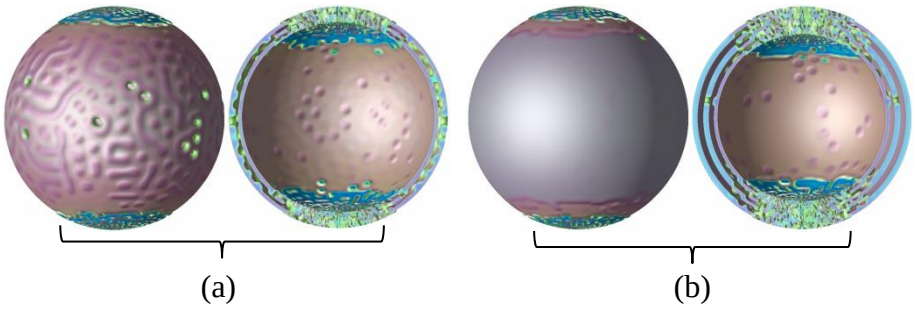

Figure 6.4: Lamella systems with interfacial surfaces, the pore surface having the interior radius fixed at $r_a = 3$ and the pore sizes are (a) *d = 1* (b) *d = 1.5*.

The lamella system confined by the similar interfaces having the affinity to the majority segment of the polymer system in a pore surface with interior radius fixed at $r_a = 3$ shows concentric lamella parallel to the pore surface. In the pore surface with pore sizes *d = 1*, shows mixed lamella system where standing-up lamella is packed inside the womb of the outer layer of the concentric lamella sheet and a few spots of the perforated morphology on the interior layer of the lamella sheet in the pore surface as shown in Figure 6.4(a). This type of the mixed lamella is a novel nanostructure where standing lamella and concentric lamella coexist to gather in the spherical pore geometry. However, the pore surface with the pore size *d = 1.5* shows concentric lamella sheets as shown in Figure 6.4(b). There are three lamella sheets in the pore surface with a smooth

exterior sheet and there are still very few spots of the perforated morphology on the interior lamellar sheet in the pore surface. Results show that the lamella under the influence of the concentric surface confinement in the spherical pore surface induces the structure in the form of the lamellar sheets which are parallel to the pore surface.

In the second case, we consider the pore surface with interior radius fixed at $r_a = 5$ and the exterior radius of the pore surface varied to expand the pore size of the system. The polymer system is confined by the parallel spherical surface having affinity to the major block of the polymer system in the spherical shell.

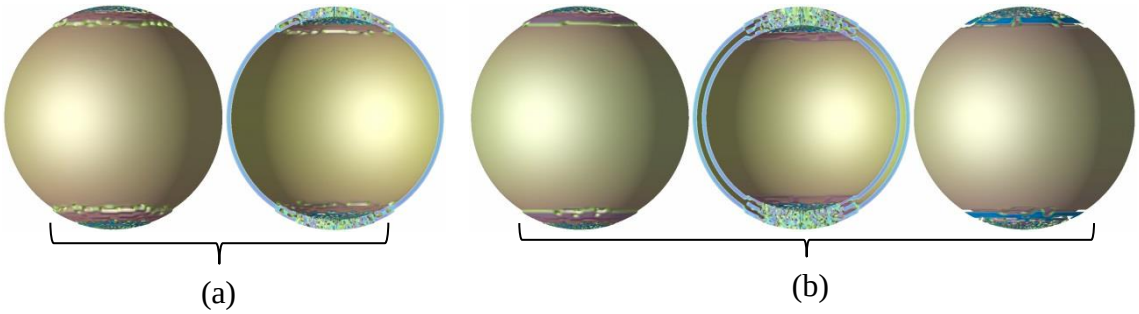

Figure 6.5: Lamella systems confined by interfacial interfaces, with pore surface having the interior radius fixed at $r_a = 5$ and the pore sizes are (a) *d = 1* (b) *d = 1.5*.

The results for the asymmetric lamella forming system confined by the symmetric parallel spherical interfaces having preferential affinity to the majority block of the polymer system show concentric lamellae sheets parallel to the pore surface in a pore surface with the interior radius of the pore fixed at $r_a = 5$. The pore surface with the pore size *d* = 1, induces a single smooth surfaced lamella sheet parallel to the pore surface in the pore geometry as shown in Figure 6.5(a). The spherical pore surface having the pore size *d =1.5,* displays two concentric parallel lamella smooth surface sheets in the pore surface as shown in Figure 6.5(b). Results predict concentric smooth lamellae sheets parallel to the pore surface in the pore geometry under confined parallel interfaces in the pore geometry.

In the third case, results are obtained and discussed with the interior radius of the pore shell fixed at $r_a = 7$ and the exterior radius r_b of the pore surface varied for five grid

points to expand the pore size of the surface. The interacting similar interfaces parallel to the pore surface applied on the polymer system have affinity with the majority segment of the polymer system.

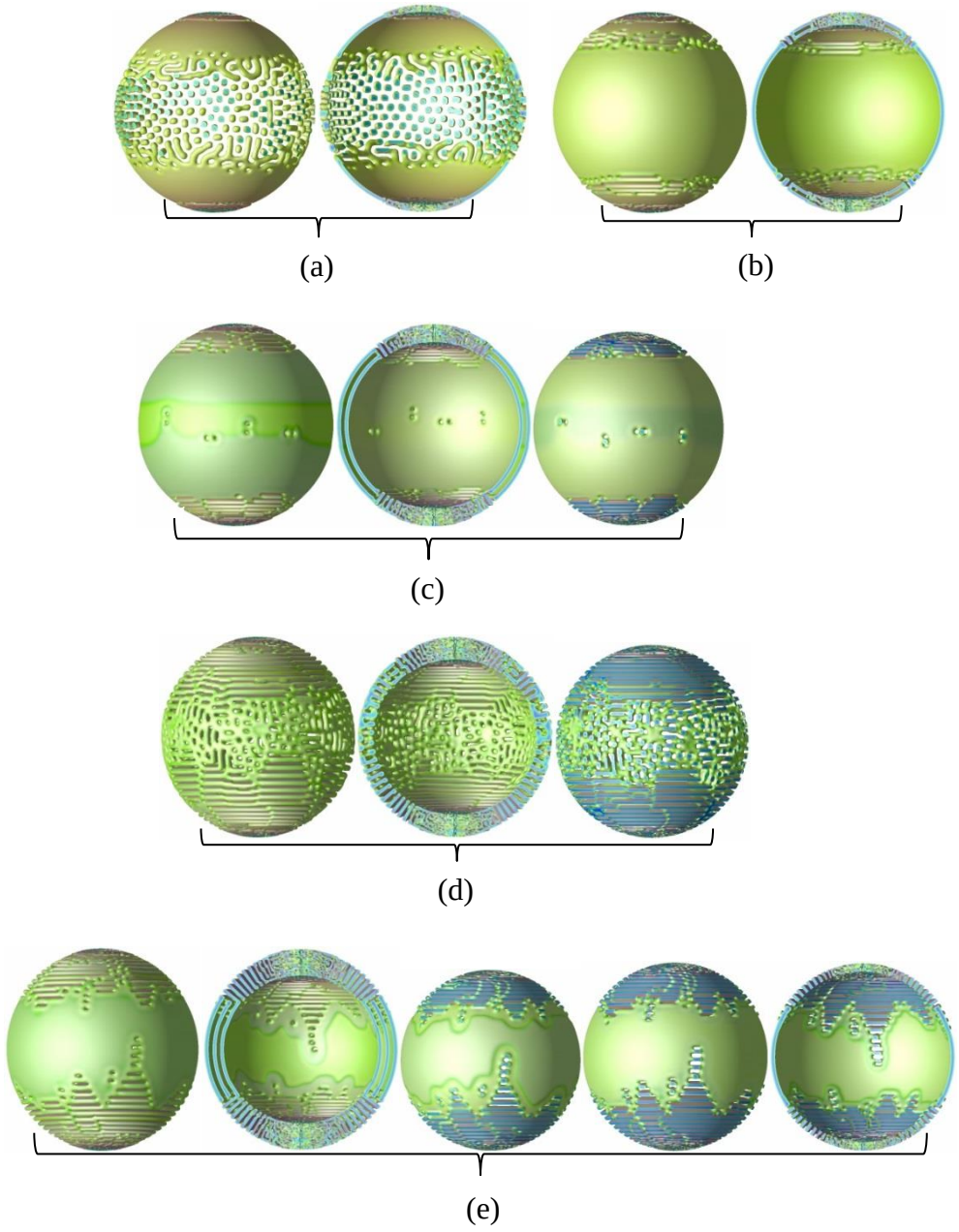

Figure 6.6: lamella systems confined by interacting interfaces, with the pore surface having the interior radius fixed at $r_a = 7$ and the pore sizes are (a) *d = 1* (b) *d = 1.5* (c) *d = 2.0* (d) *d = 2.5* (e) *d = 3.0.*

The pore surface with the interior radius fixed at $r_a = 7$, the polymer system was confined by parallel spherical interfaces in spherical pore geometry and shows evolution of different morphologies of lamella forming system. In the first case, the pore surface with pore size *d = 1*, shows interesting mixed nanostructures which induce lamellar

sheets, so called standing-up lamellae, perpendicular cylinders, spheres and perforated morphologies in the spherical pore surface as shown in Figure 6.6(a). Results predict coexistence of the lamellar, cylindrical and spherical forming systems in the spherical pore surface confined by the similar interfaces which is quite a novel nanostructure in the field. The hybrid nanostructures were also reported confined by dissimilar interfaces in planar thin films [92] which are a different case from spherical geometry. However, hybrid morphology of the parallel and perpendicular lamella confined in spherical pores under dissimilar interfaces, were reported in the computational work [8] but this work shows only the coexistence of the parallel and perpendicular morphologies of lamella system. The pore surface with the pore size $d = 1.5$, induces smooth lamellar sheet with perforated holes on top and bottom of the surface as shown in Figure 6.6(b). However, the pore surface having a pore size $d = 2.0$, induces two lamellar sheets with a few perforated holes on the interior lamellar sheets as well as exterior lamellar sheets in the spherical pore surface as shown in Figure 6.6(c) along with an interior layer. The interior layer of the structure shows that the both layers are also interconnected by the few neck-bridges. Perforated holes are results of the bilayer lamellar sheets. For the pore surface with pore size $d = 2.5$, induces stack lamellar system on top and bottom of the pore surface and perforated lamella in the middle of the layers in the pore surface as shown in Figure 6.6(d) along with interior layer on the right hand side of the image. Interior layer of the pore system shows that layers are interconnected by the neck-bridges to each other in the pore geometry. The pore surface having pore size $d = 3.0$, induces the mixed structure of lamellar sheets, a few perforated holes and stacked lamellar on the top and bottom surfaces of the spherical pore system as shown in Figure 6.6(e). Results were also show that the lamella system under wetting surfaces evolves into the stacked lamellar morphology from lamellar sheets morphology with respect to the size of the pore surface. Results were obtained with various sizes of pore surface

show evolution of the lamellar morphologies from a hybrid system to lamellar sheets, lamellar sheets to the perforated holes, perforated holes to lamellar sheets again and finally lamellar sheets to the stacked lamella system in the spherical pore surface. All these variations in the lamella morphology are results of the variation in the thickness of the lamellar sheets with respect to the size of the pore surface in the spherical pore geometry. The evaluation of the lamellar morphology has been investigated with respect to the size effect in the spherical surface [8], which shows that with increasing shell thickness, the structure gradually changes from a single lamellar sheet to two lamellae sheets and when the film thickness is small, the perforated morphology forms in the lamellar sheet. However, results of this study show that after the lamellar sheet and the perforated morphology, the next destination is the stacked lamellar morphology in the spherical pore surface.

6.2.2. Cylindrical forming system confined in spherical pores

In this section, results were obtained and discussed for cylindrical forming system confined in spherical pore geometry with various sizes of the pore surfaces. The cylindrical system of diblock copolymer systems were investigated in spherical pores with neutral surfaces as well as with interacting parallel spherical interfaces, having preferential affinity to the majority segment of the polymer system. The CDS parameters for the cylindrical forming system were used in this study are shown in table 10.

Table 10: CDS parameter system for cylindrical forming system

τ	f	u	v	B	D	A
0.30	0.40	0.50	1.50	0.02	0.50	1.50

I. Cylindrical forming system in neutral spherical pores

In this section we consider cylindrical forming system confined by neutral spherical surfaces with various pore surface sizes. Results were obtained in a pore surface with the interior radius fixed at $r_a = 3$ not shown here but in this case we get very defective nanostructures due to the strong curvature effect in the pore surface.

In the first case, we consider the pore surface with the interior radius fixed at $r_a = 5$ and the exterior radius r_b which were increased by the five in each system to expand the pore surface size.

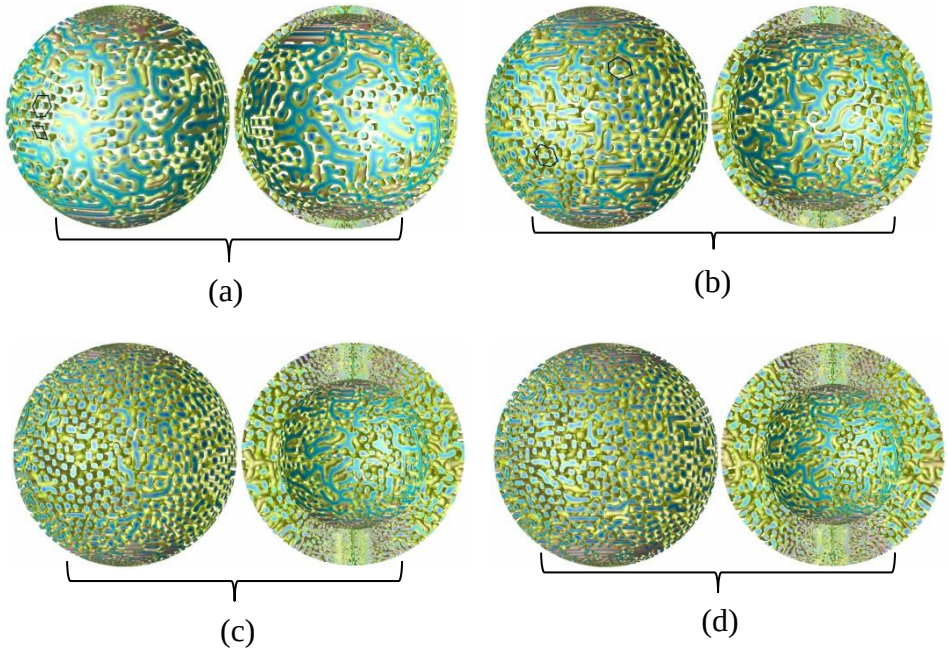

Figure 6.7: Cylindrical forming system confined in neutral spherical pores with the interior radius of the pore surface fixed at $r_a = 5$ and the pore sizes are (a) *d = 0.5* (b) *d = 1* (c) *d = 2.5* (d) *d = 3.0.*

The cylindrical forming system in the neutral spherical surfaces shows a few parallel to the pore surface cylinders and perpendicular to the pore surface cylinders with majority. In the pore surface with pore size *d = 0.5,* it shows a mixed structure of cylinders perpendicular to the pore cylinders and cylinders parallel to the pore curved cylinders in the pore surface as shown in Figure 6.7(a). The perpendicular to the pore surface cylinders are in hexagonal and rhombus packing arrangements in the pore geometry. In

this pore surface a few defective spheres in the pore surface can be observed. The defective spheres were formed due to the size effect in the pore geometry. Increasing the pore size of the surface *d = 1,* defective spheres interconnect with neighbouring cylinders to form long curved cylinders oriented parallel to the pore surface in the pore geometry as shown in Figure 6.7(b). This pore-sized system also shows short straight cylinders perpendicular to the pore surface. Cylinders in the spherical pore geometry turn to be perpendicular to the pore surface with respect to the increase in the size of the pore surface. For the pore surface having pore size *d = 2.5,* short straight cylinders were induced, oriented perpendicular to the pore surface as shown in Figure 6.7(c). Notice that in this pore size system, there are short straight cylinders perpendicular to the pore surface on the exterior surface and long curved cylinders parallel to the pore surface on the interior pore surface of the pore geometry. This clearly shows that long curved cylinder parallel to the pore conforms due the curvature effect in the pore geometry. The pore surface with pore size *d = 3.0,* also shows a similar story that there are short straight cylinders perpendicular to the pore surface, while we can observe long curved cylinders on the interior surface of the pore geometry as shown in Figure 6.7(d). Perpendicular to the pore cylinders are in the hexagonal, square and rhombus packing arrangements in the pore geometry.

In the second case, results were obtained and discussed with interior radius of the pore shell were fixed at $r_a = 7$, while the exterior radius r_b of the pore surface were increased to expand the pore surface.

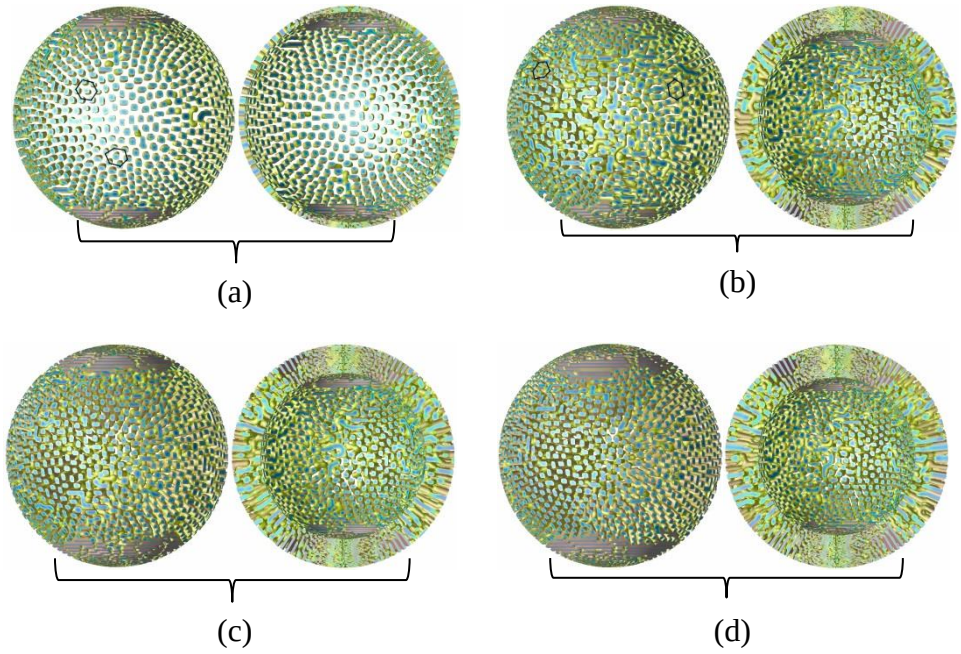

Figure 6.8: Cylindrical forming system confined in neutral spherical pores with the interior radius of the pore surface fixed at $r_a = 7$ and the pore sizes are (a) *d = 0.5* (b) *d = 2.0* (c) *d = 2.5* (d) *d = 3.0.*

The nanostructures were obtained by confined neutral spherical pore surfaces, with the interior radius were fixed at $r_a = 7$, showing short straight cylinders oriented perpendicular to the pore surface in the pore geometry. In the spherical pore system with the pore size *d = 0.5*, the pore shell induces a short straight cylinder packed in rhombus and triangular arrangements, while there are very few defective spheres in the pore geometry as shown in Figure 6.8(a). The pore surface *d = 2.0* also induces short straight cylinders oriented perpendicular to the pore surface as shown in Figure 6.8(b). In this size of pore surface, there are a few tilted short cylinders and curved cylinders parallel to the pore surface. The pore systems *d = 2.5* and *d = 3.0* also display short cylinders with a few curved cylinders parallel to the pore surface in the pore geometry as shown in Figure 6.8(c,d). Results in the spherical pore geometry show that under the influence of the curvature of the pore geometry cylinders tend to form curved cylinders, while, when increasing the size of the pore surface cylinders reorient and become

straight short cylinders perpendicular to the pore surface in the pore geometry. Straight short cylinders are hexagonally packed in the spherical pore geometry. Parallel to the pore cylinders have defects in order to accommodate themselves among the perpendicular cylinders and curvature influence. The results of this study are consistent with the experimental results [68] which were obtained in the spherical pore surfaces, where perpendicular, hexagonally packed and parallel to the pore surface cylinders are observed. Hexagonally packed perpendicular cylinders were also obtained in the experimental work [65]. Parallel and perpendicular cylinders confined in spherical pores were also obtained by the CDS method in Cartesian coordinate system using symmetric boundary conditions on the parallel interfaces of the spherical pore [8]. In this work Pinna *et al* also performed scanning force microscopy experiments on thin films floated on the half-spherical shell on a silicon wafer and obtained the perpendicular and parallel cylinders which are consistent with the results of this study see Figure 9(f) there in.

II. Cylinder forming system with interfacial surfaces

In this section, we consider the cylindrical forming system confined by parallel spherical interfaces having preferential affinity with the majority segment of the polymer system in the spherical pores. Results were obtained by the applying preferential interacting interfaces having a strength of interaction $\alpha = 0.2$ to the majority block of the polymer system in the pore surface.

In the first case, results were obtained and discussed for the pore surface with the interior radius fixed at $r_a = 5$ and the pore thickness is increased by the exterior radius of the spherical surface.

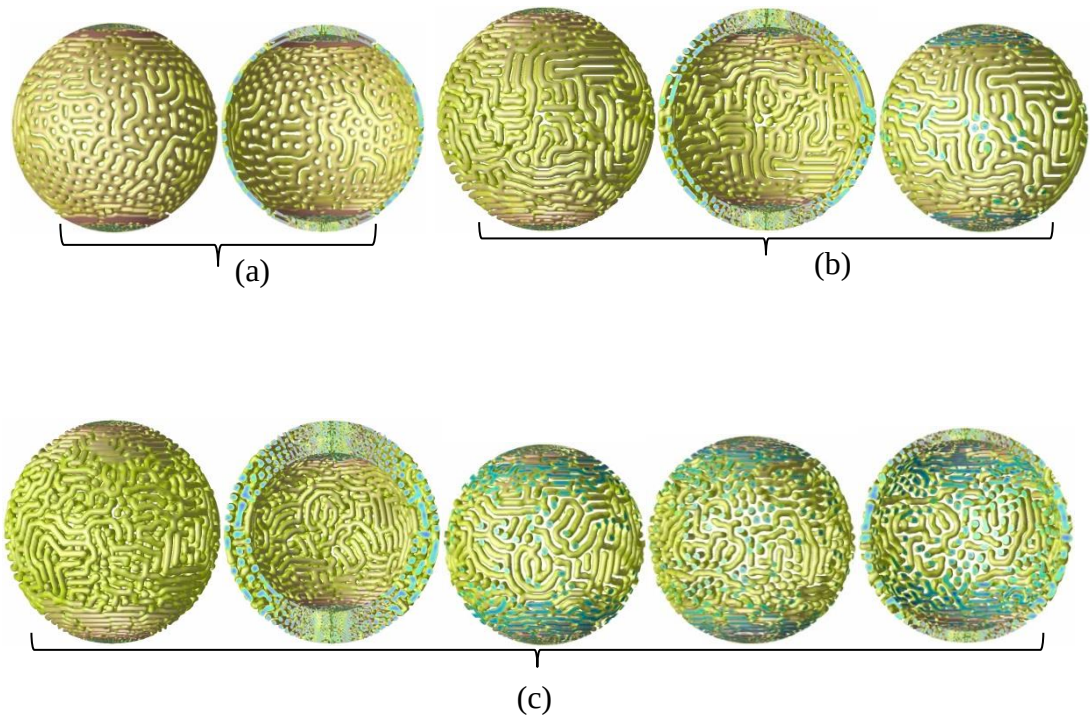

Figure 6.9: Cylinder system confined by parallel spherical interfaces in a spherical pore with the interior radius fixed at $r_a = 5$ and the pore surface sizes are (a) *d = 1* (b) *d = 1.5* (c) *d = 2.5*.

The cylindrical forming system confined between the parallel spherical surface walls in a pore system with the interior radius fixed at $r_a = 5$, shows mixed morphologies of perforated holes and long curved cylinder in the spherical pore surface. The spherical pore surface with pore size *d = 1*, shows mixed patterns of perforated holes and parallel to the pore cylinder in the single-layered spherical pore surface as shown in Figure 6.9(a). The perforated holes induced in the pore surface have rhombus, curved lines, straight lines and L-shaped packing arrangements on the pore surface. Perforated holes morphology was also obtained by the experimental work [31] shown in Figure 6(a) there in, which is consistent with the results shown in Figure 6.9(a). The coexistence of the cylinders parallel to the pore and perforated holes were also reported in the planar geometry [93]. The coexistence of both morphologies were also verified by Pinna *et al* on the surface of the sphere both computationally and experimentally [8] while their experimental image (shown in Figure 10(d) there in) shows consistency with this study. However, the pore surface with pore size *d = 1.5* shows bi-layered structure and induces

long curved cylinders, short straight cylinders, a few perforated holes and defective spheres in the pore surface as shown in Figure 6.9(b). Both layers are interconnected by cross-sectional cylinders, as one can observe by exterior view of the interior layer of the nanostructure shown on the right hand side of the image shown in Figure 6.9(b). The pore surface with pore size $d = 2.5$ a tri-interconnected layered nanostructure and shows long curved cylinders, short straight cylinders oriented perpendicular to the pore surface through cross-sections of the pore surface, as shown in Figure 6.9(c). There are a few defective spheres observed in the pore surface while there are very few perforated holes in the nanostructure.

Parallel to the pore cylinders were also obtained by both experimental and computational work [8] and their obtained results were shown by Figure 9(a) and Figure 9(c) there in, are consistent with this study. The coexistence of parallel, perpendicular and perforated morphology of cylindrical forming system were also reported in the computational study of the planar cylinders [92]. The cylinders parallel to the pore surface in the spherical geometry were reported in the experimental work [31] see Figure 6(c) there in.

In the next, we consider the pore surface with interior radius fixed at $r_a = 7$, while the exterior radius r_b of the pore surface was increased to expand the pore surface and pore surface walls have affinity with the majority block of the polymer system.

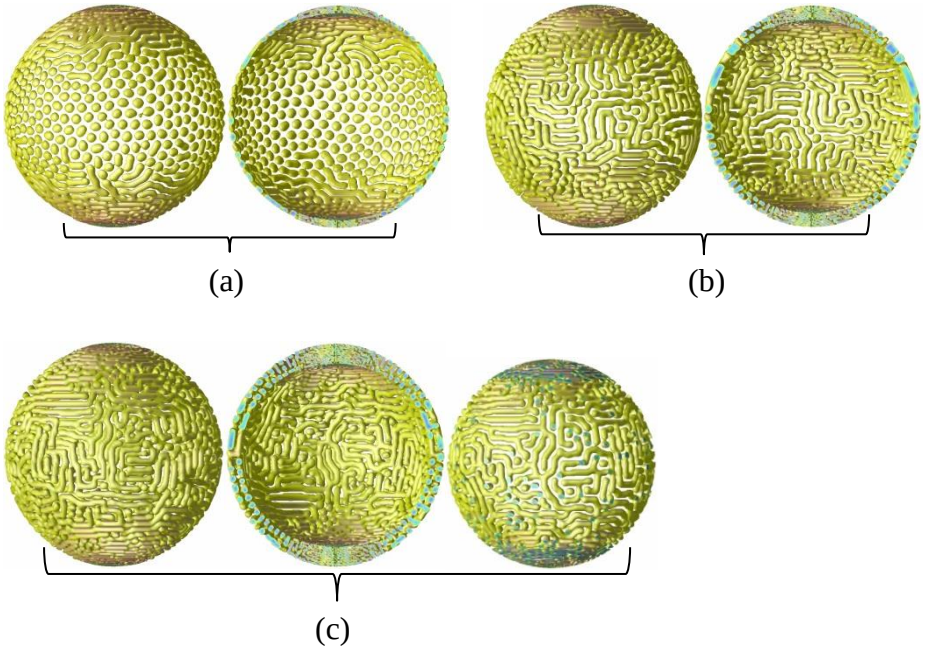

Figure 6.10: Cylinder system confined by parallel spherical interfaces in a spherical pore with the interior radius fixed at $r_a = 7$ and the pore surface sizes are (a) *d = 1* (b) *d = 1.5* (c) *d = 2.0.*

Results in the pore surface with the interior radius fixed at $r_a = 7$ and confined by parallel spherical surfaces having preferential affinity to the major segment of the polymer system show long curved cylinders, short straight cylinders and defective spheres in the spherical shells. The first system with narrow pore size *d = 1* shows defective squeezed spheres in the middle of the surface, long as well as short curved cylinders and perforated holes on the top and bottom of the spherical pore surface as shown in Figure 6.10(a). The next pore surface with pore size *d = 1.5,* displays a single layered nanostructure as shown in Figure 6.10(b). This nanostructure induces long curved cylinders, short cylinders parallel to the pore surface and defective spheres in the pore surface. However, this pore-sized surface-perforated morphology did not conformed in the spherical pore surface due to the size of the system. The spherical shell with pore size *d = 2.0* is a bi-layered nanostructure which induces the long curved cylinders, straight cylinder parallel to the pore surface, short cylinders perpendicular to the pore surface through cross section of the pore surface and defective spheres in the pore surface as shown in Figure 6.10(c). Similar cylindrical coils wrapping around each

other in the surface of sphere can be found in experimental work [85], where shown by Figure 5 therein.

6.2.3. Sphere forming system confined in spherical pores

In this section, a spherical forming system is investigated in spherical pore shell with various pore sizes by cutting off the spherical surface from its interior pore surface. Results are obtained with modified CDS parameters for sphere forming system, with high temperature in the neutral pore surfaces, while, in the results obtained with interfacial surfaces, CDS parameters for sphere forming system with low temperature were used in the pore geometry.

I. Sphere forming system confined in neutral spherical surfaces

In this subsection, results were obtained and discussed for spherical forming systems in the neutral spherical pore surfaces with various pore thicknesses and pore radii of the systems. Results were obtained by the new modified CDS parameter system with high temperature as shown in table (11).

Table 11: Modified CDS parameter system for sphere forming system with high temperature

τ	f	u	v	B	D	A
0.25	0.40	0.50	1.5	0.02	0.50	1.50

In the first case, results are obtained and discussed for a pore surface with the interior radius fixed at $r_a = 3$, while the exterior radius r_b increased to expand the pore thickness of the system. Results were obtained in the neural pore surfaces with the modified CDS parameter system with high temperature as shown in table (11).

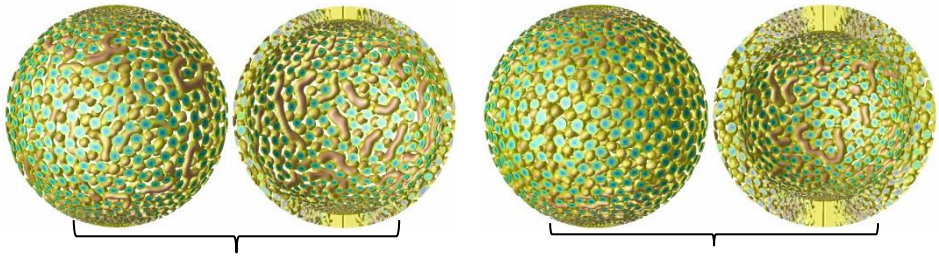

(a) (b)

Figure 6.11: Modified sphere system in the neutral pore surfaces with the interior radius of the pore surface fixed at $r_a = 3$ and the pore sizes are (a) *d = 0.5* (b) *d = 1.0.*

The results show that spheres are packed in the pore surface with thick defective cylinders in the neutral pore surfaces with the interior radius of the pore surfaces was fixed at $r_a = 3$. These defective cylinders were formed in the pore geometry by the merger of two or more spheres due to the influence of curvature. The pore surface with the pore size *d = 0.5* shows a single-layered nanostructure with packings of the spheres including defective thick cylinders as shown in Figure 6.11(a). However, the pore surface having pore size *d = 1* show defective thick cylinders on its interior surface only, while the exterior surface shows sphere packing in the pore surface as shown in Figure 6.11(b). Results show that defective cylinders form because of the strong curvature influence in the pore geometry.

In the second case, we consider the pore surface with the interior radius of the pore surface fixed at $r_a = 5$ and the exterior radius r_b were varied to obtained different pore thicknesses of the spherical pore shells. Results were obtained in the neutral spherical pore surfaces with modified CDS parameter system with high temperature.

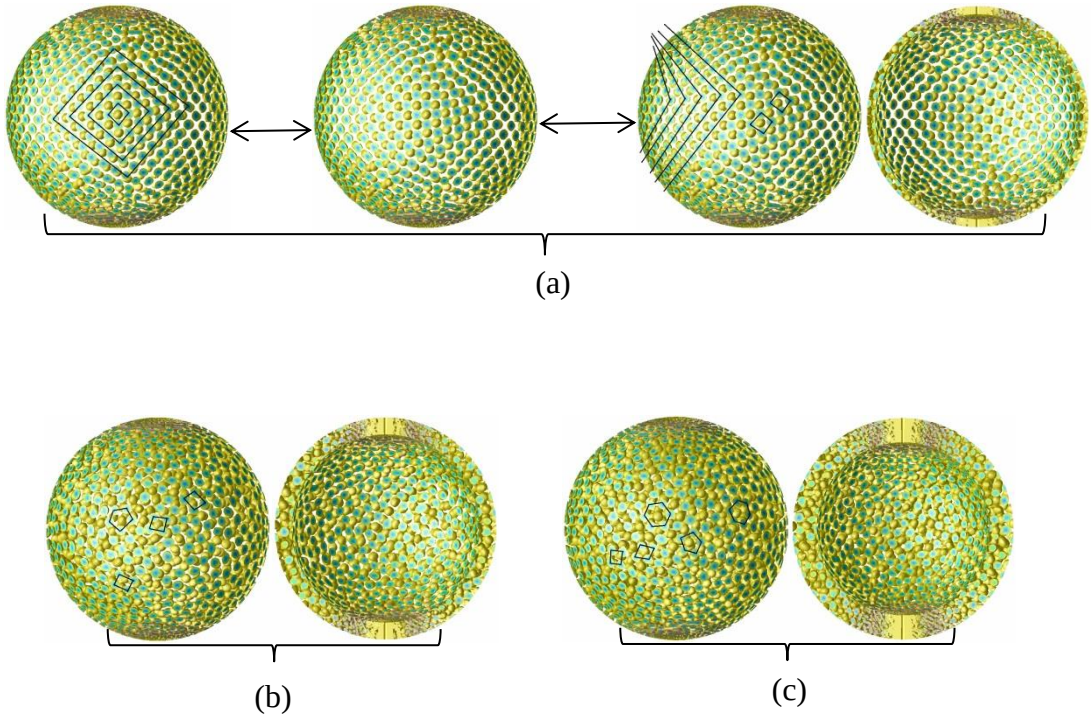

Figure 6.12: Modified sphere system in the neutral pore surfaces with the interior radius of the pore surface fixed at $r_a = 5$ and the pore sizes are (a) *d = 0.5* (b) *d = 1.0* (c) *d = 1.5.*

Results in the neutral spherical pores with the interior radius fixed at $r_a = 5$ were obtained with modified CDS parameter system for sphere forming system show packing arrangements of sphere system in the pore geometry, such as packing along the vertices of the concentric squires, packing along the quadrilateral vertices, square packing, pentagon packing, hexagonal packing and rhombus packing inside the pore surface. The narrow spherical pore system *d = 0.5,* shows very interesting packings of the sphere system in the spherical pore geometry as shown in Figure 6.12(a). This pore surface induces spheres in the packing arrangement along the vertices of the concentric squares in the pore geometry. The spheres in the outer layer (cut off in half) are shifted with respect to the spheres in the interior layer so that the sphere from the interior layer emanates in the middle of the squared-packed spheres of the outer layer. It is interesting that the sphere system on the curved surface is still able to persist in the square packing arrangement. Increasing the pore thickness of the pore surface *d = 1,* we can observe square packing, rhombus packing and pentagon packing of the sphere system on the

pore surface as shown in Figure 6.12(b). However, in this pore surface packing along the vertices of the concentric squares and quadrilaterals did not conform to the pore geometry, due to the size effect. In the pore surface *d = 1.5,* spheres are induced square, rhombus, pentagon, and hexagonal arrangements in the pore geometry as shown in Figure 6.12(c).

In the second case we consider the pore surface with interior radius of the pore system fixed at $r_a = 7$ and the pore surface size was extended by the exterior radius r_b of the spherical shells.

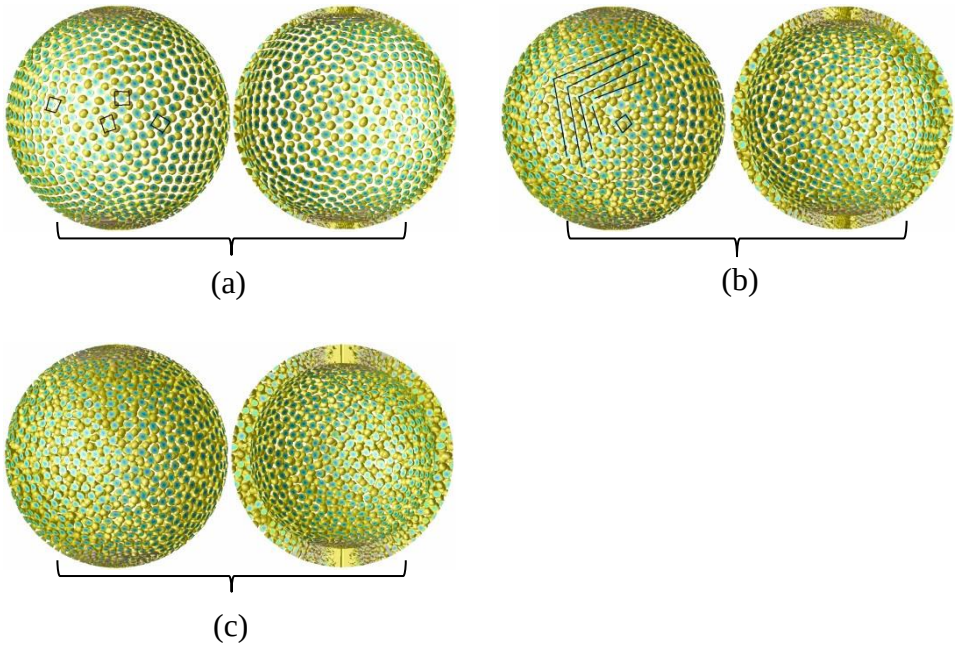

Figure 6.13: Sphere system obtained by modified CDS parameter system in the neutral pore surfaces with the interior radius of the pore surface fixed at $r_a = 7$ and the pore sizes are (a) *d = 0.5* (b) *d = 1.0* (c) *d = 1.5.*

The modified sphere system obtained in a pore surface with interior radius fixed at $r_a = 7$ show square packing and rhombus packing arrangements in the spherical pore geometry. The pore surface with pore size *d = 0.5,* shows square and rhombus packing arrangements of the spheres in the spherical shell as shown in Figure 6.13(a). Body-centred-cubic nanodomains were packed in the concentric layers of nano structure in

their intrinsic packing arrangements in both layers of the nano structure. The interior layer of the spherical pore shell was shifted so that the nanodomains in the interior layer emanates from the centre of four nano domains of the outer layer in the pore structure. The pore surface with pore size *d =1* also induces sphere system in square and rhombus arrangements in the pore surface as shown in Figure 6.13(b). In this pore surface sphere were conformed in distorted concentric square arrangements which can be observed in Figure 6.13(b) shown by strips on the image. Results show more shifting of the interior layer with respect to the exterior layer of the microstructure due to the size effect. The pore surface having pore size of the system *d =1.5*, shows more distorted square and rhombus packing arrangements of the nanodomains on account of the internal energy of the polymers system as shown in Figure 6.13(c).

II. Sphere system with interfacial surfaces

In this subsection, the sphere system is investigated by confining interacting parallel spherical surfaces having preferential affinity with the majority block of the polymer system in the spherical shell surfaces with various thicknesses of the pore systems. Interaction strength between the surface walls and the majority segment of the polymer system applied is $\alpha = 0.2$. CDS parameters for sphere forming system with low temperature were used in the simulation results, which are shown in table (12).

Table 12: CDS parameters for sphere forming system with low temperature

τ	f	u	v	B	D	A
0.20	0.40	0.50	2.30	0.01	0.50	1.50

In the first case, we consider the spherical pore shell with the interior radius fixed at $r_a = 5$ and the exterior radius r_b varied to expand the thicknesses of the pore shells.

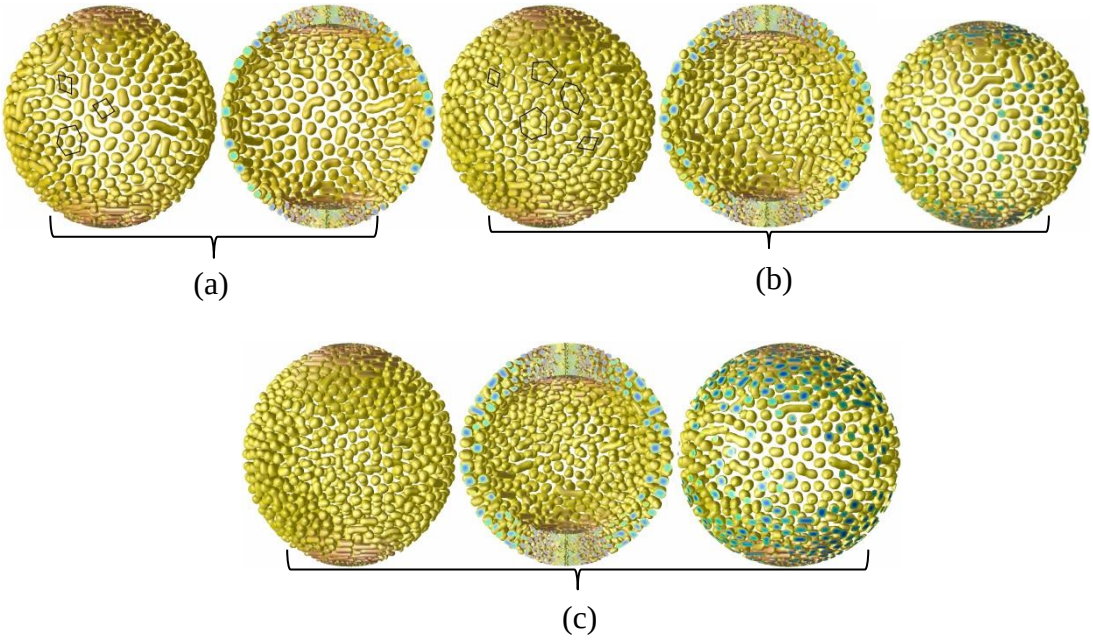

Figure 6.14: Sphere system confined by parallel to the pore walls, with the interior radius of the pore surface fixed at $r_a = 5$ and the pore surface sizes are (a) *d = 1.5* (b) *d = 2.0* (c) *d = 2.5.*

Results obtained in the spherical pore shell under confinement of the parallel spherical interfaces show square and rhombus packing arrangements along with the defective short cylinders in the pore geometry. The pore shell with pore size *1.5,* induces nano domains in a single-layered nano structure with square and rhombus packing arrangements in the spherical pore shell as shown in Figure 6.14(a). Some of the nano domains preserved their classical pentagonal and hexagonal conformation in the pore shell under the influence of the confinement and curvature. However, some of the nanodomains are packed in the square and rhombus arrangements in the spherical pore surface. Rhombus packing arrangement of the sphere system forms which is due to the curved surface effect in the pore geometry and originally this packing arrangement is the square packing arrangement of the sphere system. There are short curved cylinders and straight short cylinders parallel to the pore surface in the pore shell. The defective cylinders form due to the merger of two or more spheres. In the pore shell with size *2.0* spheres are induced in a bi-layered nanostructure with the interior layer shifted with respect to the outer layer of the nanostructure as shown in Figure 6.14(b). The spheres

in the pore surface show skewed hexagonal, pentagonal and rhombus formations with few defective short cylinders in the pore surface. Short defective cylinders are parallel to the pore surface and perpendicular to the pore surface (see in the interior layer on the right hand side of the system) while there are more defective cylinders in the interior layer as compared to the outer layer of the nanostructure which the role of the curvature in the formation of the defective short cylinder in the pore geometry. The pore shell having pore size $d = 2.5$ also induces sphere system in a single layered nanostructure with less defective cylinders as compared to previously-sized systems as shown in Figure 6.14(c). This system also shows twisted hexagonal, pentagonal and squared arrangements of the nanodomains in the pore shell. The less defective spheres in the pore shell show that the size effect is also one of the key reasons behind the formation of the defective cylinders in the pore geometry.

In the second case, we consider a pore shell with the interior radius fixed at $r_a = 7$ and the pore shell size was increased by the exterior radius r_b of the pore shell. The results were obtained with the surface preference to the majority segment of the polymer system in the pore geometry.

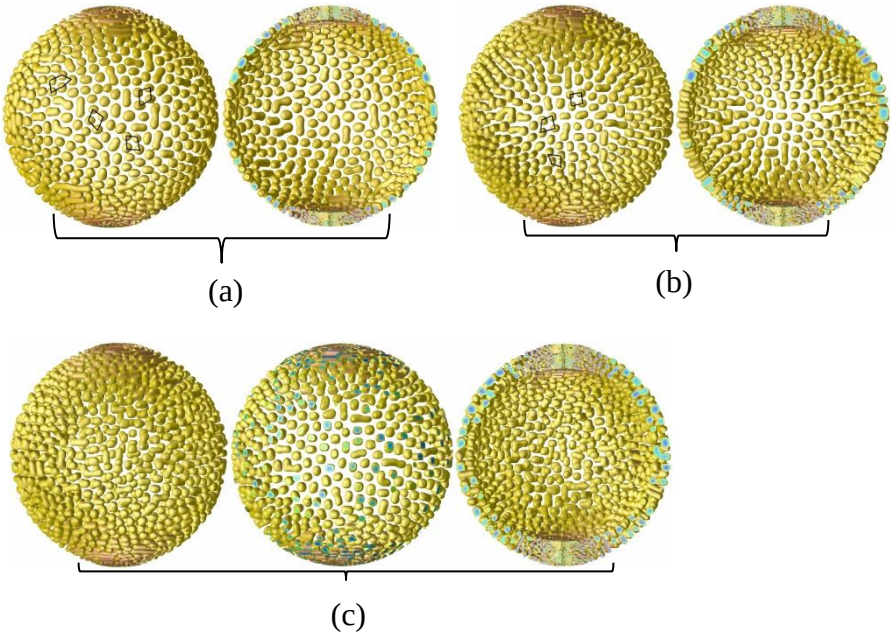

Figure 6.15: Sphere system confined by parallel to the pore walls, with the interior radius of the pore surface fixed at $r_a = 7$ and the pore surface sizes are (a) *d = 1.5* (b) *d = 2.0* (c) *d = 2.5.*

Nanodomains in the spherical pore shell with the interior radius fixed at $r_a = 7$ confined by parallel spherical interfaces show more skewed hexagonal, pentagonal and square packing arrangements in the pore geometry as compared to previous pore shell systems, while in this pore system a less defective system can be observed, nanodomains are small in size. The pore shell with pore size *d = 1.5* shows a single-layered nanostructure with skewed pentagonal, square and rhombus packing arrangement of the micro domains as shown in Figure 6.15(a). The pore shell also induces the short curved and straight cylinder oriented parallel to the pore shell. The pore shell having pore size *d =2.0* also show a single-layered nanostructure with square and rhombus packing arrangements of the nanodomains in the pore geometry as shown in Figure 6.15(b). There are skewed nanodomains in the respect of the size and shape as well in the pore surface. Defective cylinders in the pore shell are short straight cylinders parallel to the pore surface and one arc-shaped cylinder evident on the pore surface. In the pore surface with size of the pore *d = 2.5* displays spheres in the bi-layered nanostructure as shown in Figure 6.15(c.) This pore shell also shows the skewed pentagonal, square, and

rhombus packing arrangements in the both layers of the nanostructure in the pore geometry. Defective cylinders can be seen on the surface of the outer layer and the interior layer of nanostructure. There are a few straight cylinders perpendicular to the pore shell which can be seen clearly in the interior layer of the pore shell surface. However, in this pore system spheres are not skewed in respect of their size and shape in the nanostructure.

6.3. Summary

Lamella systems in neutral spherical pore shells show, concentric lamella (onion-like structure), standing lamella, stacked lamella and perforated lamella morphologies in the pore geometry. In the absence of the interfacial surfaces, results show that the stacked lamella morphology conformed in the pore geometry with respect to the pore size. In the presence of the interfacial surfaces, The obtained results predict the coexistence of lamella, cylinder and sphere morphologies in the pore geometry. Interfacial spherical surfaces also show the conformation of the stacked lamellar system with respect to the size of the pore surface. The confinement-induced lamella evolves in patterns such as concentric lamella, perforated lamella, mixed concentric lamella and stacked lamella. In the case of confined cylinders with neutral surfaces, cylinders parallel to the pore and perpendicular to the pore cylinders observed in the pore surfaces. The confinement induces cylinders perpendicular to the pore surface with respect to the pore size. In the presence of the interfacial pore walls, perforated holes and parallel to the pore cylinders observed in the pore geometry. The conformations of the short cylinders perpendicular to the pore surface were observed with respect to the pore size of the surface. Long curved cylinders, short cylinders and perforated holes were observed in the nanostructure in the concentric layers. Pore geometry induces the spheres in square, rhombus, pentagon, hexagon packing arrangements in the absence of the interfacial pore

walls. However, these packing arrangements of the sphere forming system were distorted with respect to the size of the system. In the presence of the interfacial surfaces, spheres packed in the concentric layers were observed in the pore geometry. The square and rhombus packing arrangements in the presence of interacting surfaces was observed in confined nanostructures.

CHAPTER SEVEN

7. Conclusions and Future work

7.1. Block copolymers confined in the circular annular pores

Using the CDS method employed in the polar coordinate system we obtained novel nanostructures in the circular pore geometry for lamella, cylinder and sphere forming systems. The asymmetric lamella forming system in the neutral film interfaces shows perpendicular to the exterior circumference and parallel to the interior circumference tendency in the circular pore system. Grain boundaries confined in the circular pore geometry show various formations of lamella including Y-shape, U-shape, W-shape, V-shape and T-junctions. Fingerprint morphology confined in the neutral circular pore with various pore thicknesses induced clusters of perforated holes, isolated perforated holes and star lamella with perforated hole at the centre of star. Close to the exterior pore boundary, lamellae conforms concentric parabolic patterns having openings in the direction of outer boundary, however for larger system sizes these parabolic patterns evolve into the parallel lamella strips normal to the outer circular boundary. The pore system with large interior radii shows parallel strips lamellae normal to the circular pore boundaries. The interplay of both interfacial circular walls and curvature influence induces lamella into the concentric circular rings in the circular pore geometry. In the presence of interfacial circular walls, concentric alternating lamella (onion-like) nanostructure were obtained in the circular pores which are strongly consistent with experimental results. Results show that under the influence of curvature and interfacial circular walls, the microdomains tend to form concentric lamella in the pore geometry. Symmetric lamella system induces defective nanostructures in the circular pore geometry.

The cylindrical forming system in the neutral circular annular pore system shows, the novel packing arrangements along the spiral lines. However, in the larger pore systems spiral packing arrangements alters and system regains in the classical hexagonal packing arrangements in the circular pore system. While, in the presence of interacting circular walls microdomains induces packing arrangements in the concentric circular rings in the pore geometry.

Similarly, the sphere forming system confined in circular annular pores shows, packing arrangements along the spiral lines, parabolic lines with opening along the outer boundary and hexagonal packing arrangements in the pore system. A new set of CDS parameters for sphere forming system were also introduced in the study. Results obtained with modified CDS parameters show that small system size induces sphere along the spiral curve, while large circular pore system induces sphere in the classical hexagonal packing arrangements. In the presence of interfacial circular walls, sphere system with modified CDS parameters squeezed down in size and shape. Sphere system under geometric confinement of annular circular pores with interfacial circular walls show, packing arrangements in the concentric circular rings. Results shows that under the influence of the curvature nanodomains show spiral packing arrangements while due to the interplay of both curvature and interfacial circular walls microdomains forms packing arrangements in the concentric circular rings in the pore geometry

7.2. Block copolymers confined in cylindrical pores

The lamella forming system confined in the neutral cylindrical pores show mixed orientations like helical strip lamella, various formations of strip lamella and lamellar sheets parallel to the pore axis. In the small pore radius, helical strip lamella conforms in the neutral cylindrical pores, while in the large pore radius lamellar sheets conforms in the cylindrical pore geometry. Results show that curvature influences the lamella

system to form helical strips around the pore axis while, in the minimal curvature effect lamella tend to form lamellar sheets parallel to the pore axis. In the presence of the parallel to the pore interfacial surfaces, the pore system induces smooth concentric cylindrical layers and the numbers of concentric layers depend on the size of the system. However, in the presence of the perpendicular to the pore interfacial surfaces, cylindrical geometry induces lamella into the smooth cylindrical lids perpendicular to the pore surface. In this case, the system shows strong segregation limit in the narrow sized surfaces under perpendicular one dimensional confinement. In the presence of both parallel and perpendicular interfacial surfaces, cylindrical confinement induces lamella into a single circular ring cylinder.

The cylinder forming system under geometric confinements of the neutral cylindrical pore show mixed orientations of microdomains, perpendicular to pore surface and parallel to the pore surface. Cylinders perpendicular to the pore were packed in square, rhombus and hexagonal arrangements in the neutral pore geometry. In the neutral pore surfaces, system induces short straight cylinders perpendicular to the pore surface and curved cylinders parallel to the pore cylinders in the pore geometry. However, in the presence of parallel interfacial surfaces with small pore radius, microdomains show parallel to the pore surface orientation and wrapped around the pore system. In the presence of the parallel interfacial surfaces cylinders were packed in the concentric cylindrical layers.

In the narrow pore size system, coexistence of perforated morphology and parallel to the pore cylinders were observed in the pore geometry. Results show that the interplay of both curvature and interfacial parallel cylindrical surfaces alter the orientation of the perpendicular cylinders to the parallel coil cylinders wrapped around the cylindrical axis. In the large pore radius with parallel interfacial surfaces, cylinders show mixed orientation in the pore geometry. In the short length pore surface, we obtained standing

cylinders which were packed in the concentric circles in the pore system. Cylindrical forming systems were also investigated with various lengths of the narrow sized cylindrical pores, with one dimensional confinement (parallel interfacial surfaces) and two dimensional confinements (parallel and perpendicular interfaces). In this case coexistence of perforated holes with parallel to the pore cylinders were observed, however, under two dimensional confinements in the small pore length, cylindrical rings arranged perpendicularly one on other were observed.

The sphere forming system obtained in neutral cylindrical pores with CDS parameter system with low temperature show, sphere packing along with defective short and long curved cylinders perpendicular to the pore surface. The sphere forming systems were obtained with a new set of CDS parameter system with high temperature. In this case we obtained perfect sphere systems in the cylindrical pores without any defective cylinders. The sphere system obtained with modified CDS parameters and with high temperature show, packing arrangements along the perimeters of the concentric quadrilateral in the narrow sized pore surface. This packing arrangements look like diagonal lines on the cylindrical pore surface. The modified sphere system under preferential surfaces squeezed down in size and shape in the pore surface. Sphere forming system confined in the cylindrical pore with interfacial surfaces show, packing arrangements into concentric circular layers. In the presence of the perpendicular and parallel interfacial surfaces, pore geometry induces spheres into the circular rings arranged in parallel and perpendicular layers. In this case we obtained in small sized and short length cylindrical pore, the coexistence of spheres and cylinder segments induced into a circular ring. Results show that cylindrical pore geometry induces spheres into the layers of circular rings.

7.3. Block copolymers confined in spherical pores

Lamella systems in neutral spherical pore shells show, concentric lamella (onion like structure), standing lamella, stacked lamella and perforated lamella morphologies in the pore geometry. In the absence of the interfacial surfaces, results show that the stacked lamella morphology conformed in the pore geometry with respect to the pore size. In the presence of the interfacial surfaces, we obtained the nanostructure which predicted the coexistence of lamella, cylinder and sphere morphologies in the pore geometry. Interfacial spherical surfaces also show the conformation of the stacked lamellar system with respect to the size of the pore surface. The confinement induced lamella evolves in the patterns like concentric lamella, perforated lamella, mixed concentric lamella and stacked lamella. In the case of confined cylinders with neutral surfaces, parallel to the pore cylinders and perpendicular to the pore cylinders observed in the pore surfaces. The confinement induces cylinders perpendicular to the pore surface with respect to the pore size. In the presence of the interfacial pore walls, perforated holes and parallel to the pore cylinders observed in the pore geometry. The conformations of the short cylinders perpendicular to the pore surface were observed with respect to the pore size of the surface. The long curved cylinders, short cylinders and perforated holes were observed in the nano structure in the concentric layers. Pore geometry induces the spheres in square, rhombus, pentagon, hexagon packing arrangements in the absence of the interfacial pore walls. However, these packing arrangements of the sphere forming system distorted with respect to the size of the system. In the presence of the interfacial surfaces, spheres packed in the concentric layers were observed in the pore geometry. The square and rhombus packing arrangements in the presence of interacting surfaces was observed in confined nanostructures.

7.4. Future work

For future work following projects can be carried out.

I. To study Block copolymers confinement's in circular pores, cylindrical pores and spherical pores by applying electric field and shear flow using the CDS method employed in curvilinear coordinate systems.

II. To study and investigate block copolymer confined in circular pores, cylindrical pores and spherical pores by using asymmetric boundary conditions on the pore interfaces in the circular pores, cylindrical pores and spherical pores.

III. To study block copolymer under various different confinements, in addition to the circular pore, cylindrical pore and spherical pore geometries, study will also be carried out under geometric confinements of ellipsoid and hyperboloid.

IV. The study and investigate block copolymers using two order parameters for diblock copolymers/homopolymer mixture confined in the circular pores, cylindrical pores and spherical pores using physically motivated discretization.

References

[1] M. Folkes, *Processing, Structure and Properties of Block Copolymers.* Springer Science & Business Media, 2012.

[2] P. Wu, G. Ren, C. Li, R. Mezzenga and S. A. Jenekhe, "Crystalline diblock conjugated copolymers: Synthesis, self-assembly, and microphase separation of poly (3-butylthiophene)-b-poly (3-octylthiophene)," *Macromolecules,* vol. 42, pp. 2317-2320, 2009.

[3] S. An-Chang and L. Baohui, "self-assembly of diblock copolymers under confinement," *RSC,* vol. 9, pp. 1398-1413, 2013.

[4] H. Xiang, K. Shin, T. Kim, S. I. Moon, T. J. McCarthy and T. P. Russell, "From cylinders to helices upon confinement," *Macromolecules,* vol. 38, pp. 1055-1056, 2005.

[5] K. Shin, S. Obukhov, J. Chen, J. Huh, Y. Hwang, S. Mok, P. Dobriyal, P. Thiyagarajan and T. P. Russell, "Enhanced mobility of confined polymers," *Nat Mater,* vol. 6, pp. 961-965, print, 2007.

[6] Q. Wang, "Symmetric diblock copolymers in nanopores: Monte Carlo simulations and strong-streching theory," *J. Chem. Phys.,* vol. 126, pp. 024903-1-024903-11, 2007.

[7] P. Chen, X. He and H. Liang, "Effect of surface field on the morphology of a symmetric diblock copolymer under cylindrical confinement," *J. Chem. Phys.,* vol. 124, pp. 104906-1-104906-6, 2006.

[8] M. Pinna, S. Hiltl, X. Guo, A. Boker and A. V. Zvelindovsky, "Block Copolymer Nanocontainers ," *ACSNANO,* vol. 4, pp. 2845-2855, 2010.

[9] J. Feng, H. Liu and Y. Hu, "Mesophase seperation of diblock copolymer confined in a cylindrical tube studeid by dissipative particle dynamics," *Macromol, Theory Simul,* vol. 15, pp. 674-685, 2006.

[10] P. Chen and H. Liang, "Origin of microstructures from confined asymmetric diblock copolymers," *Macromolecules,* vol. 40, pp. 7329-7335, 2007.

[11] M. Yiyong and E. Adi, "Self-assembly of diblock copolymers," *Chem Soc Rev,* vol. 41, pp. 5969-5985, 2012.

[12] M. Pinna and A. V. Zvelindovsky, "Large scale simulation of block copolymers with cell dynamics," *Eur. Phys. J. B,* vol. 85, pp. 210, JUN, 2012.

[13] J. Feng and E. Ruckenstein, "Morphologies of AB diblock copolymer melt confined in nanocylindrical tubes," *Macromolecules,* vol. 39, pp. 4899-4906, 2006.

[14] b. Yu, P. Sun, T. Chen, Q. Jin, D. Ding, B. Li and A. Shi, "Confinement-induced novel morphologies of block copolomers," *PRL,* vol. 96, pp. 138306-1-138306-4, 2006.

[15] K. Shin, H. Xiang, S. I. Moon, T. Kim, T. J. McCarthy and T. P. Russell. Curving and frustrating flatland. *Science 306(5693),* pp. 76-76. 2004. . DOI: 10.1126/science.1100090.

[16] Y. Wu, G. Cheng, K. Katsov, s. w. Sides, J. Wang, J. Tang, G. H. Fredrickson, M. Moskovits and G. D. Stucky, "Composite mesostructures by nano-confinement," *Nature Publishing Group,* vol. 3, pp. 816-822, 2004.

[17] G. J. A. Sevink, A. V. Zvelindovsky and Fraaije, J. G. E. M, "Morphology of symetric block copolymer in a cylindrical pore," *Journal of Chemical Physics,* vol. 115, pp. 8226-8230, 2001.

[18] C. Lam, "Applied Numerical Methods for partial differential equations," *Prentice Hall*, 1994.

[19] R. Yang, B. Li and A. Shi, "Phase behaviour of binary blends of diblock copolymer/homopolymer confined in spherical nanopores," *Langmuir*, vol. 28, pp. 1569-1578, 2012.

[20] M. Pinna, X. Guo and A. V. Zvelindovsky, "Block copolymer nanoshells," *Polymer*, vol. 49, pp. 2797-2800, 2008.

[21] B. Yu, P. Sun, T. Chen, Q. Jin, D. Ding, B. Li and A. Shi, "Self-assembly of diblock copolymers confined in cylindrical nanopores," *J. Chem. Phys.*, vol. 127, pp. 114906-1-114906-15, 2007.

[22] T. Chantawansri L., A. W. Boss, A. Hexemer, H. D. Ceniceros, c. J. Garcia-cervera, E. J. Kramer and G. H. Fredrickson, "Self-Consistent field theory simulations of block copolymer assembly on a sphere," *Physical Review E*, vol. 75, pp. 031802-1-031802-17, 2007.

[23] X. He, H. Liang, M. Song and C. Pan, "Possiblity of design of Nanodevices by confined macromolecular self-assembly," *Macromol, Theory Simul*, vol. 11, pp. 379-382, 2002.

[24] W. Li and R. A. Wickham, "Self-Assembled Morphologies of a diblock copolymer melt confined in a cylindrical nanopore," *Macromolecules*, vol. 39, pp. 8492-8498, 2006.

[25] M. W. Matsen and F. S. Bates, "Unifying Weak- and Strong-Segregation Block Copolymer Theories," *Macromolecules*, vol. 29, pp. 1091-1098, 01/01, 1996.

[26] F. S. Bates and G. H. Fredrickson, "Block copolymer thermodynamics: theory and experiment," *Annu. Rev. Phys. Chem.*, vol. 41, pp. 525-557, 1990.

[27] N. Hadjichristidis, A. Hirao, Y. Tezuka and F. Du Prez, *Complex Macromolecular Architectures: Synthesis, Characterization, and Self-Assembly*. John Wiley & Sons, 2011.

[28] M. Pinna, *Mesoscale Modelling of Block Copolymer Systems*. Germany: VDM Verlag, 2010.

[29] C. M. M. a. M. E. Cates, "Harmonic Corrections near the Ordering Transition," *EPL (Europhysics Letters)*, vol. 13, pp. 267, 1990.

[30] S. R. Ren and I. W. Hamley, "Cell Dynamics Simulations of Microphase seperation in block copolymers," *Macromolecules*, vol. 34, pp. 116-126, 2001.

[31] D. A. Rider, J. I. L. Chen, C. Eloi, A. C. Arsenault, T. P. Russell, Ozin G. A and I. Manners, "Controlling the Morphologies of Organometallic Block Copolymers in the 3-Dimensional Spatial Confinement of Colloidal and Inverse Colloidal Crystals," *Macromolecules*, vol. 41, pp. 2250-2259, 2008.

[32] P. Dobriyal, H. Xiang, M. Kazuyuki, J. Chen, H. Jinnai and T. P. Russell, "Cylindrically Confined Diblock Copolymers," *Macromolecules*, vol. 42, pp. 9082-9088, 11/24, 2009.

[33] A. K. Khandpur, S. Foerster, F. S. Bates, I. W. Hamley, A. J. Ryan, W. Bras, K. Almdal and K. Mortensen, "Polyisoprene-polystyrene diblock copolymer phase diagram near the order-disorder transition," *Macromolecules*, vol. 28, pp. 8796-8806, 1995.

[34] G. H. Fredrickson, "Surface ordering phenomena in block copolymer melts," *Macromolecules,* vol. 20, pp. 2535-2542, 10/01, 1987.

[35] R. Choksi and X. Ren, "On the Derivation of a Density Functional Theory for Microphase Separation of Diblock Copolymers," *Journal of Statistical Physics,* vol. 113, pp. 151-176, 2003.

[36] C. M. M. a. M. E. Cates, "Harmonic Corrections near the Ordering Transition," *EPL (Europhysics Letters),* vol. 13, pp. 267, 1990.

[37] I. W. Hamley, *Introduction to Soft Matter.* England: John Wiley & Sons, Ltd, 2007.

[38] S. Kim, W. Li, G. H. Fredrickson, C. J. Hawker and E. J. Kramer, "Order–disorder transition in thin films of horizontally-oriented cylinder-forming block copolymers: thermal fluctuations vs. preferential wetting," *Soft Matter,* 2016.

[39] F. H. Schacher, P. A. Rupar and I. Manners, "Functional block copolymers: nanostructured materials with emerging applications," *Angewandte Chemie International Edition,* vol. 51, pp. 7898-7921, 2012.

[40] W. Li, R. A. Wickham and R. A. Garbary, "Phase diagram for a diblock copolymer melt under cylindrical confinement," *Macromolecules,* vol. 39, pp. 806-811, 2006.

[41] Y. Mai and A. Eisenberg, "Self-assembly of block copolymers," *Chem. Soc. Rev.,* vol. 41, pp. 5969-5985, 2012.

[42] V. Bart, U. K. Jaeup, L. C. Tanya, H. F. Glenn and W. M. Mark, "Self-Consistent field theory for diblock copolymers grafted to a sphere," *Soft Matter,* vol. 7, pp. 5049-5452, 2011.

[43] B. Yu, B. Li, Q. Jin, D. Ding and A. Shi, "Confined Self-Assembly of Cylinder-forming diblock copolymer: effects of confing geometries," *softMatter, RSC Publishing,* vol. 7, pp. 10227-10240, 2011.

[44] J. G. Son, J. Chang, K. K. Berggren and C. A. Ross, "Assembly of sub-10-nm block copolymer patterns with mixed morphology and period using electron irradiation and solvent annealing," *Nano Letters,* vol. 11, pp. 5079-5084, 2011.

[45] I. Hamley, "Nanostructure fabrication using block copolymers," *Nanotechnology,* vol. 14, pp. R39, 2003.

[46] M. Ma, E. L. Thomas, G. C. Rutledge, B. Yu, B. Li, Q. Jin, D. Ding and A. Shi, "Gyroid-forming diblock copolymers confined in cylindrical geometry: A case of extreme makeover for domain morphology," *Macromolecules,* vol. 43, pp. 3061-3071, 2010.

[47] V. A. J.M.G. Cowie, *Polymers: Chemistry and Physics of Modern Materials.* CRC Press, 2008.

[48] D. E. Angelescu, J. H. Waller, R. A. Register and P. M. Chaikin, "Shear-Induced Alignment in Thin Films of Spherical Nanodomains," *Adv Mater,* vol. 17, pp. 1878-1881, 2005.

[49] M. Matsen, "Electric field alignment in thin films of cylinder-forming diblock copolymer," *Macromolecules,* vol. 39, pp. 5512-5520, 2006.

[50] S. Pujari, R. A. Register and P. M. Chaikin, "Shear induced alignment of standing lamellar block copolymer thin films," in *2011 AIChE Annual Meeting, 11AIChE,* 2011, .

[51] J. N. L. Albert and T. H. Epps III, "Self-assembly of block copolymer thin films," *Materials Today*, vol. 13, pp. 24-33, 6, 2010.

[52] X. Wang, S. Li, P. Chen, L. Zhang and H. Liang, "Microstructures of lamella-forming diblock copolymer melts under nanorod-array confinements," *Polymer*, vol. 50, pp. 4964-4972, 2009.

[53] A. Daud Júnior, F. M. Morais, S. Martins, D. Coimbra and W. A. Morgado, "Microphase separation of diblock copolymer with moving walls," *Brazilian Journal of Physics*, vol. 34, pp. 405-407, 2004.

[54] V. Weith, A. Krekhov and W. Zimmermann, "Stability and orientation of lamellae in diblock copolymer films," *J. Chem. Phys.*, vol. 139, pp. 054908, 2013.

[55] I. W. Hamley, "Cell dynamics simulations of block copolymers," *Macromolecular Theory and Simulations*, vol. 9, pp. 363-380, 2000.

[56] S. Pujari, M. A. Keaton, P. M. Chaikin and R. A. Register, "Alignment of perpendicular lamellae in block copolymer thin films by shearing," *Soft Matter*, vol. 08, pp. 5358-5363, 2012.

[57] N. E. Voicu, S. Ludwigs and U. Steiner, "Alignment of Lamellar Block Copolymers via Electrohydrodynamic-Driven Micropatterning," *Adv Mater*, vol. 20, pp. 3022-3027, 2008.

[58] G. J. A. Sevink and A. V. Zvelindovsky, "Block copolymers confined in a nanopores: Pathfinding in a curveing and frustrating flatland," *Journal of Chemical Physics*, vol. 128, pp. 084901-1-084901-16, 2008.

[59] M. Pinna, X. Guo and A. V. Zvelindovsky, "Diblock copolymers in a cylindrical pore," *J. Chem. Phys.,* vol. 131, pp. 214902-1-214902-7, 2009.

[60] M. W. Matsen and M. Schick, "Stable and Unstable Phases of a Diblock Copolymer Melt," *Physical Review Letters,* vol. 72, pp. 2660-2663, 1994.

[61] P. Chen, H. Liang and A. Shi, "Microstructures of a cylinder-forming diblock copolymer under spherical confinement," *Macromolecules,* vol. 41, pp. 8938-8943, 2008.

[62] P. Chi, Z. Wang, B. Li and A. Shi, "Soft confinement-induced morphologies of diblock copolymers," *Langmuir,* vol. 27, pp. 11683-11689, 2011.

[63] P. Broz, S. Driamov, J. Ziegler, N. Ben-Haim, S. Marsch, W. Meier and P. Hunziker, "Toward Intelligent Nanosize Bioreactors: A pH-Switchable, Channel-Equipped, Functional Polymer Nanocontainer," *Nano Lett.,* vol. 6, pp. 2349-2353, 10/01, 2006.

[64] W. Chen, H. Wei, S. Li, J. Feng, J. Nie, X. Zhang and R. Zhuo, "Fabrication of star-shaped, thermo-sensitive poly(N-isopropylacrylamide)–cholic acid–poly(ε-caprolactone) copolymers and their self-assembled micelles as drug carriers," *Polymer,* vol. 49, pp. 3965-3972, 8/26, 2008.

[65] A. Knoll, A. Horvat, K. S. Lyakhova, G. Krausch, G. J. A. Sevink, R. Magerle and R. Magerle, "Phase Behavior in Thin Films of Cylinder-Forming Block Copolymers," *Physical Review Letters,* vol. 89, pp. 035501-1, 2002.

[66] A. Knoll, R. Magerle and G. Krausch. Phase behavior in thin films of cylinder-forming ABA block copolymers: Experiments. *J. Chem. Phys. 120(2),* pp. 1105-1116. 2004. . DOI: http://dx.doi.org/10.1063/1.1627324.

[67] A. Knoll, K. S. Lyakhova, A. Horvat, G. Krausch, G. J. A. Sevink, A. V. Zvelindovsky and R. Magerle, "Direct imaging and mesoscale modelling of phase transitions in a nanostructured fluid," *Nat Mater,* vol. 3, pp. 886-891, print, 2004.

[68] H. Takeshi, T. Atsunori, Y. Hiroshi and S. Masatsugu, "Spontaneous formation of polymer nanoparticles with inner micro-phase separation structures," *Soft Matter,* vol. 4, pp. 1302-1305, 2008.

[69] P. Tang, F. Qiu, H. Zhang and Y. Yang, "Phase seperation patterns for diblock copolymers on spherical surfaces: A finite volume method," *Physical Review E,* vol. 72, pp. 016710-1-016710-7, 2005.

[70] W. Li, R. A. Wickham and R. A. Garbary, "Phase Diagram for a Diblock Copolymer Melt under Cylindrical Confinement," *Macromolecules,* vol. 39, pp. 806-811, 01/01, 2006.

[71] G. H. Griffths, B. Vorselaars and M. W. Matsen, "Unit Cell Approximation for diblock copolymer brushes grafted to spherical particles," *Macromolecules,* vol. 44, pp. 3649-3655, 2011.

[72] M. Serral, M. Pinna, A. V. Zvelindovsky and J. B. Avalos, "Cell dynamics simulations of sphere-forming diblock copolymers in thin films on chemically patterned substrates," *Macromolecules,* vol. 49, pp. 1079-1092, 2016.

[73] J. D. Hoffman, *Numerical Methods for Engineers and Scientist.* United States: McGRAW-HILL, 1992.

[74] S. Sirca and M. Horvat, *Computational Methods for Physicists.* Springer, 2010.

[75] S. P. Thampi, S. Ansumali, R. Adhikari and S. Succi, "Isotropic Discrete Laplacain operators from lattice hydrodynamics," *Journal of Computational Physics*, vol. 234, pp. 1-7, 2012.

[76] S. A and O. Y, "Spinodal decomposition in 3-space," *Physical Review E,* vol. 48, pp. 2622-2654, 1993.

[77] R. Dessí, M. Pinna and A. V. Zvelindovsky, "Cell dynamics simulations of cylinder-forming diblock copolymers in thin films on topographical and chemically patterned substrates," *Macromolecules,* vol. 46, pp. 1923-1931, 2013.

[78] T. Ohta and K. Kawasaki, "Equilibrium morphology of block copolymer melts," *Macromolecules,* vol. 19, pp. 2661-2632, 1986.

[79] L. Ludwik, "Theory of Microphase Separation in Block Copolymers," *Macromolecules,* vol. 13, pp. 1602-1617, 1980.

[80] J. Feng and E. Ruckenstein. Long-range ordered structures in diblock copolymer melts induced by combined external fields. *J. Chem. Phys. 121(3),* pp. 1609-1625. 2004. . DOI: http://dx.doi.org/10.1063/1.1763140.

[81] M. Patra and M. Karttunen, "Stencils with isotropic discretization error for differential operators," *Numerical Methods for Partial Differential Equations,* vol. 22, pp. 936-953, 2006.

[82] "Clipart - Blue grid sphere", *Openclipart.org*, 2016. [Online]. Available: https://openclipart.org/detail/183675/blue-grid-sphere. [Accessed: 11- Apr- 2016].

[83]"Create_grid_with_VTK"[online]available:http://www.corephysics.com/wiki/index.php [accessed: 11-Apr- 2016]

[84] X. Zhang, B. C. Berry, K. G. Yager, S. Kim, R. L. Jones, S. Satija, D. L. Pickel, J. F. Douglas and A. Karim, "Surface morphology diagram for cylinder-forming block copolymer thin films," *ACSNANO,* vol. 2, pp. 2331-2341, 2008.

[85] L. Li, K. Matsunaga, J. Zhu, T. Higuchi, H. Yabu, M. Shimomura, H. Jinnai, R. C. Hayward and T. P. Russell, "Solvent-driven evolution of block copolymer morphology under 3D confinement," *Macromolecules,* vol. 43, pp. 7807-7812, 2010.

[86] H. Xiang, K. Shin, T. Kim, S. Moon, T. McCarthy and T. Russell, "The influence of confinement and curvature on the morphology of block copolymers," *Journal of Polymer Science Part B: Polymer Physics,* vol. 43, pp. 3377-3383, 2005.

[87] X. Hongqi, s. Kyusoon, K. Taehyung, I. Sung Moon, T. J. McCarthy and T. P. Russell, "- Block Copolymers under Cylindrical Confinement," - *Macromolecules*, vol. 37, pp. 5660-5664, 2004.

[88] D. Chen, S. Park, J. Chen, E. Redston and T. P. Russell, "A simple route for the preparation of mesoporous nanostructures using block copolymers," *ACSNANO,* vol. 3, pp. 2827-2833, 2009.

[89] J. M. Shin, M. P. Kim, H. Yang, K. H. Ku, S. G. Jang, K. H. Youm, G. Yi and B. J. Kim, "Monodipserse Nanostructured Spheres of Block Copolymers and Nanoparticles via Cross-Flow Membrane Emulsification," *Chem. Mater.,* vol. 27, pp. 6314-6321, 09/22, 2015.

[90] M. J. Fasolka and A. M. Mayes, "BLOCK COPOLYMER THIN FILMS: Physics and Applications1," *Ann. Rev. Mat. Res.,* vol. 31, pp. 323-355, 2001.

[91] B. Yu, L. Baohui, Q. Jin, D. Ding and A. Shi, "Self-Assembly of Symmetric Diblock Copolymers Confined in Spherical Nanopores," *Marcomolecules*, vol. 40, pp. 9133-9142, 2007.

[92] K. S. Lyakhova, G. J. A. Sevink, A. V. Zvelindovsky, A. Horvat and R. Magerle, "Role of dissimlar interfaces in thin films of cylinder-forming block copolymers," *J. Chem. Phys.*, vol. 120, pp. 1127-1137, 2004.

[93] A. Horvat, K. S. Lyakhova, G. J. A. Sevink, A. V. Zvelindovsky and R. Magerle, "Phase behaviour in thin films of cylinder-forming ABA block copolymers: Mesoscale modelling," *J. Chem. Phys.*, vol. 120, pp. 1117-1126, 2004.